

SEPARATION OF LITHIUM FROM BRINES

A THESIS SUBMITTED TO
THE GRADUATE SCHOOL OF NATURAL AND APPLIED SCIENCES
OF
MIDDLE EAST TECHNICAL UNIVERSITY

BY
BARIŞ ERDOĞAN

IN PARTIAL FULFILLMENT OF THE REQUIREMENTS
FOR
THE DEGREE OF DOCTOR OF PHILOSOPHY
IN
CHEMICAL ENGINEERING

FEBRUARY 2015

Approval of the thesis:

SEPARATION OF LITHIUM FROM BRINES

submitted by **BARIŞ ERDOĞAN** in partial fulfillment of the requirements for the degree of **Doctor of Philosophy in Chemical Engineering Department, Middle East Technical University** by,

Prof. Dr. Gülbin Dural Ünver
Dean, Graduate School of **Natural and Applied Sciences** _____

Prof. Dr. Halil Kalıpçılar
Head of Department, **Chemical Engineering** _____

Prof. Dr. H. Önder Özbelge
Supervisor, **Chemical Engineering Dept., METU** _____

Assoc. Prof. Dr. Yusuf Uludağ
Co-supervisor, **Chemical Engineering Dept., METU** _____

Examining Committee Members:

Assoc. Prof. Dr. Naime Aslı Sezgi
Chemical Engineering Dept., METU _____

Prof. Dr. H. Önder Özbelge
Chemical Engineering Dept., METU _____

Prof. Dr. Halil Kalıpçılar
Chemical Engineering Dept., METU _____

Prof. Dr. Niyazi Bıçak
Chemistry Dept., ITU _____

Assoc. Prof. Dr. Çerağ Dilek Hacıhabiboğlu
Chemical Engineering Dept., METU _____

Date: _____ 06.02.2015

I hereby declare that all information in this document has been obtained and presented in accordance with academic rules and ethical conduct. I also declare that, as required by these rules and conduct, I have fully cited and referenced all material and results that are not original to this work.

Name, Last name : Barış Erdoğan

Signature :

ABSTRACT

SEPARATION OF LITHIUM FROM BRINES

Erdoğan, Barış

Ph.D., Department of Chemical Engineering

Supervisor: Prof. Dr. H. Önder Özbelge

Co-supervisor: Assoc. Prof. Dr. Yusuf Uludağ

February 2015, 184 pages

Lithium is one of the valuable and promising metals having extensive potential use in long lasting rechargeable batteries in automotive and electronics industry. Regarding scarcity of world lithium reserves, the most efficient method must be utilized in lithium separation and purification process. The scope of this study is to increase the efficiency of lithium separation by liquid-liquid extraction and adsorption methods with various materials synthesized throughout the study.

In liquid-liquid extraction method, N-alkyl formamides (hexyl formamide, octyl formamide, dibutyl formamide, dihexyl formamide) were synthesized and lithium separation performances were evaluated. Hexyl formamide was found to have a distribution coefficient of 0.14 for LiCl in dilute concentrations at 25 °C which is the largest value cited in the literature for a single solvent so far.

In adsorption method, lithium manganese oxides (LiMnO) were synthesized with solid-solid and hydrothermal reaction procedures under different temperature and Li/Mn ratios. The performance of the adsorbent with the highest capacity value was characterized at different pH, lithium and foreign ion (Na, K, Mg) concentrations. It was found out that, LiMnO adsorbent has a capacity value of 22.8 mg Li/g adsorbent at pH:10.2 in dilute lithium chloride solutions with a very high selectivity towards foreign ions such as sodium, potassium and magnesium.

In order to employ LiMnO adsorbents in an adsorption column, micron sized particles were impregnated into millimeter sized beads made of poly(styrene-maleic anhydride-glycidyl methacrylate) (PSMA) by precipitation method. PSMA has been utilized in bead formation process for the first time in this study and gave superior results compared to previous analogs in terms of its swelling and self-crosslinking ability. The column performance filled with PSMA-LiMnO beads were evaluated with artificial brine, concentrated brine taken from Çamaltı Salina (İzmir) and boron clay extract taken from Bigadiç. The lithium concentration in brines was increased from 0.43 ppm to 1675.6 ppm while reducing the foreign ion concentrations significantly in adsorption column. The post treatment of the column product with LiMnO resulted in a solution with 3200 ppm Li. That concentration is above the required minimum concentration for Li_2CO_3 production, which is the raw material for lithium battery industry.

The adsorption method, utilizing new PSMA-LiMnO beads in a column was found as a promising candidate for practical use in conventional separation of lithium from brines.

Keywords: Lithium separation, brines, N-alkyl formamide, lithium manganese oxides, organic metal oxide support

ÖZ

TUZLU SULARDAN LİTYUM AYRIŞTIRILMASI

Erdoğan, Barış

Doktora, Kimya Mühendisliği Bölümü

Tez Yöneticisi: Prof. Dr. H. Önder Özbelge

Ortak Tez Yöneticisi: Doç. Dr. Yusuf Uludağ

Şubat 2015, 184 sayfa

Lityum, otomotiv ve elektronik endüstrisi içerisinde uzun ömürlü, şarj edilebilir pillerde oldukça fazla kullanım alanı bulan değerli ve gelecek vaadeden bir metaldir. Dünya lityum rezervlerinin kısıtlı olması, lityum ayrıştırma ve saflaştırma işlemlerinde mümkün olan en verimli yöntemin kullanılmasını gerektirmektedir. Bu çalışmanın amacı, sentezlenen çeşitli malzemeler kullanılarak sıvı-sıvı özütlemesi ve adsorpsiyon yöntemleri ile lityum ayrıştırma işlemlerinin verimini artırmaktır.

Sıvı-sıvı özütlemesi yönteminde N-alkil formamitler (hekzil formamit, oktil formamit, dibutil formamit, dihekzil formamit) sentezlenmiş ve lityum ayrıştırma performansları hesaplanmıştır. Hekzil formamit, seyreltik LiCl çözeltileri için 25 °C'de 0.14 değeri ile literatürde tek bir çözücü için bahsedilen en yüksek dağılım katsayısını vermiştir.

Adsorpsiyon yönteminde, lityum mangan oksitler (LiMnO) katı-katı ve hidrotermal reaksiyon yöntemleri ile farklı sıcaklık ve Li/Mn mol oranlarında sentezlenmiştir. En yüksek kapasite değerini veren adsorbentin performansı farklı pH, lityum ve rakip iyon (Na, K, Mg) derişimlerinde karakterize edilmiştir. LiMnO adsorbentlerin kapasite değeri seyreltik lityum klorür çözeltileri için pH:10.2'de ve sodyum, potasyum, magnezyum gibi rakip iyonlar varlığında, lityuma karşı yüksek selektivite ile 22.8 mg Li/g olarak bulunmuştur.

Lityum mangan oksit parçacıkları poli(stiren-maleik anhidrit-glisidil metakrilat) (PSMA) içine emdirilerek mikron boyutundan milimetre boyutunda boncuklara çevrilmiş ve adsorpsiyon kolonunda kullanılmıştır. PSMA ilk defa bu çalışmada boncuk sentezinde kullanılmış, şişme ve kendi kendine çapraz bağlanma özellikleri ile önceki benzerlerinden üstün sonuçlar vermiştir. Yapay tuzlu su, Çamaltı konsantre deniz suyu ve Bigadiç bor kili özütü ile yapılan deneyler sonucunda PSMA-LiMnO boncukları ile doldurulmuş kolonun performansı ölçülmüştür. Tuzlu sular içerisinde bulunan lityum konsantrasyonu 0.43 ppm'den 1675.6 ppm'e kadar çıkartılmış ve rakip iyonların konsantrasyonu kayda değer biçimde düşürülmüştür. Kolon ürünü çözelti LiMnO ile direk muamele edildiğinde 3200 ppm Li derişimine ulaşılmıştır. Bu değer lityum pil endüstrisinde hammadde olarak kullanılan Li_2CO_3 üretimi için gerekli minimum konsantrasyon değerinin üzerindedir.

PSMA-LiMnO boncukları kullanılarak uygulanan adsorpsiyon tekniği, tuzlu sulardan endüstriyel lityum ayırıştırma yöntemleri arasına girmeye aday, umut vaadeden bir metot olarak değerlendirilmiştir.

Anahtar kelimeler: Lityum ayırıştırma, tuzlu sular, N-alkil formamit, lityum mangan oksit, organik metal oksit destek

To my grandmother

ACKNOWLEDGEMENTS

I wish to express my sincere gratitude to my supervisor Prof. Dr. H. Önder Özbelge for his support, guidance and help, in all the possible way, throughout my study. Without his encouragements and practical solutions to problems, I would not have achieved this work with success. I would also like to express my special thanks to my co-supervisor Assoc. Prof. Dr. Yusuf Uludağ for his helpful comments and suggestions. I also wish to thank to Prof. Dr. Niyazi Bıçak for his great leadership in synthesis reactions held on throughout the study.

I would like to especially thank to Bilal Bayram for his advices and contributions to see the whole picture during the study. I would also thank to Bilsen Aytekin for her cooperation during the laboratory studies.

Heartfelt thanks to my colleagues who helped me, opened my mind and shared the hard times, Emine Kayahan, Hasan Zerze, Saltuk Pirgaloğlu, Eda Açık, Merve Akkuş, Canan Yeniova, Özge Mercan, Sevler Gökçe Avcıoğlu.

I should like to acknowledge Faculty Members of Chemical Engineering Department during my studies at METU, Kerime Güney for her great help in AAS analysis, Turgut Aksakal in finding all possible chemicals and equipments located in the department, Ertuğrul Özdemir in building the vapor pressure measurement set-up, Yavuz Güngör in XRD measurements, Gülten Orakçı in GC and HPLC measurements, Gülüstan Görmez and Naciye Kaya for solving bureaucratic problems throughout the study.

I wish to thank to my parents, Nevin and Mustafa Erdoğan, my sister Nihan Erdoğan, and my uncle Raşit Ülkü for their love and encouragement. I would like to thank to my grandmother Nermin Ülkü for her great wisdom of life and endless love towards me.

And lastly, I would like to thank to my dear friends who are always besides me through the study, Şaziye, Uğur, Barış, Esen, Eylem, Ozan, Ceren, Soner, Bilgen, Başar, Burcu, Mert, Dominic, Iğın, Pelin, Burak, Şafak, Aslı, Ulaş Barış, Onur, Ufuk, Salih, Aytaç.

The financial support provided by TÜBİTAK through the projects 109M499 and 113M919 is gratefully acknowledged.

TABLE OF CONTENTS

ABSTRACT.....	v
ÖZ.....	vii
ACKNOWLEDGEMENTS.....	x
TABLE OF CONTENTS.....	xii
LIST OF TABLES.....	xv
LIST OF FIGURES.....	xix
LIST OF SYMBOLS.....	xxii

CHAPTERS

1 INTRODUCTION.....	1
1.1 The usage areas of lithium and its compounds.....	1
1.1.1 Ceramics and glass.....	2
1.1.2 Electrochemical applications.....	2
1.1.3 Lubricating oils.....	3
1.1.4 Ventilation systems and air conditions.....	3
1.1.5 Metallurgical use.....	3
1.1.6 Organometallic compounds.....	3
1.1.7 Nuclear reactors.....	3
1.1.8 Medicines.....	4
1.1.9 Hydrogen storage.....	4
1.2 Lithium Sources.....	4
1.2.1 Minerals.....	5
1.2.2 Clays.....	6
1.2.3 Brines.....	6
1.3 Conventional lithium separation process from minerals and clays.....	7
1.4 Conventional lithium separation processes from brines.....	8

1.4.1	Clayton Valley, Nevada	9
1.4.2	Salar de Atacama, Chile	11
1.4.3	Salar de Hombre Muerto, Argentina	13
1.4.4	Searles Lake, California	14
1.4.5	Lakes in Turkey.....	15
1.5	Literature survey on lithium separation methods from brines.....	15
1.5.1	Liquid-liquid extraction	16
1.5.2	Adsorption.....	18
2	EXPERIMENTAL METHODS	27
2.1	Materials	27
2.2	Synthesis and experimental procedures	27
2.2.1	Synthesis of N-alkyl formamides.....	27
2.2.2	Synthesis of lithium manganese oxide adsorbents.....	28
2.2.3	Synthesis of lithium manganese oxide precursors	30
2.2.4	Synthesis of poly (styrene-maleic anhydride-glycidyl methacrylate) (PSMA) [90]	30
2.2.5	Liquid-liquid extraction procedure	31
2.2.6	Polymer enhanced ultrafiltration procedure.....	31
2.2.7	Batch adsorption procedure	32
2.2.8	LiMnO bead preparation	33
2.2.9	Column experiment procedure	34
2.3	Equipment	35
2.3.1	Measurement of metal ion concentration in aqueous solutions	35
2.3.2	Measurement of organic content in aqueous solutions	36
2.3.3	Spectroscopic methods.....	36
2.3.4	Thermal analysis	36
2.3.5	Bead characterization	37
2.3.6	Physical properties of the synthesized formamide.....	37
3	RESULTS AND DISCUSSIONS.....	39
3.1	Synthesis and characterization of materials employed in lithium separation.....	39
3.1.1	Synthesis and characterization of N-alkyl formamides	39
3.1.2	Synthesis and characterization of lithium manganese oxide.....	44

3.1.3	Synthesis and characterization of lithium manganese oxide-polymer beads.....	64
3.1.4	Acquisition of lithium containing brines from nature.....	75
3.2	Liquid-liquid extraction by N-alkyl formamides	78
3.3	Adsorption via lithium manganese oxide adsorbents.....	87
3.3.1	Effect of pH on adsorption.....	87
3.3.2	Effect of initial lithium concentration on adsorption.....	88
3.3.3	Kinetics of the adsorption process	89
3.3.4	Equilibrium Isotherms	90
3.3.5	Stability experiments	93
3.3.6	Selectivity experiments.....	94
3.4	Separation of lithium by PSMA-LiMnO beads in an adsorption column...	95
3.4.1	The breakthrough plots for solutions containing lithium chloride only.....	95
3.4.2	The breakthrough plots for solutions containing foreign ions	102
3.4.3	The breakthrough plots for the artificial and real brine solutions.....	106
3.4.4	Recovery of lithium and regeneration of the beads	110
3.4.5	Separation of lithium by a post-treatment with LiMnO particles following column adsorption.....	125
4	CONCLUSIONS	129
	RECOMMENDATIONS	133
	REFERENCES	135
APPENDICES		
A.	ALTERNATIVE MATERIALS EMPLOYED IN LITHIUM SEPARATION.....	143
B.	XRD MEASUREMENTS OF SYNTHESIZED LITHIUM MANGANESE OXIDES.....	165
C.	SEM PHOTOGRAPHS OF SYNTHESIZED PSMA-LiMnO BEADS	173
D.	THE FEASIBILITY STUDY TO RECOVER LITHIUM CARBONATE FROM ÇAMALTI SALINA AND BORON CLAY EXTRACT.....	175
	CURRICULUM VITAE.....	183

LIST OF TABLES

TABLES

Table 1.1 Areas of usage and consumption ratios for lithium compounds.....	2
Table 1.2 Lithium production and reserves.....	5
Table 1.3 Commercially valuable lithium minerals.....	6
Table 1.4 Commercially important brines	7
Table 1.5 Clayton Valley, Brine Composition.....	9
Table 1.6 Salar de Atacama, Brine Composition.....	11
Table 1.7 Salar de Hombre Muerto, Brine Compositon	13
Table 1.8 Searles Lake, Brine Composition.....	14
Table 1.9 The compositon of lakes in Turkey.....	15
Table 1.10 Lithium chloride solubility in different alcohols	16
Table 1.11 The distribution coefficients of various solvents for lithium, sodium, potassium and calcium ions [21, p. 137].....	17
Table 3.1 Surface tension values for the N-alkyl formamides at 10 °C.....	42
Table 3.2 The densities of the N-alkyl formamides at different temperatures.....	43
Table 3.3 LiCl, NaCl and KCl solubilities in hexyl formamide	44
Table 3.4 Methods employed in synthesis of lithium manganese oxide adsorbents.	45
Table 3.5 Optimization plan constructed by applying factorial design for the upper and lower limits of four variables versus acquired adsorbent capacity (response)....	47
Table 3.6 Effect of oven temperature on capacity of adsorbents synthesized by Hydrothermal-1 procedure.....	48
Table 3.7 Effect of gel/water ratio on capacity of adsorbents synthesized by Hydrothermal-1 procedure.....	49
Table 3.8 Effect of Li/Mn ratio on capacity of adsorbents synthesized by Hydrothermal-1 procedure.....	49

Table 3.9 Effect of autoclave temperature on capacity of adsorbents synthesized by Hydrothermal-1 procedure.....	50
Table 3.10 Finding crystal system and lattice constant of LiMnO	63
Table 3.11 Different solvent-polymer couples utilized for LiMnO bead synthesis by precipitation method	65
Table 3.12 PSMA beads synthesized with different GMA content at 70 °C (Benzyl peroxide molar ratio:0.01, monomer/solvent ratio: 0.33)	67
Table 3.13 The amount of the components used in bead synthesis	71
Table 3.14 BET results of PSMA-LiMnO beads.....	75
Table 3.15 The composition of the concentrated brine in Çamaltı Salina.....	76
Table 3.16 Leaching of lithium ions from boron clay	77
Table 3.17 The composition of the clay extract taken from Bigadiç.....	77
Table 3.18 The effect of pH on distribution coefficient of LiCl for the formamides at 25 °C, 10 ml water/10 ml formamide ratio (The initial LiCl concentration was 1.4 M)	79
Table 3.19 The effect of temperature on distribution coefficient values for different formamides at pH:4, 10 ml water/10 ml formamide ratio, initial lithium concentration of 1.4 M Li.	79
Table 3.20 ΔH° and ΔS° values calculated from Van't Hoff plots	81
Table 3.21 Equilibrium data between extract and raffinate phase for the formamide-water-lithium chloride system at 25 °C, pH: 4 and 10 ml water/10 ml hexyl formamide.....	82
Table 3.22 Artificial concentrated seawater composition and the resulting distribution coefficient values in selectivity experiments.....	84
Table 3.23 The selectivity values of hexyl formamide for lithium near foreign (Na, K, Mg, Ca) ions in sea water.....	85
Table 3.24 Composition of the concentrated sea water taken from Çamaltı Salina and resulting distribution coefficients (25 °C, 10 ml HeFo/10 ml water, pH:7.4)	85
Table 3.25 The effect of pH on recovery of lithium from hexyl formamide.....	86
Table 3.26 The effect of pH on recovery of lithium from hexyl formamide (Second recovery)	86

Table 3.27 Capacity values of adsorbents at different pHs (Total volume: 100 ml, Adsorbent amount: 0.02 g).....	88
Table 3.28 Capacity value of the adsorbents at different initial lithium concentrations (pH:10.2 and adsorbent amount: 0.02 g).....	88
Table 3.29 The stability of lithium manganese oxide particles in lithium recovery..	93
Table 3.30 Selectivity of lithium manganese oxides with respect to Na, K and Mg.	94
Table 3.31 The column operating conditions for the pH dependency of adsorption process.....	96
Table 3.32 The column operating conditions for different initial lithium concentration in adsorption process	97
Table 3.33 The column operating conditions for different flow rates in adsorption process.....	99
Table 3.34 The column operating conditions for different bead sizes in adsorption process.....	101
Table 3.35 The column operating conditions for feed solutions containing NaCl ..	102
Table 3.36 The column operating conditions for feed solutions containing KCl	104
Table 3.37 The column operating conditions for feed solutions containing MgCl .	105
Table 3.38 The column operating conditions for artificial brine solutions.....	106
Table 3.39 The column operating conditions for concentrated brine solution taken from Çamaltı Salina	108
Table 3.40 The column operating conditions for boron clay extract taken form Bigadiç	109
Table 3.41 The initial and final concentrations in the feed tank before and after the operation.....	109
Table 3.42 Elution process data of the column after Run 3.	111
Table 3.43 The elution of the column saturated with artificial brine solution and swept by tap water.....	114
Table 3.44 The comparison of the artificial brine and elution solution composition after sweeping by tap water.....	114
Table 3.45 The second adsorption-sweeping-elution process composition with the feed solution having concentration of elution process in Run 18	115

Table 3.46 The elution of the column saturated with artificial brine solution and swept by acidic water at pH 6.1.	116
Table 3.47 The comparison of the artificial brine and elution solution composition after sweeping by acidic solution (pH 6.1)	117
Table 3.48 The second adsorption-sweeping(at pH:6.1)-elution process composition with the feed solution having concentration of elution process in Run 26.....	117
Table 3.49 The elution of the column saturated with concentrated brine solution and swept by demineralized water.....	118
Table 3.50 The comparison of the real concentrated brine and elution solution composition after sweeping by deionized water	119
Table 3.51 The elution of the column saturated with concentrated brine solution and swept by acidic water at pH 6.1.	120
Table 3.52 The comparison of the real concentrated brine and elution solution composition after sweeping by acidic water at pH 6.1	120
Table 3.53 The elution of the column saturated with clay extract and swept by tap water.....	122
Table 3.54 The comparison of the boron clay extract and elution solution composition after sweeping with tap water	123
Table 3.55 The elution of the column saturated with clay extract and swept by acidic water at pH 6.1	123
Table 3.56 The comparison of the boron clay extract and elution solution composition after sweeping with acidic water.....	124
Table 3.57 The initial and final concentrations of the adsorption process done with column effluent.....	125
Table 3.58 The amount of eluted ions and concentrations in elution process of post-treatment	126
Table 3.59 Li concentration, Li/foreign ion ratio, Li loss in each separation step starting from artificial brine	127
Table 3.60 Li concentration, Li/foreign ion ratio, Li loss in each separation step starting from clay extract	128

LIST OF FIGURES

FIGURES

Figure 1.1 The process scheme of Clayton Valley	10
Figure 1.2 Production scheme of LiCO_3 in Salar de Atacama.....	12
Figure 1.3 Lithium insertion/extraction mechanisms (a) Lithium extraction (b) Lithium insertion O: redox side; □: ion exchange side	21
Figure 1.4 Breakthrough curve for 150 days operation	23
Figure 2.1 Continuous ultrafiltration set-up [92]	32
Figure 2.2 Scheme of the set-up for column experiments	34
Figure 2.3 Photos of the set-up for column experiments	35
Figure 2.4 Vapor pressure measurement set-up	37
Figure 3.1 Synthesis pathway of N-alkyl formamides.....	40
Figure 3.2 Temperature dependence of viscosity for N-alkyl formamides	42
Figure 3.3 Temperature-vapor pressure relation for hexyl formamide.....	43
Figure 3.4 Hydrothermal-1 procedure in ten steps.....	46
Figure 3.5 Heating curve for MnO and LiOHH_2O reaction system	52
Figure 3.6 Heating curve for MnO_2 and LiOHH_2O reaction system.....	52
Figure 3.7 Heating curve for MnCO_3 and LiOHH_2O reaction system	53
Figure 3.8 Heating curve for Mn_3O_4 and LiOHH_2O reaction system.....	54
Figure 3.9 FTIR spectrum of spinel lithium manganese oxide synthesized by MnCO_3 and LiOHH_2O (Li/Mn: 1/1) F30, before (LMO) and after (HMO) acid leaching	55
Figure 3.10 FTIR spectrum of spinel lithium manganese oxide synthesized by MnCO_3 and LiOHH_2O (Li/Mn: 1/0.8 mole ratio) F31, before (LMO) and after (HMO) acid leaching.....	56
Figure 3.11 FTIR spectrum of spinel lithium manganese oxide synthesized via MnCO_3 and LiOHH_2O (Li/Mn: 0.8/1 mole ratio) F32, before (LMO) and after (HMO) acid leaching.....	57

Figure 3.12 FTIR spectra for three different adsorbents (after acid leaching) having different Li/Mn molar ratios(F30-Li/Mn:1, F31-Li/Mn:1/0.8, F32-Li/Mn:0.8).....	58
Figure 3.13 Effect of acid leaching process on lattice proton at different times for adsorbents synthesized by Hydrothermal-1 procedure	59
Figure 3.14 The adsorbents synthesized with three different methods.....	59
Figure 3.15 XRD spectrum of the spinel lithium manganese oxide LMO (450 °C, Li/Mn=1).....	61
Figure 3.16 XRD spectrum of the spinel lithium manganese oxide HMO (450 °C, Li/Mn=1).....	61
Figure 3.17 Structure of poly maleic anhydride-styrene-glycidyl methacrlate (PSMA)	67
Figure 3.18 FTIR spectra of poly (styrene-maleic anhydrid-glycidyl methacrylate) terpolymer (PSMA)	69
Figure 3.19 ¹³ C-NMR spectra of PSMA.....	70
Figure 3.20 SEM photographs for Bead T16.....	72
Figure 3.21 SEM photographs for Bead T16 after acid leaching	72
Figure 3.22 SEM photographs for Bead T18.....	73
Figure 3.23 SEM photographs for Bead T21	73
Figure 3.24 SEM photographs for Bead T22.....	74
Figure 3.25 Van't Hoff Plots for hexyl formamide (a), octyl formamide (b), dibutyl formamide (c).....	80
Figure 3.26 Effect of initial LiCl concentration on k of hexyl formamide at pH:4. The plots were drawn for three different water/formamide volume ratios (1:1, 1:2, 1:3) at 10 °C.	81
Figure 3.27 The lithium concentration in extract (formamide) and raffinate (water) phases at 25 °C and pH:4 for 10 ml water/10 ml hexyl formamide.....	83
Figure 3.28 The kinetics of adsorption process	89
Figure 3.29 The equilibrium concentration of lithium in solution vs uptake of lithium ions.....	90
Figure 3.30 Langmuir isotherm curve for LiMnO at 25 °C.....	91
Figure 3.31 Freundlich isotherm curve for LiMnO at 25 °C.	92
Figure 3.32 The breakthrough curves at different pH values	96

Figure 3.33 The breakthrough curves at different initial lithium concentrations.	98
Figure 3.34 The breakthrough curves at different flow rates.	100
Figure 3.35 The breakthrough curves for different bead sizes.	101
Figure 3.36 The breakthrough curve for sodium chloride feed solution	103
Figure 3.37 The breakthrough curve for potassium chloride feed solution	104
Figure 3.38 The breakthrough curve for magnesium chloride feed solution.	105
Figure 3.39 The effluent lithium concentration in a column fed with artificially prepared brine solution.	107
Figure 3.40 The effluent lithium concentration in a column fed with concentrated brine solution from Çamaltı Salina	108
Figure 3.41 The elution curve after Run 3	110
Figure 3.42 The change of ion concentrations in sweeping process applied after Run 12.	112
Figure 3.43 The molar ratio of potassium and magnesium with respect to lithium during sweeping process	113
Figure 3.44 The change of ion concentrations in sweeping process applied after Run 14.	121

LIST OF SYMBOLS

Calcite	Calcium carbonate
Gypsum	Calcium sulfate dihydrate
Sylvinite	NaCl and KCl mixture
Glaserite	Potassium sulfate
Soda ash	Sodium carbonate
PEUF	Polymer enhanced ultrafiltration
ΔH°	Standard enthalpy change
ΔS°	Standard entropy change
R_g	Universal gas constant
T	Absolute temperature
k	Distribution coefficient
HeFo	Hexyl formamide
OcFo	Octyl formamide
DbFo	Dibutyl formamide
DhFo	Dihexyl formamide
EMK	Ethyl methyl ketone
AAS	Atomic Absorbance Spectrophotometer
CF	Cross Flow
UF	Ultrafiltration
LiMnO	Lithium manganese oxide adsorbent
GMA	Glycidyl methacrylate
AIBN	Azobisisobutyronitrile
NMP	N-methyl pyrrolidone
PSMA	Poly (styrene-maleic anhydride-glycidyl methacrylate)
FTIR	Fourier Transform Infrared Spectroscopy

NMR	Nuclear Magnetic Resonance
TGA	Thermogravimetric Analysis
DTA	Differential Thermal Analysis
SEM	Scanning Electron Microscopy
BET	Brunauer–Emmett–Teller
LMO	Lithium manganese oxides before acid leaching
HMO	Lithium manganese oxides after acid leaching
CTAB	Cetyl tert butyl ammonium bromide
PolyMMA-co-BA	Polymethyl methacrylate-co-butyl acrylate
PET	polyethylene terephthalate
PE	Polyethylene
PS	Polystyrene
PS-Br	Brominated poly styrene
THF	Tetrahydrofuran
DMF	Dimethylformamide
DMSO	Dimethyl sulfoxide
PVC	Polyvinylchloride
S	Selectivity
C_e	Lithium concentration in solution at equilibrium
Q_e	Uptake amount of lithium at equilibrium (mg/g)
K_{ads}	Empirical equilibrium constant (L/mg)
Q_m	Theoretical maximum adsorption capacity (mg/g)
MWCO	Molecular weight cut-off
F_p	Flux of permeate
C_f	Feed concentration
C_p	Permeate concentration
R	Retention
PES	Poly ether sulfone
C-PEG	Comb like poly ethylene glycol
TLC	Thin Liquid Chromatography

CHAPTER 1

INTRODUCTION

Lithium is one of the most valuable and promising metals having extensive potential use especially in design of new generation battery systems. The four main reasons that make lithium metal attractive as a battery anode material are its light weight, high voltage, high electrochemical equivalence, and good conductivity [1]. Demand to this chemical is expected to grow in the future due to its application in long lasting rechargeable batteries in automotive and electronics industry.

1.1 The usage areas of lithium and its compounds

The lithium consumption in the world first stepped up by the demand of US Atom Energy Commission (AEC) in 1950 till 1960s. In the following years as the technology level in the world evolved, new application areas for lithium emerge and showed great variety from batteries to medicines today [2]. The areas of usage and consumption ratios are given in Table 1.1 [3].

Table 1.1 Areas of usage and consumption ratios for lithium compounds

Area of usage	Consumption ratio (%)
Ceramics and glass	31
Batteries	23
Lubricating oils	10
Ventilation systems and air conditions	5
Production of aluminum	3
Other	28

Areas of usage for lithium and its compounds can be grouped into nine sections in detail.

1.1.1 Ceramics and glass

Small ionic radius resulting in a high ionic charge makes lithium a superb flux material in production of ceramics. Lithium tetraborate is a good example of this kind, it fastens the clay and glaze formations in the production of glass [4].

1.1.2 Electrochemical applications

The battery technology was based on cadmium and nickel until 1990's. After that lithium based batteries got in charge with their superior performance resulting from their higher energy/weight ratio (energy density). Besides, lithium-ion batteries do not have memory effect, and a slow loss of charge when not in use [5]–[7]. The electronic devices spread away to all over the world, and energy requirements of concerned developed technologies get increasing. One of the most important electronic devices are hybrid or electrical cars which are presented as the vehicles of the future recently. This increasing demand on energy will inevitably bring a very important role to the lithium metal in the future [8].

1.1.3 Lubricating oils

Lithium is used in oils as a cation within the structure of the surfactants. Lithium containing oils have lower freezing points, improved viscosity, surface tension and water compatibility [9].

1.1.4 Ventilation systems and air conditions

The concentrated aqueous solution of lithium bromide has low vapor pressure so that it can be used in the air conditioning systems. Lithium bromide solutions can be replaced with chlorofluorocarbon which is a harmful compound to the environment [10].

1.1.5 Metallurgical use

Lithium forms alloys with numerous metals. Lead and aluminum alloys are the most important ones. Lead alloys are used for bearings of railroad cars. Aluminum alloys have been used in structural components of aircraft since 1957. Low weight and high stability make the aluminum-lithium alloys unique for aircraft manufacturers [11].

1.1.6 Organometallic compounds

The production of organometallic compounds is one of the major usage areas of lithium metal such as n-butyl lithium [12]. These compounds are formed by the reaction of dispersions of lithium metal with organic halogens. N-butyllithium is also used as an initiator in polymer synthesis [13] and widely used in agriculture and pharmaceutical chemical synthesis [14].

1.1.7 Nuclear reactors

Lithium-6 is used as a source material in production of tritium which is a fuel in fusion reactors [15]. Also it is utilized as an absorbent material for neutrons [16]. Besides, the low density, high heat capacity and high latent heat of evaporation makes lithium one of the best cooling materials in nuclear reactors [17]. As the

nuclear technology evolves with the fusion reactors, the importance of lithium metal will increase.

1.1.8 Medicines

Lithium compounds have been used in medicines since 1900's. It is used in treatment of bipolar disorder and for related diagnoses, such as schizoaffective and cyclic major depression. The healing mechanism of the lithium ion in the body cannot be understood completely [18].

1.1.9 Hydrogen storage

Hydrogen was stored in the form of lithium hydrate in World War 2. Lithium hydrate can be reacted by seawater easily and it gives hydrogen gas as a product. In the literature Ichikawa et al utilized lithium amide and lithium hydride in 1:1 ratio and found a new promising material for the storage of hydrogen. These materials absorb or desorb the hydrogen gas depending on the medium temperature [19]. In another study, Xiong et al. produced a new material by using lithium and sodium aminoborates which was published in "Nature Materials" [20]. These new generation materials are promising in storage of hydrogen gas in future.

1.2 Lithium Sources

In nature, lithium cannot be found in pure form, rather it is found in complex form most of the time with aluminum and silicates. The lithium reserves on earth crust are found at low concentrations; between 7 and 60 ppm [21]. The lithium reserves and production amount of lithium compounds in 2012 and 2013, for different countries are given in Table 1.2 [22]–[24].

Table 1.2 Lithium production and reserves

Country	Mine production (tons)		Amount of reserve (tons)
	2012	2013	
United States	*	*	38,000
Argentina	2,700	3,000	850,000
Australia	12,800	13,000	1,000,000
Brazil	150	150	46,000
Canada	690	480	180,000
Chile	13,200	13,500	7,500,000
China	4,500	4,000	3,500,000
Portugal	560	570	60,000
Zimbabwe	1,060	1,100	23,000
World (Total)	35,000	35,000	13,000,000

* *Commercial secret*

Identified lithium resources for Bolivia is 9 million tons and it is not processable due to lack of infrastructure.

Lithium and its compounds were mainly produced conventionally from three sources as, minerals, clays and brines. Spent lithium ion batteries (LIB) can also be considered as secondary resources of lithium, yet there is not an industrial production of lithium from LIB contemporarily.

1.2.1 Minerals

Geologists state that 145 of minerals on earth contain some amount of lithium ($\% > 0.002 \text{ Li}_2\text{O}$) and 25 of these minerals contain significant amount of lithium ($\% > 2 \text{ Li}_2\text{O}$). Minerals which are commercially valuable in the production of lithium are listed in Table 1.3 [25]–[28].

Table 1.3 Commercially valuable lithium minerals

Minerals	Formula	Lithium content (%)
Spodumene	$\text{LiAlSi}_2\text{O}_6$ or $\text{Li}_2\text{OAl}_2\text{O}_3\cdot 4\text{SiO}_2$	3.73
Lepidolite	$\text{LiKAl}_2\text{F}_2\text{Si}_3\text{O}_9$ or $\text{LiFKFAl}_2\text{O}_3\cdot 3\text{SiO}_2$	3.56
Amblygonite	LiAlFPO_4 or $2\text{LiFAl}_2\text{O}_3\cdot \text{P}_2\text{O}_5$	4.74
Triphylite	LiFePO_4 or $\text{Li}_2\text{O} \cdot 2\text{FeOP}_2\text{O}_5$	4.40
Petalite	$\text{LiAlSi}_4\text{O}_{10}$ or $\text{Li}_2\text{OAl}_2\text{O}_3\cdot 8\text{SiO}_2$	2.27
Bikitaite	$\text{LiAlSi}_2\text{O}_6\cdot \text{H}_2\text{O}$	3.28
Eucryptite	LiAlSiO_4	5.53
Zabuyelite	Li_2CO_3	18.75

The biggest lithium mineral producers were Sons of Gwalia (Australia) with 150,000 tons, Bikita (Zimbabwe) with 55,000 tons, and Tanco (Canada) with 21,000 tons in 2002 [29].

1.2.2 Clays

Clays are fine-grained rocks that consist of mostly metal oxides and silicates. Hectorite is one of the famous clays which is rich in lithium and magnesium having 0.3 to 0.6 % Li [21]. The by-product of boron mine in Bigadiç-Balıkesir in Turkey can be considered as a rich lithium clay which has 0.3 % Li.

1.2.3 Brines

Besides minerals, brines are another important lithium sources. The concentration of lithium in brines is lower than minerals but the total amount of lithium in brines makes up to 66 % of the world lithium resources. The brines with a commercial importance in production of lithium are listed in Table 1.4 [21].

Table 1.4 Commercially important brines

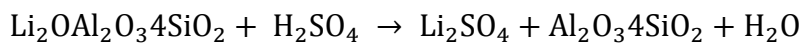
Country	Brine	Li conc (ppm)
Chile	Salar de Atamaca	1500
China	Zabuye Lake	970
Argentina	Salar de Hombre Muerto	600
USA	Clayton Valley	450
-	Seawater	0.17

1.3 Conventional lithium separation process from minerals and clays

Spodumene which is an igneous rock is used chiefly for lithium production among the commercial lithium minerals. Approximately 250 kg of spodumene is required to produce 1 kg of lithium.

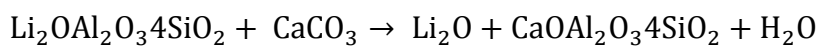
Minerals are treated by two major methods which are acid, alkaline processes. There is also chlorination process used barely.

In acid process, minerals are roasted with sulfuric acid at 250-400 °C to dissociate silicate structure. Spodumene must be first converted from α - phase to β - phase at 1100 °C before treatment with sulfuric acid. The general reaction scheme is shown below [30]:



Finally, lithium carbonate is acquired by the addition of soda ash after the required evaporation and pH adjustment steps.

In alkaline process, spodumene is calcined via limestone at 825-1050 °C. The resulting product is mixed with water to have lithium hydroxide and further treated with hydrochloric acid to have lithium chloride. The reaction scheme is shown below [31];



In chlorination process, which is not widely used, the mineral is roasted with chlorine gas or hydrochloric acid at 880-1100 °C and lithium chloride is produced as a final product [32].

1.4 Conventional lithium separation processes from brines

There are five important brines in which lithium is produced commercially in all over the world. These sources can be listed as; Clayton Valley (Nevada), Salton Sea (California), Searless Lake (California) in North America and Salar da Atacama (Chile), Salar de Hombre Muerto (Argentina) in South America. Among these lithium sources Salar de Atacama has the highest lithium production with two plants; SQM and Chemetall (Rockwood Lithium) [33], [34]. The plant on Humbre Muerto was partly closed in 1999 due to the price reduction of SQM. Olarez Salina which is placed near Humbre Muerto currently takes investment by Orocobre, which is the largest lithium resource developer in Argentina [35]. Among those plants, Simbol Materials which is on Salton Sea in California is the newest one and it has started its production in September 2011 [36]. Although Bolivia has the largest lithium reserves in brines with 9 million tons capacity, there is no production of lithium due to lack of infrastructure in high hills where those resources are located [37]. China also declared to produce lithium from the high lakes in Tibet like Zabuye Lake and continues its research on the field since 2002 [38].

Due to the dilute concentration of lithium in even the most favorable brine, solar evaporation of the brine to further concentrate it has been a necessary first step in all of the world's current lithium brine production. After the evaporation of excess water in large pools, suitable precipitation agents are employed and unwanted salts are separated. Thereafter, lithium is acquired in desired purity. Currently all the conventional processes utilize evaporation and precipitation techniques. The other techniques like ion-exchange, adsorption or membrane separation does not take place in the processes. On the other hand, it is known that POSCO which is located in South Korea will start production of lithium from seawater by 2015 [39]. Due to

the extremely dilute concentration of lithium in sea water, it is supposed that Koreans will employ an additional technique like adsorption or ion exchange in addition to evaporation and precipitation. POSCO claims that the production time for lithium carbonate will be reduced to 8 hours from 12 months which also implies the utilization of additional processes other than evaporation and precipitation [40].

Lithium production processes in four different brines were described and listed below.

1.4.1 Clayton Valley, Nevada

Production of lithium from this deposit was initiated in 1966 by Foote Chemicals. The plant changed hands to Chemetall in 1998 and now has a capacity of 6400 tons of lithium carbonate per year. The valley has a 400 ppm lithium concentration initially but after years of operation its lithium concentration now reduced to 160 ppm. The concentration of lithium and other major ions in Clayton Valley is listed in Table 1.5.

Table 1.5 Clayton Valley, Brine Composition

Ion	Concentration (ppm)	Concentration (ppm)
	1966 [41]	1998 [42]
Na	7.5	4.69
K	1	0.4
Li	400	163
Mg	600	190
Ca	500	450
Cl	11.7	7.26
CO ₃	-	74
B	-	67
Br	-	23

In Clayton Valley, lithium production starts with the evaporation of water in large ponds. In the first four ponds, brine gets concentrated while some amount of calcite (calcium carbonate) and gypsum (calcium sulphate dihydrate) precipitates. After 10

months of evaporation period, slaked lime (calcium hydroxide) is added to the brine, so that gypsum and magnesium hydroxide is precipitated (magnesium concentration in brine reduces to 2-3 ppm). Meanwhile the brine becomes basic and calcium starts to precipitate by absorption of carbon dioxide near sylvinite (NaCl, KCl salt). Sylvinite is sent to a different plant for the recovery of potassium. Afterwards, glaserite ($K_3Na[SO_4]_2$), potassium chloride, and remaining gypsum and calcite precipitates in the last three ponds, then the final brine containing 5000 ppm lithium is sent to lithium carbonate plant [21, p. 101]. In this plant, concentrated brine is first treated with slaked lime so that the whole remaining magnesium and some part of remaining sulfate and borate ions are separated. Next, calcium in the brine coming from lime is withdrawn by adding small amount of soda ash (sodium carbonate) to the mixture which is followed by heating the brine to 93 °C and adding stoichiometric amount of soda ash to precipitate lithium carbonate as a final product. During this process some excess amount of water is added to the brine in order to prevent the precipitation of other salts. The final product is accepted to be in industrial grade due to its 400 ppm boron content. The whole lithium production scheme in Clayton Valley is shown in Figure 1.1.

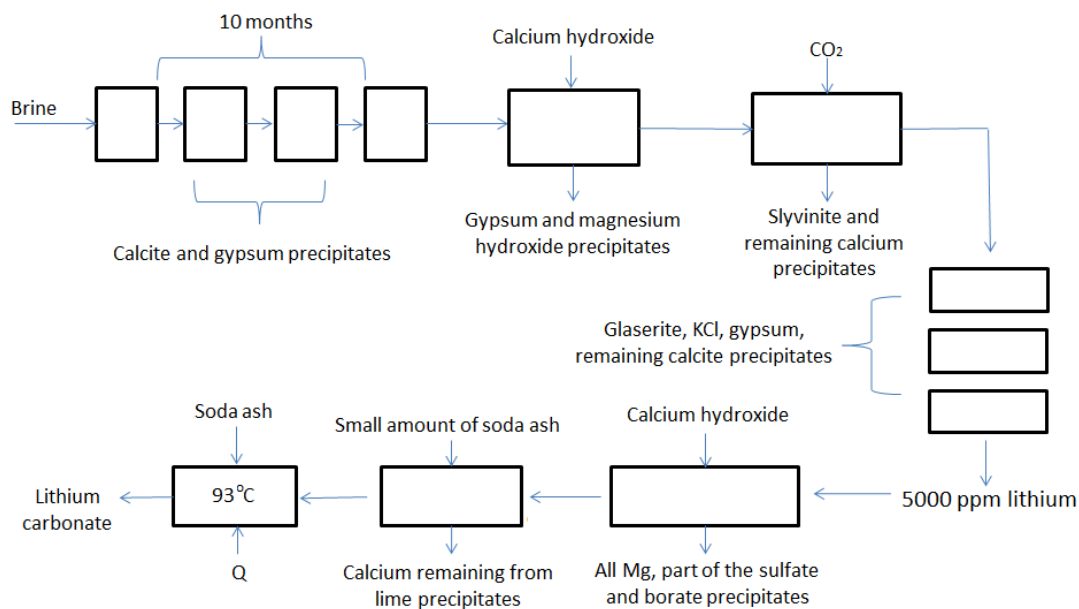


Figure 1.1 The process scheme of Clayton Valley

1.4.2 Salar de Atacama, Chile

The most suitable conditions such as high lithium concentration and high evaporation regimes for the production of lithium from brines are present in this playa. Salar de Atacama, a few Andean Salars and the Tibetan region of China are the only places in the world where the humidity is low enough to allow bischoffite ($\text{MgCl}_2 \cdot 6\text{H}_2\text{O}$) and lithium salts to be crystallized in solar ponds on a commercial scale. The prosperous conditions of the lake attracted many investors to the playa, so that two different plants, SQM and Chemetall were built on this district. The salt concentration in Salar de Atacama is shown in Table 1.6 [43, p. 483].

Table 1.6 Salar de Atacama, Brine Composition

Ion	Na	K	Mg	Li	Ca	B	HCO₃
Concentration (ppm)	91000	23600	9650	1570	450	440	230

The general process scheme that shows the production of lithium compounds from Salar de Atacama is shown in Figure 1.2 [44].

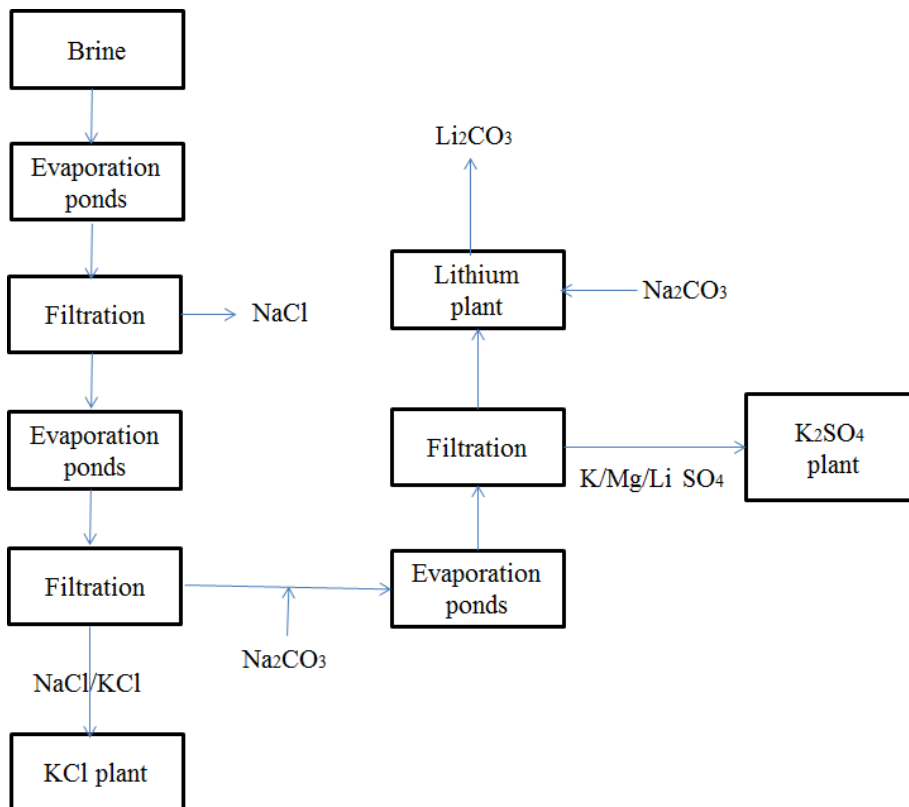


Figure 1.2 Production scheme of LiCO_3 in Salar de Atacama

1.4.2.1 Chemetall (Rockwood Lithium)

The process in Chemetall starts with the evaporation of water in large ponds and precipitation of sodium chloride in first pond, following by calcium chloride addition and precipitation of sylvinite, carnalite ($\text{KCl} \cdot \text{MgCl}_2 \cdot 6\text{H}_2\text{O}$), bischoffite and lithium carnalite ($\text{LiCl} \cdot \text{MgCl}_2 \cdot 6\text{H}_2\text{O}$) [45]. The brine which is concentrated up to 4-6 % lithium concentration in ponds, contains also 8000 ppm boron is sent to boron extraction column. In this operation, boron is treated with alcohol-kerosene mixture whose pH is adjusted to 2 by HCl solution. By this way the concentration of boron ions in brine is reduced below 5 ppm in expense of losing 5-10 % lithium. After that operation, lime is added to the solution so that magnesium and sulfate ions are separated. Finally by the addition of soda ash and heating, lithium carbonate is obtained [46].

1.4.2.2 SQM

SQM differs from other plants in terms of their production of by products like potassium nitrate, sylvinit and other salts which bring them an economical advantage near competitors. Like other plants, SQM lithium carbonate production process starts in ponds with evaporation of water. In ponds, sodium chloride settles down first following by potassium and sulfate salts which are sent to potassium sulfate and boric acid plants. Sylvinit which settles down in following ponds is sent to potassium nitrate plant. At that step in the process, brine lithium concentration reaches up to 1 % and sent to ponds again to reach 6 % lithium. Meanwhile, magnesium concentration reaches 1.8 % and boron concentration reaches 0.8 % approximately. After that, the concentrated brine is sent to lithium carbonate plant and similar to Chemetall after removal of boron, lime is added to the brine and magnesium, sulfate ions are separated. In the last step lithium carbonate is precipitated by the addition of soda ash and heating the brine [21, p. 122].

The production capacity of SQM is around 18000 tons of lithium carbonate per year. After they break into market in 1988, the lithium prices lowered by half and this reduced price considerably stimulated the lithium market and cause most of the lithium producers from ores (which are relatively high-cost producers) close their plants.

1.4.3 Salar de Hombre Muerto, Argentina

Lithium production from this brine was initiated by FMC in 1997. The composition of lithium and other major ions in the lake is listed in Table 1.7 [43].

Table 1.7 Salar de Hombre Muerto, Brine Compositon

Ion	Na	K	Ca	Mg	Li	B
Concentration (ppm)	15	76	210	72	2.1	7.8

Different from other lithium production methods, adsorption of lithium by alumina was firstly utilized in this plant. The recovery of lithium starts with evaporation of

water by sunlight in large ponds similar to other plants until the concentration of lithium reaches up to 600 ppm. Then the brine is sent to polycrystal alumina column and lithium is captured by alumina particles. After that, the column is washed with water and 1 % lithium chloride solution is acquired in column effluent which could then be concentrated in solar ponds to the desired concentration for further processing with lime and soda ash to produce lithium carbonate. The eluted column would next be given a saturated sodium chloride wash to recover the entrained lithium and to raise the ionic concentration in the alumina [47]. In preparing alumina adsorbents to employ in lithium adsorption columns, lithium chloride is reacted with alumina in saturated sodium chloride solution and forms $\text{LiCl}/\text{Al}(\text{OH})_3$ crystals in which lithium chloride is present in amounts up to a 0.2 mole fraction. The alumina adsorbent has a strong affinity for the lithium in high ionic solutions; oppositely the lithium can be eluted in dilute solutions [21, p. 131].

FMC announced that, the process they have with alumina adsorbents has 20 % better efficiency than other conventional solar evaporation, magnesium and sulfate precipitation processes. However after SQM break into lithium market, the decreasing prices of lithium carbonate result in partly closed plant and an agreement to purchase lithium carbonate from SQM [21, p. 132].

1.4.4 Searles Lake, California

Searles Lake is operated by American Potas and Chemical Co. The brine composition is given in Table 1.8 [42].

Table 1.8 Searles Lake, Brine Composition

Ion	Na	K	Ca	Mg	Li	B
Concentration (ppm)	118400	15700	16	-	60	4120

The brine in Searles Lake is evaporated in triple-effect evaporators. In these evaporators, the tanks are at different pressures and the vapor boiled off in one tank can be used to heat the next, and only the first tank (at the highest pressure) requires

an external source of heat. During the evaporation process, sodium chloride, burkeite ($3\text{Na}_2\text{SO}_4 \cdot \text{Na}_2\text{CO}_3$) and dilithium sodium phosphate (licons) are crystallized. Licons are then converted to phosphoric acid and lithium carbonate by a reaction. In this reaction, licons are firstly baked in an oven and organic residues are cleaned, then licons are reacted with sulfuric acid at 115 °C and splitted into phosphoric acid and lithium, sodium sulfates. Lastly, sulfates react with soda ash and lithium carbonate is obtained [21, p. 134] .

1.4.5 Lakes in Turkey

There is no commercial production of lithium compounds in Turkey. Tuz Lake has the highest lithium composition with 325 ppm but high magnesium content in the lake blocks the production of lithium. The composition of ions in some of the lakes in Turkey is listed in Table 1.9 [48].

Table 1.9 The compositon of lakes in Turkey

Lake	Lithium	Magnesium	Potassium	Sodium
Acı Lake	16	4108	1000	46000
Burdur Lake	3	970	46	5550
Tersakan Lake	34	6300	2000	23500
Boluk Lake	36	8800	2000	50000
Tuz Lake	325	37500	12000	61000

1.5 Literature survey on lithium separation methods from brines

Lithium is currently produced by evaporation and precipitation processes from brines conventionally. However the high concentration of the foreign ions in brines with lithium, force the researchers to develop an additional method to be integrated in conventional processes. Liquid-liquid extraction and adsorption methods have been the most investigated methods cited in the literature so far.

1.5.1 Liquid-liquid extraction

In this method, lithium in water is extracted by a proper solvent into another phase. The solvability power of the utilized solvents towards lithium and foreign ions like sodium, potassium and magnesium determine the performance of the extraction process. In literature, it is seen that various organic solvents are studied in the extraction of lithium from brines. Most commonly, organic alcohols were studied and their performance was found to be the best among other solvents [49], [50]. The solvability power of these alcohols generally increases with the decrease in the carbon number of the alkyl chains. At the same time, selectivity of those alcohols towards lithium ion decreases correspondingly. In 1966, Hermann reported that, lithium, sodium and potassium chlorides and carbonates were dissolved in long alcohols containing 3-8 carbons. For n-butanol the solubility of lithium is 10.57 grams LiCl per 100 grams of n-butanol [51]. The solubility of lithium chloride in various alcohols and tetrahydrofuran (THF) reported in different studies are tabulated in Table 1.10 [21, p. 136].

Table 1.10 Lithium chloride solubility in different alcohols

Solvent	Lithium chloride solubility (g LiCl/g solvent)
N-butanol	10.6
Isopropyl alcohol	12.0
Propanol	16.2
Isobutanol	7.3
Pentanol	8.1
2-ethyl heksanol	9.0
Alyl alcohol	4.4
Tetrahydrofuran	4.6

The lithium concentration in sea water is almost constant at 0.173 mg/L (0.173 ppm). The lithium concentration is very low but the total quantity occurring in sea water is tremendous and estimated to be 2.4×10^{11} tons. The limited lithium content on earth brings attention to this huge source in sea water. The low concentration of lithium in sea water makes the pretreatment process inevitable. In the pretreatment process, concentration of lithium is increased from 0.17 ppm to 30 ppm [52] by solar

energy. Than with a suitable solvent, lithium is extracted from aqueous phase to an organic phase and finally by evaporating solvent or precipitation of lithium with a proper anion would achieve the separation. The drawback of this process is the high concentration of foreign ions in sea water which are magnesium (1290 ppm), sodium (10770), potassium (380 ppm) and calcium (410 ppm) [53]. Another drawback is the low distribution coefficient of the extraction solvents utilized in the process, which makes the 5-10 evaporation and condensation cycles unavoidable. The solvents utilized in extraction processes and their distribution coefficients towards lithium, sodium, potassium and calcium ions are given in Table 1.11.

Table 1.11 The distribution coefficients of various solvents for lithium, sodium, potassium and calcium ions [21, p. 137]

Solvent	Distribution coefficient				Separation factor		
	k_{Li}	k_{Na}	k_K	k_{Ca}	S_{Na}^{Li}	S_K^{Li}	S_{Ca}^{Li}
n- butanol	0.058	0.023	0.020	0.017	2.5	2.9	3.4
Sec-butanol	0.044	0.022	0.021	0.020	2.0	2.09	2.1
Isobutanol	0.018	0.009	0.009	0.005	2.0	2.00	3.6
Pentanol	0.011	0.008	0.005	0.006	1.38	2.20	1.8
Isopentanol	0.01	0.006	0.007	0.005	1.66	1.43	2.0
2-ethylhexanol	0.001	0.007	0.004	0.006	0.57	1.00	0.7
2-ethylisohexanol	0.005	0.006	0.005	0.006	0.83	1.00	0.8
Octanol	0.005	0.007	0.006	0.006	0.71	0.83	0.8
2,4-Dimethyl-3-pentanol	0.006	0.007	0.008	0.014	0.86	0.75	0.4
o-Chlorophenol	0.018	0.0056	0.0020	0.013	3.21	0.90	1.4
p-Chlorophenol	0.0119	0.0049	0.01	0.012	2.43	1.19	1.0
o-Cresol	0.045	0.019	0.03	0.006	2.36	1.50	7.5
m-Cresol	0.007	0.014	0.013	0.0008	0.50	0.53	8.8
p-Cresol	0.011	0.01	0.006	0.0012	1.0	1.83	9.2
Cresol	0.008	0.019	0.0049	0.009	0.42	1.63	0.9
Molar sol. Of phenol/benzene	0.011	0.003	0.005	0.011	3.67	2.20	1.0
p-sec-Butylphenol/benzene	0.005	0.017	0.0013	0.009	0.29	3.85	0.6
p-1,1,3,3-Tetramethyl-(butyl)phenol/benzene	0.002	0.003	0.007	0.003	0.67	0.29	0.7

Table 1.11 (continued)

p-tert- Butylphenol/benzene	0.012	0.0089	0.008	0.012	1.35	1.50	1.0
--------------------------------	-------	--------	-------	-------	------	------	-----

1.5.2 Adsorption

Separation of lithium via adsorption method is the most convenient technique to be integrated in conventional lithium production processes which are evaporation and precipitation. However, there is no industrial application of adsorption method contemporarily. In this method, simply lithium ions are separated selectively from aqueous solutions through physical or chemical adsorption. Research on adsorbents focuses mostly on alumina and manganese oxide up to now.

The usage of alumina was first investigated by Goodenough in 1960 [54]. According to this study, when aluminum chloride or aluminum hydroxide mixed with neutral or basic water, it combines with lithium ions and precipitates in the form of a gel as aluminium hydroxide. After that, lithium was separated from alumina by various solvents and purified. The patents written by the followers of Goodenough claimed that brines including high concentration of calcium and magnesium showed the optimum separation values at 81 °C and pH value of 6.8 [55]. The separation factors and optimum values change with brine source and physical conditions, also in these studies separation of lithium from the precipitated gel was done by high temperature water.

In Salton Sea, lithium was separated via alumina adsorbents and 99 % of lithium was recovered from the brine but the process was found to be too expensive. The alumina adsorption was investigated by many scientists with different brines. In 1986, Rothbaum et al. studied the lithium recovery from waste water of a geothermal energy plant by alumina in order to minimize the effect of lithium content on the environment [56]. According to the study, after the separation of silica from water, sodium aluminate was added to the water and at pH equals to 10, gelation occurs. After that, the gel was washed with 60 °C water and the remaining gel was recovered by washing it with sodium hydroxide solution. Unfortunately the purity of the

resultant lithium product was low. In the studies on geothermal water in France and England, lithium separation was explored by aluminium chloride and most of the lithium was gathered from water but the resultant product could not be acquired in desired purity [57].

Alumina adsorption to separate lithium was also studied with sea water [52]. According to the study, 50 % mixture of magnesium hydroxide and aluminum hydroxide was added to the brine and after the gel was formed, it was washed with 0.05 M HCl solution and lithium concentration was increased nearly seven fold. At the end, approximately 40 % of lithium could be recovered from sea water. In another study, brine in Dead Sea was concentrated from 30 ppm to 680 ppm by aluminum chloride in 1978 [58], however to adjust the pH of brine, 73 tons of lime stone was used for each ton of brine and to wash the precipitated gel, 19000 tons of water and 92 tons of HCl was used. In 1981, Epstein et al carried a research and used isoamyl alcohol to dissolve the gel [59]. After that, they extracted lithium from alcohol by water, but the final product still contains 1.2 % Ca, 0.4 % Mg and large amount of alcohol was lost in the process. Ryabtsev et al. investigated the structure of the precipitated gel and they stated that the gel has a chemical formula with $\text{LiCl} \cdot 2\text{Al}(\text{OH})_3 \cdot m\text{H}_2\text{O}$ and a layered structure [60]. They noted that gel was formed in a layered structure which resulted in a molecular-sieve effect that could only be penetrated by lithium. They further stated that, up to 40 % of the lithium in this compound could be released by a water wash, and then be replaced (the adsorption reaction) by contact with a lithium-containing strong brine. During the preparation of the adsorbent, equimolar amount of LiCl and AlCl_3 was used and the capacity was turned out to be 7 mg Li/g adsorbent. This capacity reduces to 5-6 mg Li when PVC was used as a binder. In the study, the capacity loss of the adsorbent after each use and the final lithium product purity were not mentioned.

In another study conducted in 2007, the effect of pH and mixing time on the efficiency of alumina adsorption was investigated at 25 °C by response surface methodology (RSM). In this study, alumina gel was dissolved in n-hexanol, 2-ethyl hexanol and methyl-iso-butyl acetone to separate lithium chloride [61]. The optimum

values were found as Al/Li mol ratio: 4.7, pH: 7.2 and 3 hours of mixing time with a 95 % of lithium retention capacity.

By the increase in usage of lithium ion battery technology, the research on finding a more efficient anode material was also increased. For this reason lots of different metal oxides (Zr, Ti, Sb, Cs, Rb, Ni, Mg, Na, Al, Co, Fe, V, Sn Mn) were synthesized and investigated [62]–[70]. These metal oxides were also recognized as adsorbents to be employed in lithium separation processes and most of them were studied in terms of their separation efficiency. After it was realized that metal oxides which include manganese give better separation factor among other adsorbents, the research on this subject focused on manganese including adsorbents. The first article about the subject was published by Shen in 1986 [71], where it was investigated the mechanism of lithium insertion/extraction on manganese oxides and found out that the insertion/extraction mechanism of lithium ions towards manganese adsorbent occurs tapotactically which does not disrupt the crystal structure. After that, in another study carried by Ooi et al., the crystal system of the lithium manganese oxide was shown to be spinel, besides it was said that, manganese has +3 and +4 oxidation states in closed cubic packed (ccp) oxygen system [72]. In the continuation study of the same group, lithium addition and extraction mechanism was described in three ways as redox type, specific ion-exchange and non-specific ion exchange. The synthesis conditions determine which type dominates [73]. In another study again by Ooi et al., the researchers showed that, adsorbents synthesized below 500 °C works with redox type and adsorbents synthesized above 500 °C works with ion exchange mechanism. In their conclusion they also stated that, lithium extraction/insertion mechanism mostly happens to be with ion-exchange mechanism. In Figure 1.3, the mechanisms of ion-exchange and redox were shown [74].

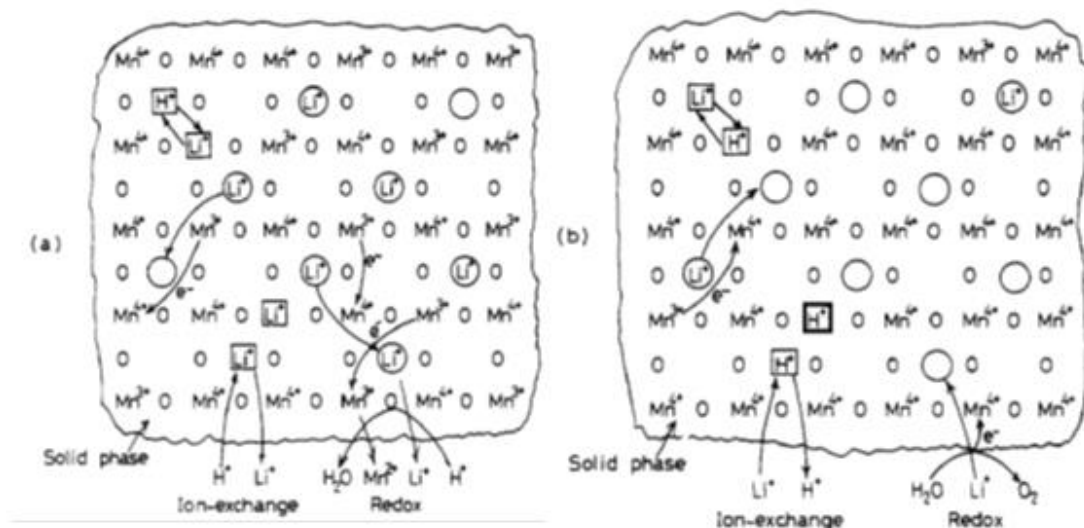


Figure 1.3 Lithium insertion/extraction mechanisms (a) Lithium extraction (b) Lithium insertion O: redox side; □: ion exchange side

Manganese oxide is known to adsorb most of the metals onto its surface, even it is known that the heavy metal balance in oceans are controlled by the manganese oxide nodules in water [75]. In literature, there are many articles about synthesis of LiMnO_2 adsorbents. In these articles, synthesis studies were conducted with different precursors, temperatures and molar ratios of Li/Mn. The gathered performance values investigated under different pH values, temperature and initial lithium concentrations in feed solution. In the studies of Ooi et al where the adsorption mechanism of LiMn_2O_4 described, the adsorbents were synthesized by solid-solid reaction [72]–[74] in 1989-1992. In these syntheses, MnOOH and MnCO_3 were utilized as manganese source while LiCO_3 was utilized as lithium source. Reaction takes place at temperatures between 400-800 °C, for 4 hours. Li/Mn mol ratio was adjusted to 0.2, 0.5 and 0.8. The resultant product was mixed with 0.5 M HCl for two days and lithium ions were exchanged with hydrogen ions. After that adsorbents were dried in oven at 70 °C and put into LiOH solution to investigate the exchange mechanism between hydrogen and lithium ions. In 1995, Feng and Ooi investigated the synthesis of LiMn_2O_4 and NaMn_2O_4 with a hydrothermal method [76]. In this method, NaOH or LiOH was mixed with $\gamma\text{-MnO}_2$ in a desired mol ratio and put into an autoclave where the reaction takes place at 170 °C. After 24 hours synthesis time, the product was washed with water and left for drying at room temperature for 3 days. After the synthesis, it was observed that, lithium manganese oxide was in

spinel type and sodium manganese oxide was in birnessite type. In the same study, the selectivity of the adsorbents towards lithium ions with foreign ions like sodium, potassium and magnesium was investigated. The selectivity order of the ions can be listed as $\text{Li}^+ < \text{Na}^+ < \text{Cs} = \text{K}$ for sodium manganese oxide and $\text{Na}^+ < \text{Li}^+ < \text{K}^+ < \text{Rb}^+ < \text{Cs}^+$ for lithium manganese oxide at pH=4, which means actually low selectivity for lithium. Roziere and Burns made a similar study in 1995 but synthesized the adsorbents with three different reactant groups as lithium carbonate-manganese carbonate, lithium nitrate- γ -manganese oxide and lithium nitrate- β -manganese oxide in solid-solid medium [77]. They fixed the molar ratio of Li/Mn as 0.8 and oven temperature as 400 °C. The synthesized adsorbents were then mixed with 0.2 M HCl solution for 48 hours and dried in an oven at 60 °C. The lithium extraction ability of the resultant product was measured by 0.1 M LiCl solution but only the mechanisms were reported, no capacity value was noted. In 2001, Chitrakar et al. published an article, and claimed that they found the highest lithium adsorption capacity with their lithium manganese adsorbent as 40 mg Li/g adsorbent [70]. There are some other studies which has an adsorbent capacity near 40 mg, however they used concentrated lithium chloride solutions. The selectivity of the synthesized adsorbent has a formula of $\text{Li}_{1.6}\text{Mn}_{1.6}\text{O}_4$ with a high selectivity to lithium and decreasing selectivity in order with $\text{Na}^+ > \text{K}^+ > \text{Mg}^{2+} > \text{Ca}^{2+}$. In Chitrakar's adsorbent synthesis procedure γ - MnOOH and LiOH were autoclaved at 120 °C for 1 day. LiMn_2O_4 was taken as a product and dried at 60 °C. After that it was placed into an oven operating at 400 °C for 4 h, $\text{Li}_{1.6}\text{Mn}_{1.6}\text{O}_4$ was taken as an intermediate final product. Thereafter, 1.5 g of $\text{Li}_{1.6}\text{Mn}_{1.6}\text{O}_4$ was mixed with 2 L 0.5 M HCl solution and $\text{H}_{1.6}\text{Mn}_{1.6}\text{O}_4$ was taken as a final product. The same synthesis also described for reflux method with same procedure except that the reaction took place for 8 hours. Adsorbents which are synthesized by using an autoclave gave slightly higher capacity values than the adsorbents synthesized by reflux method.

Another important study about lithium manganese adsorbents were conducted by Yoshizuka et al. [78]. In their first paper which was published in 2002, they made the synthesis of the adsorbents by using Mn_3O_4 and LiOH as reactants. Li/Mn ratio was adjusted to 0.5 and the synthesis was done in two steps, one of which was at 425 °C, 5 h and the other was 500 °C, 5 h in electrical oven. The resulting product was

cooled in oven slowly for 12 h and after that mixed with 1 M HCl to form HMn_2O_4 . Adsorbent capacity was found as 10.5 mg Li/g adsorbent approximately and it was observed that as pH of the initial lithium chloride solution increases, the capacity value also increases. In another study by the same group [79], the adsorbent capacity was increased by changing the Mn/Li ratio to 1.5 and keeping the other variables constant during the synthesis. In the following study in 2006, the researchers investigate the application of the adsorbents in recovery of lithium from sea water by designing an adsorption column operating at 200 L/h [80]. After the column was filled with 60 kg of lithium manganese oxide, it was fed with 140 m^3 of sea water in 30 days. Finally, the column was washed with HCl solution and after drying, 151.7 g of precipitated salt was acquired. This salt has a composition of 10.35 % LiCl, 38.3 % NaCl, 0.89 % KCl, 36.9 % CaCl_2 and 5.3 % MnCl_2 . In another run in the same column for 150 days, the final composition was found as 33.3 % LiCl, 20.4 % NaCl, 3.3 % KCl, 8.2 % MgCl_2 , 13.4 % CaCl_2 and 19.4 % MnCl_2 . The breakthrough curve gathered from the column was reported as in Figure 1.4 [80].

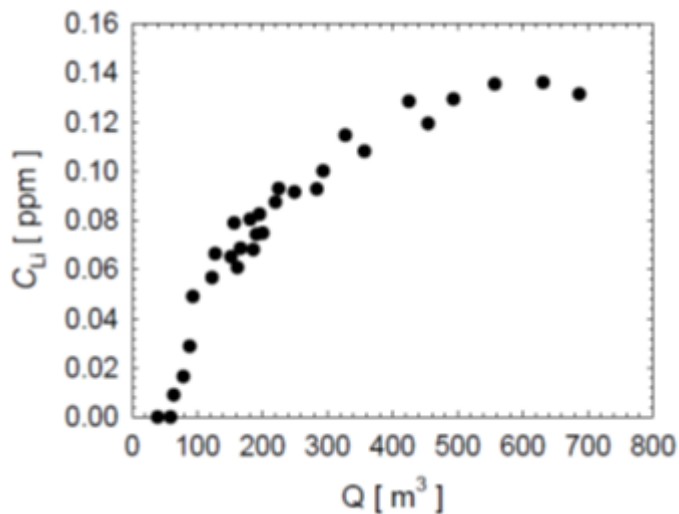


Figure 1.4 Breakthrough curve for 150 days operation

Yoshizuka et al. published their last study on lithium adsorption in 2011. In this article, they integrated additional ion exchangers on lithium chloride separation process in order to purify lithium chloride more and get rid of foreign ions like sodium and magnesium [81]. The process started with feeding sea water into the adsorption column, filled with lithium manganese oxide. Then column was eluted

with HCl solution to extract lithium. Afterwards, the elution solution with 160 ppm lithium concentration was fed to DIAION SK110 ion exchanger to separate Mg, Ca, Sr and Mn. After that, the brine was fed to an ion exchange column filled with 1-phenyl-1,3-tetradecanedione to separate manganese and magnesium further and finally reach 900 ppm Li concentration. Afterwards the water was evaporated and by addition of ammonium carbonate, lithium carbonate was precipitated. The final product acquired has a purity of 99.9 % and the total process had an efficiency value of 56 %.

Kima et al. investigated the structure of lithium manganese oxide in 2003 and tried to impregnate Ti and Fe into the structure [64]. In this study, solid-solid reaction system was chosen and lithium carbonate was used as a lithium source while manganese carbonate was used as a manganese source. For iron and titanium resource, FeOOH and TiO₂ were employed. In this article no separation experiments were done but the crystal systems of the resulting products were described and selectivity of the new adsorbents were discussed.

In 2006, Wang et al. studied the parameters affecting the capacity of the lithium manganese oxide adsorbents synthesized by solid-solid method. They analyze the effect of Li/Mn ratio, heating time, heating temperature, precursors, leaching conditions etc. [82]. They used manganese carbonate as single manganese source, lithium carbonate and lithium hydroxide as lithium sources. In their conclusion, it was stated that, LiOH and MnCO₃ pair gave highest capacity values and as Li/Mn ratio increases lithium adsorption capacity of the adsorbents increase also. It was found out that when LiOH and MnCO₃ were used and Li/Mn ratio was adjusted to 1, adsorbents worked most efficiently and give 23 mg/g capacity value.

Wang et al. published another article in 2008 and they synthesized the adsorbents with MnCl₂, LiOH and H₂O₂ by hydrothermal process [83]. They performed the adsorption experiments under constant pH by using an ammonium chloride-ammonia buffer and investigated the effect of ionic strength and temperature on capacity. It was found out that ionic strength decreases the efficiency of the adsorption process, which was explained by the formation of an ionic layer on adsorption surface that increases the diffusion resistance of lithium ions into the

adsorbent particle. In their study, they also measured the values of ΔH , ΔG and ΔS during adsorption and they found out that the lithium adsorption process is endothermic which means increasing capacity with the increase in temperature. In another aspect, they explained the increase in capacity by temperature in terms of requirement of heat during exchange. The exchange of $\text{Li}^+ - \text{H}^+$ need first the bond breaking of O–H and also the sorption of Li^+ or the insertion of Li^+ for a diffusion process, which was an endothermic process; i.e., the rise of temperature favors adsorbate to transport within the pores of the adsorbent.

Wang et al. published another article in 2009 and discussed the effect of pH on the capacity of adsorbents [84]. They found out that, as pH increases from 8 to 12 the capacity value increases from 8 mg/g to 35 mg/g.

Insertion of alternative metals into lithium manganese oxide spinels was another subject studied by the researchers. For instance, Ma et al. investigated the insertion of antimony and used Sb_2O_3 as reactant with MnO_2 and repeat the synthesis experiments under different temperature and mole ratios [63]. They found out that adsorbents having a molar ratio of $\text{Sb}/\text{Mn}=0.05$ and $\text{Li}/(\text{Sb}+\text{Mn})=0.5$ synthesized at $800\text{ }^\circ\text{C}$ gave 20 % better capacity values with respect to ordinary lithium manganese oxide. In another study which tries to impregnate Mg onto adsorbent structure, it was found that Mg tends to stabilize the crystal structure of the adsorbent [85]. In this work, $\text{MnCl}_2 \cdot 4\text{H}_2\text{O}$, $\text{Mg}(\text{NO}_3)_2 \cdot 6\text{H}_2\text{O}$ LiOH ve H_2O_2 were employed as reactants.

Lithium manganese oxide synthesis was also done with ultrasonic pyrolysis method by Özgür et al in 2010 by using lithium nitrate and manganese nitrate as reactants [86]. The surface area of the resultant adsorbents were similar to adsorbents synthesized with ordinary solid-solid reaction but the morphology of the adsorbents were found smoother. The total capacity of the adsorbents decrease a little but the kinetics of the adsorption get increased so that the adsorption equilibrium was reached in less time with respect to ordinary synthesized adsorbents.

CHAPTER 2

EXPERIMENTAL METHODS

2.1 Materials

The chemicals used throughout the study were reagent grade chemicals that were purchased from Sigma Aldrich or Merck, unless otherwise stated. N-alkyl formamides, lithium manganese oxides, beads used in adsorption experiments and functional polymers were synthesized and characterized in this study.

2.2 Synthesis and experimental procedures

2.2.1 Synthesis of N-alkyl formamides

The formamides were synthesized by action of dry formic acid on primary and secondary amines with appropriate alkyl groups. In a typical procedure, one mole of the amine compound was placed in a conical flask equipped with a pressure equalized dropping funnel. The flask was mounted in an ice bath on a magnetic stirrer. While stirring vigorously, one mole of formic acid (57.5 g of 85 % solution) was added drop wise via the dropping funnel. An ammonium formate salt was formed as white precipitate or waxy product. Soon after the formic acid addition, the flask was transferred into silicon oil bath and attached to a Dean-Stark trap and a

reflux condenser. To the flask, there was added 60 mL toluene to remove water azeotropically. The temperature of the oil bath was maintained at 140 °C. In all cases the water evolution was completed (1.0 mol) within 45-50 min in these conditions. After removal of toluene the residual liquid was distilled under vacuum. The products so obtained were optically clear.

2.2.2 Synthesis of lithium manganese oxide adsorbents

2.2.2.1 Solid-solid-1 [79]

5 g (0.022 mol) Mn_3O_4 and 0.792 g (0.033 mol) LiOH was mixed and grounded for 15 min in a ceramic crucible (setting Mn/Li=2). Then the mixture was sintered at 425 °C for 5 h in oven and cooled at room temperature for 1.5 h. Then, the blend was mixed and grounded again for 15 min. After that, it was sintered at 500 °C for 5 h in oven and cooled for 12 h in the oven. Spinel type $LiMn_2O_4$ was acquired.

2.2.2.2 Solid-Solid-2 [73], [74], [87]

Mn source ($MnCO_3$, MnO , MnO_2) and $LiOH.H_2O$ were weighed and put into ceramic crucibles according to the molar ratio of Li/Mn and grounded for 15 minutes. The crucibles were placed into oven which was already adjusted to a desired temperature (450 or 550 °C) and kept there for 6 hours. After that, the crucibles were removed from oven and cooled at room temperature in a dessicator.

2.2.2.3 Hydrothermal-1 [83]

4.8 g of LiOH was dissolved in 100 ml of water and 2 M LiOH solution was prepared. 3.96 g of $MnCl_2.4H_2O$ was dissolved in sufficient amount of water separately. 40 ml of 2 M LiOH solution was added dropwise into $MnCl_2$ solution with vigorous magnetic stirring (means, 0.02 mol $MnCl_2.4H_2O$ was mixed with 0.08 mol of LiOH). The color of the solution turns yellow and brown during addition. Half an hour later, 5 ml of 30 % H_2O_2 solution was added into above solution

dropwise and stirred for 2 h. A black gel was formed and aged for 1 day (The color of the solution turned to black from brown). The gel was transferred into a teflon lined stainless steel vessel and deionized water was added until 70-80 % of the vessel was reached. The vessel was placed into oven at 120 °C for 24 h. The precipitate was filtered and washed with 1 L of deionized water and dried at 60 °C for minimum 6 hours. The obtained product was placed into 350 °C oven for 5 h and cooled in room temperature. A leaching solution of 0.5 M HCl acid was prepared and 0.5 g of cooled product was mixed with 250 ml of leaching solution in batch shaker for 24 hour. Than the solution was filtered under vacuum and washed with 500 ml pure water. The acid solution can be analyzed for its lithium content. The precipitate was dried at 60 °C for minimum 6 hours.

2.2.2.4 Hydrothermal-2 [70]

4.8 g of LiOH was dissolved in 100 ml of water and 2 M LiOH solution was prepared. 1 g of γ -MnOOH was mixed with 40 ml of 2 M LiOH solution (means 0.0115 mol MnOOH was mixed with 0.08 mol of LiOH) in a teflon lined stainless steel vessel and autoclaved at 120 °C for 1 day. The precipitate was filtered and washed with 500 ml of deionized water and dried at 60 °C. The obtained product (LiMnO₂) was ready for use after kept in oven at 400 °C for 4 h.

2.2.2.5 Hydrothermal-3 [88]

Equimolar (0.7-1.5) amounts of H₂O₂ and LiOH were dissolved in sufficient amount of water in different beakers and mixed. Menawhile, 0.4 mol Mn(NO₃)₂ was dissolved in a teflon lined stainless steel autoclave and LiOH-H₂O₂ solution was dripped into it. After the solution was maintained at room temperature for 2 h, the autoclave was sealed and heated to 70-180 °C for 8 hours. The resulted black solid products were filtered and washed with plenty of water (1 L), then dried at 70 °C for 12 hours.

2.2.3 Synthesis of lithium manganese oxide precursors

2.2.3.1 MnCO₃ synthesis procedure [89]

16.9 g of manganese (II) sulfate-1-hydrate (0.1 mole) and 10.56 g of ammonium carbonate (0.11 mole) were dissolved in sufficient amount of water in separate beakers. Ammonium carbonate solution was added in small lots to the hot manganese sulfate solution (60-70 °C). The progress of the reaction could be observed by the precipitation of manganese carbonate and release of carbon dioxide bubbles. The manganese carbonate precipitate, which was flesh in color, was allowed to precipitate and washed with plenty of water several times by a decantation until the supernatant solution gives no further test for sulfate.

2.2.3.2 Mn₃O₄ synthesis procedure [89]

Manganese carbonate was taken to an oven at 80 °C for 4 hours. After that, the dried precipitate was transferred to a ceramic china dish and put into high temperature oven. The temperature of the oven was raised to 400 °C in steps of 100 °C, the decomposition of manganese carbonate was observed due to change in color to black. The material was taken out and cooled in dessicator to room temperature, then taken again in furnace and heated to 940 °C in steps of 100 °C. The product (Mn₃O₄) was kept in 940 °C for 1 hour, (the color of the material turns to brown in this step) taken out and cooled in desiccator.

2.2.4 Synthesis of poly (styrene-maleic anhydride-glycidyl methacrylate) (PSMA) [90]

0.1 mol (9.806 g) maleic anhydride, 0.1 mol (10.415 g) styrene, 0.038 mol (5.42 g) glycidyl methacrylate and 0.00238 mol (0.577 g) benzoyl peroxide were dissolved in 51.3 g ethyl methyl ketone (EMK) in a balloon flask and put into a constant temperature bath on a temperature controlled-heater magnetic stirrer. The reaction continued for 4 hours at 70 °C. The resulting mixture was precipitated in cold diethyl

ether. The white product was taken to an oven in dry atmosphere and dried at 40 °C under vacuum for 12 hours.

2.2.5 Liquid-liquid extraction procedure

The method used in the extraction experiments was as follows [91]; 10 ml formamide and 10 ml water phases were weighed into a separation funnel directly for the measurements in room temperature or weighed into an erlenmeyer for the higher temperature experiments. Erlenmeyers were then placed into a constant temperature oil bath. After thermal equilibrium was reached, the samples were mixed vigorously at constant temperature for several minutes (3-5 minutes), until the equilibrium was reached. Then the samples in the erlenmeyers were taken into the separation funnels which also kept at constant temperature by using a drying oven.

The mixing time of the samples can change according to the viscosities, densities and the interfacial tension between two phases. After phase separation was established, the water phase (raffinate) and formamide phase (extract) were taken into separate glass containers (formamides are strong solvents and they can solve the plastic containers). Then, the raffinate was analyzed by atomic absorption spectrophotometer to determine lithium concentration and by total nitrogen analyzer to determine the formamide concentration.

2.2.6 Polymer enhanced ultrafiltration procedure

Desired amount of polymer was dissolved in less than 1 L pure water in a 1 L volumetric flask. Known concentration of lithium chloride was then added to the polymer solution to obtain a final desired concentration of lithium chloride in 1 L. After that, the pH of the solution was adjusted by adding droplets of concentrated (3 M) ammonium hydroxide or hydrochloric acid solution. The solution was mixed by a magnet for at least 1.5 hours. Then pH was again adjusted if needed. After that, the solution was taken to a 1 L erlenmeyer and ultra-filtered continuously, in other words returning the retentate and permeate back to the feed solution in order to keep the feed concentration constant. Ultrafiltration pressure difference was 200kPa and

temperature was kept constant at 25 °C. Samples were taken from both the feed solution and the permeate stream at different time intervals for lithium analysis in AAS and for polymer analysis in total organic carbon analyzer.

Polymer purification and fractionation was carried out in batch ultrafilter (Amicon-Millipore Model 8050). Ultrafiltration experiments were conducted in continuous ultrafiltration set-up which is shown in Figure 2.1. The set-up mainly consists of Osmonics Sepa CF Membrane Cell (7), UF membrane (8), pressure gauge (9), pH meter (3), pH probe (2), feed tank (1), feed pump (4), rotameter (6) and pressurized air (11).

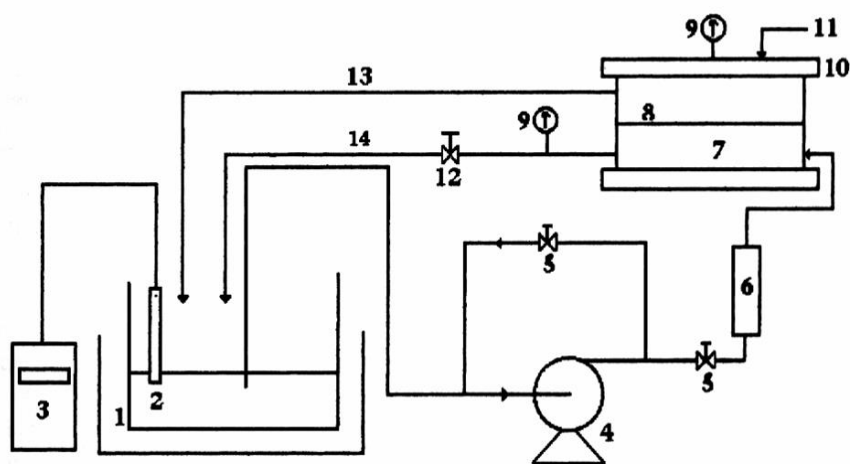


Figure 2.1 Continuous ultrafiltration set-up [92]

2.2.7 Batch adsorption procedure

Batch adsorption experiments were carried in a 250 ml flask at room temperature. 100 ml lithium chloride solution was added to 0.05 g of adsorbent (LiMnO) and mixed in a batch shaker at room temperature (25 °C). The pH of the mixture was adjusted to a desired value by 1 M ammonia and 1 M hydrochloric acid solutions. In order to attain equilibrium, shaking time was adjusted to 24 h. After mixing, the supernatant was taken and measured for ion content in AAS.

Leaching experiments were carried out by a leaching solution of 0.5 M HCl with a certain amount of product in a 250 ml erlenmeyer for 24 hour at room temperature, than the supernatant was taken for desired ion analysis in AAS.

2.2.8 LiMnO bead preparation

In LiMnO bead preparation, two methods were employed, which were suspension polymerization technique and precipitation technique

- Suspension polymerization technique

First organic and aqueous phases were prepared separately. Organic phase consists of 0.57 g glycidyl methacrylate (GMA), 1.4 g methyl methacrylate, 0.4 g ethylene glycol dimethacrylate and 0.03 g azobisisobutyronitrile (AIBN) and 2.37 ml toluene. In aqueous phase, 0.57 g sodium sulfate, 0.08 g polyvinyl pyrrolidone were dissolved in 28.4 g of water. Lithium manganese oxide particles were added to organic phase and formed a slurry. After aqueous phase reached to 65 °C in a constant temperature bath by a temperature controlled heater, the organic slurry was dripped onto aqueous phase slowly. The organic drops split into individual droplets in aqueous phase and the process was completed in 4 hours.

- Precipitation technique

In precipitation technique, 3 grams of poly (styrene-maleic anhydride-glycidyl methacrylate) (PSMA) was mixed with 1.5 g N-methyl pyrrolidone (NMP) and 1 g of LiMnO. LiMnO was added in excess amount into the mixture to be sure that NMP-PSMA solution was saturated with LiMnO content. Tap water was put into another 1 L beaker and few drops of cetyl tert butyl ammonium bromide was added. The slurry was dripped into 1 L beaker by a 5 ml volume dropper while the water was mixing with a magnet on a magnetic stirrer. After dripping process, newly formed beads continued to be mixed by the stirrer for 24 hours. Then the beads were filtered by an ordinary filter paper, washed with plenty of deionized water and dried in room temperature for 24 h.

2.2.9 Column experiment procedure

Certain amount of salt (LiCl, NaCl, KCl or $\text{MgCl}_2 \cdot 6\text{H}_2\text{O}$) was dissolved in 5 L volumetric flask to have desired final ion concentration. The solution was taken to a 10 L plastic bottle and fed to an adsorption column from the bottom. The feed solution was prepared regularly until the end of the experiment. The column has 20 mm diameter and 60 cm long which is made of borosilicate glass. It has two glass filters at the bottom and top ends in order to hold the bead content in column. The outlet of the column was sent to another 10 L plastic bottle. The flow was derived by a peristaltic pump and the flow rate was adjusted by the valve below the column and measured by a stop-watch and a 50 ml graduated cylinder. In every data point, pH measurements were done and the samples were taken to AAS for concentration measurement.

The experimental set-up was as shown in Figure 2.2 and Figure 2.3.

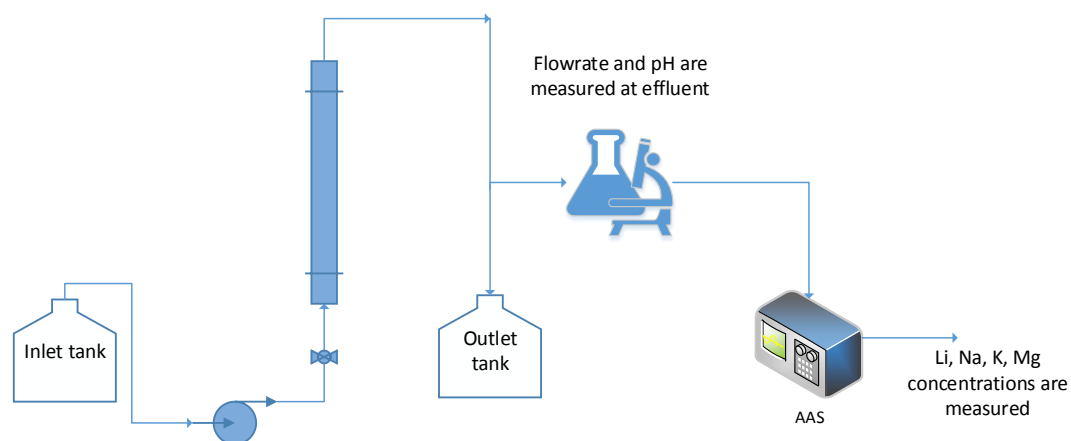


Figure 2.2 Scheme of the set-up for column experiments



Figure 2.3 Photos of the set-up for column experiments

The area under breakthrough curve was calculated with numerical integration by Trapezoidal Rule. The capacity of the beads were found by subtracting the area from the total amount of lithium fed to the column.

2.3 Equipment

2.3.1 Measurement of metal ion concentration in aqueous solutions

Lithium, sodium, potassium, magnesium and calcium contents in aqueous solutions were measured by the aid of Shimadzu Atomic Absorbance Spectrophotometer using acetylene as a fuel. Lithium, sodium and potassium ions were measured by emission technique while others were measured by absorbance using specialized lamps.

Each individual metal ion concentration was measured by first constructing a calibration curve with metal ion solutions at known concentrations.

2.3.2 Measurement of organic content in aqueous solutions

Analysis of formamide content in water in liquid-liquid extraction experiments was done by measuring the total nitrogen content by Total Nitrogen Analyzer Shimadzu TNM-1. The nitrogen content in formamides were used to calculate the total formamide content in water.

The polymer content in permeate in PEUF experiments was checked by Total Organic Carbon Analyzer. The carbon content in permeate was directly related with the polymer content which shows the filtration performance of the PEUF set-up.

2.3.3 Spectroscopic methods

The structure of the synthesized materials throughout the study were identified by Fourier Transform Infrared Spectroscopy (FTIR) using Shimadzu IR Prestige-21 FTIR spectrophotometer with a Pike Miracle ATR apparatus (KBr was used for a reference) and Nuclear Magnetic Resonance Spectroscopy using 400 MHz of Bruker NMR Spectrophotometer using CDCl_3 as solvent with Ultrashield Superconducting magnet.

The crystal structure of lithium manganese oxides were identified by using Rigaku Ultima-IV X-Ray diffractometer that generates a voltage of 40 kV and current 40 mA from Cu $K\alpha$ radiation source ($\lambda = 1.5418 \text{ \AA}$). The diffraction angle 2θ was scanned from 10° to 60° with scanning rate of $1^\circ/\text{min}$ and a step size of 0.01° .

2.3.4 Thermal analysis

The synthesis mechanism of lithium manganese oxides were identified by Thermogravimetric Analysis (TGA) and Differential Thermal Analysis (DTA) which performed simultaneously in air at a heating rate of $10 \text{ }^\circ\text{C min}^{-1}$ in alumina crucibles.

2.3.5 Bead characterization

The characterization of the beads was done by Scanning Electron Microscopy (SEM) and Brunauer–Emmett–Teller (BET) analysis. Surface area and pore size distribution measurements were done by Quantachrome Corporation Autosorb-6B, under nitrogen atmosphere at $-197\text{ }^{\circ}\text{C}$ and 1×10^{-5} - 1.0 atm. The micron sized photos of the beads were taken in SEM by QUANTA 400F Field Emission SEM machine after coating the particles with Au-Pd.

2.3.6 Physical properties of the synthesized formamide

2.3.6.1 Temperature-vapor pressure measurements

In order to measure the vapor pressure of hexyl formamide with respect to changes in temperature, an experimental set-up shown in Figure 2.4 was established.

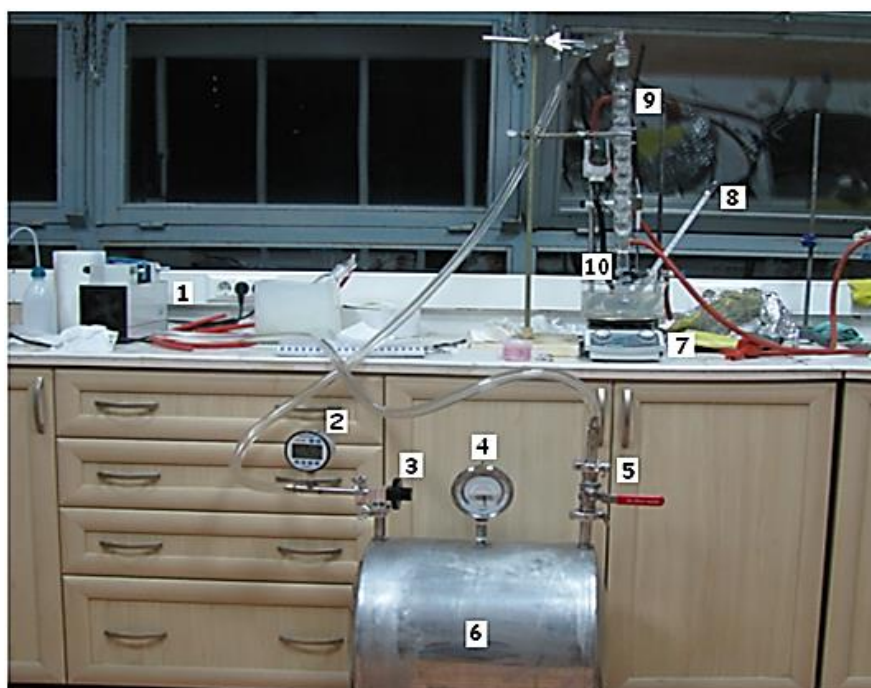


Figure 2.4 Vapor pressure measurement set-up

The name and functions of the numbered constituents are explained below for Figure 2.4;

- 1: Vacuum pump
- 2: Pressure gauge, to measure the pressure in the system
- 3: Needle valve, to adjust the pressure in the system accurately
- 4: Pressure gauge, to measure the pressure in the tank
- 5: Ball valve, controls the connection between tank and the vacuum pump
- 6: Tank
- 7: Temperature controlled heater
- 8: Thermometer, to measure the system temperature
- 9: Condenser, to condense the vapors coming from the system
- 10: The balloon flask, to hold the liquid to be measured

In this set-up, one can measure the pressure when the liquid in the system starts to boil by adjusting the pressure on top of the liquid with using a needle valve. The measured pressure where the first bubble appears actually shows the vapor pressure of the compound at that temperature. The large tank (6) here is employed in order to attain a constant pressure value during the measurements.

2.3.6.2 Viscosity measurements

The viscosity measurements were done by Brookfield LVDV-III Ultra rheometer with using a SC4-34 spindle and small sample adaptor. The device has a 0.01-250 rpm speed range. The data acquired was processed by using Brookfield Rheocalc computer program. The temperature was kept constant by using constant temperature circulating bath.

2.3.6.3 Surface tension measurements

The surface tension of the solutions was measured by using a Cole Parmer Surface Tensiomat 21 with a platinum-iridium ring (circumference: 5.965 cm). The surface tension values were measured in between 30-70 Dynes/cm.

CHAPTER 3

RESULTS AND DISCUSSIONS

The results of this thesis study were subdivided into four groups; the synthesis and characterization of the materials employed in the study, liquid-liquid extraction by N-alkyl formamides, adsorption results by lithium manganese oxide adsorbents and lastly adsorption results in a continuous column by PSMA-LiMnO beads. Additional materials synthesized and methods used in the study were summarized in APPENDIX A.

3.1 Synthesis and characterization of materials employed in lithium separation

3.1.1 Synthesis and characterization of N-alkyl formamides

3.1.1.1 NMR and FTIR

To investigate lithium extraction behavior of the formamides, four formamides bearing hexyl, octyl, dibutyl and dihexyl groups were synthesized as depicted in Figure 3.1.

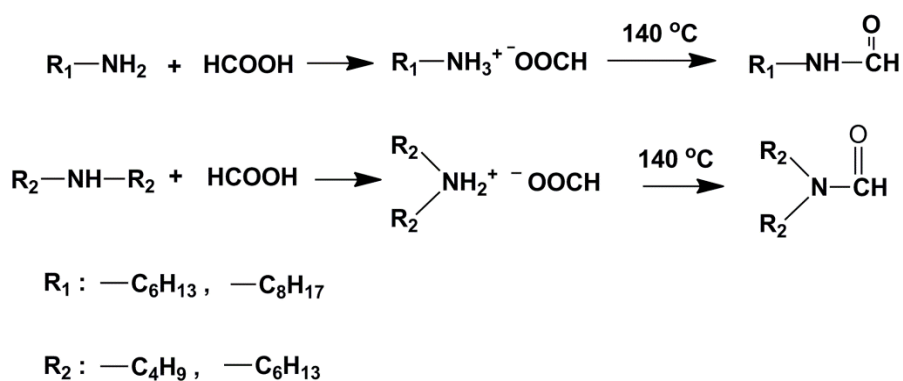


Figure 3.1 Synthesis pathway of N-alkyl formamides

The synthesis procedure was quite straightforward in which equimolar quantity of amine was mixed with formic acid and heated to 140 °C to evolve the reaction water. The products so obtained were pure enough as inferred from ¹H-NMR and FTIR spectra. It is important to note that both NMR and FTIR spectra of the formamides show very similar patterns, for instance the hexyl formamide derived from hexyl amine and formic acid exhibits a strong carbonyl vibration at 1650 cm⁻¹ and a N-H plane bending band at 1530 cm⁻¹ in the FTIR spectrum. The other peaks, N-H stretching vibration at 3350 cm⁻¹ and C-N vibration bands at 1220 and 1100 cm⁻¹ support the proposed formamide structure. ¹H-NMR spectrum of this product shows a weak signal of formamide proton at 8.0 ppm. The broad signal centered at 5.3 ppm must be associated with N-H proton. The proton signals of methylene group linked to nitrogen appears as downfield signal at 3.3 ppm, while the remaining protons of aliphatic carbons lie in between 0.9-1.6 ppm range. The residual hexyl amine in the crude product shows proton signals at 3.2 ppm as a weak triplet.

The products except dihexyl formamide were liquid at room temperature. Dihexyl formamide is a low melting solid that melting slightly above room temperature (35-40 °C). The FTIR and ¹H-NMR spectra were described in detail as listed below.

Hexyl formamide (distilled product): Boiling point (120 °C/12 mm Hg). ¹H-NMR, δ 8 (1H, s, OC-H), 5.3 (1H, b, N-H), 3.3 (2H, t, N-CH₂), 1.2-1.6 (8H, m, CH₂ of the linear chain), 0.9 (3H, t, CH₃ end group). Significant FTIR peaks: sharp peak at 1640 cm⁻¹ (C=O stretching vibration), the strong band at 1530 cm⁻¹ (N-H plane bending

vib.), broad band at 3350 cm^{-1} (N-H stretching vibration), small peak at 1100 cm^{-1} (C-N stretching vibration), sharp peak at 1220 cm^{-1} (OC-N stretching band).

Octyl formamide (distilled product): Boiling point ($123\text{ }^{\circ}\text{C}/12\text{ mm Hg}$). ^1H –NMR, δ 7.8 (1H, s), 5.1 (1H, b), 3.2 (2H, t), 1-1.4 (12H, m), 0.9 (3H, t). Significant FTIR peaks: sharp peak at 1640 cm^{-1} (C=O stretching vibration), the strong band at 1530 cm^{-1} (N-H plane bending vib.), broad band at 3350 cm^{-1} (N-H stretching vibration), small peak at 1100 cm^{-1} (C-N stretching vibration), sharp peak at 1220 cm^{-1} (OC-N stretching band).

Dibutyl formamide (distilled product): Boiling point ($135\text{ }^{\circ}\text{C}/12\text{ mm Hg}$). ^1H –NMR, δ 8 (1H, s), 3.2 (4H, t), 1.4 (4H, quin), 1.2 (4H, sex), 0.9 (6H, t). Significant FTIR peaks: sharp peak at 1640 cm^{-1} (C=O stretching vibration), the strong band at 1530 cm^{-1} (N-H plane bending vib.), broad band at 3350 cm^{-1} (N-H stretching vibration), small peak at 1100 cm^{-1} (C-N stretching vibration), sharp peak at 1220 cm^{-1} (OC-N stretching band).

Dihexyl formamide (distilled product): Boiling point ($140\text{ }^{\circ}\text{C}/12\text{ mm Hg}$). ^1H –NMR, δ 8 (1H, s), 3.2 (4H, t), 1.2-1.5 (16H, quin), 0.9 (6H, t). Significant FTIR peaks: sharp peak at 1640 cm^{-1} (C=O stretching vibration), the strong band at 1530 cm^{-1} (N-H plane bending vib.), broad band at 3350 cm^{-1} (N-H stretching vibration), small peak at 1100 cm^{-1} (C-N stretching vibration), sharp peak at 1220 cm^{-1} (OC-N stretching band).

(*s: singlet, b: broad, t: triplet, m: multiplet, quin: quintet, sex: sextet*)

3.1.1.2 Viscosity measurements

All liquids obey the Newtonian law and give the same viscosity values at all shear rates. The viscosity values decrease as the temperature increases. The results can be seen from Figure 3.2.

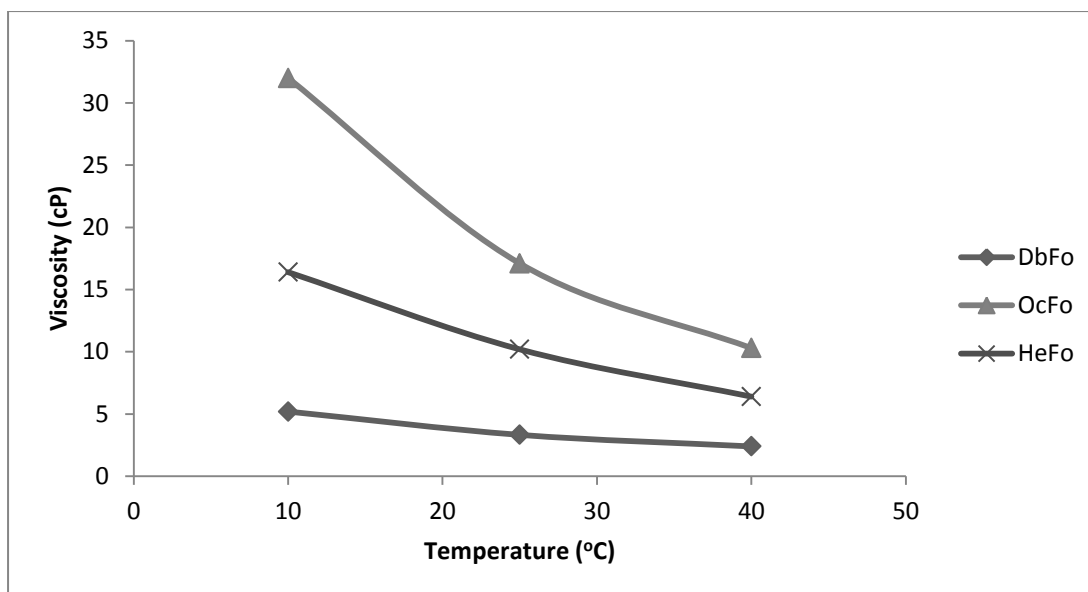


Figure 3.2 Temperature dependence of viscosity for N-alkyl formamides

3.1.1.3 Surface tension measurements

The values were measured at 10 °C and shown in Table 3.1.

Table 3.1 Surface tension values for the N-alkyl formamides at 10 °C

Formamide	Surface Tension (dynes/cm)
Hexyl formamide	37.3
Octyl formamide	35.1
Dibutyl formamide	33.5

3.1.1.4 Density measurements

Another important physical property of the N-alkyl formamides are their densities. The density measurements were done at three different temperatures by using a pycnometer and listed in Table 3.2.

Table 3.2 The densities of the N-alkyl formamides at different temperatures

N-alkyl formamide	Density (g/cm ³)		
	10 °C	25 °C	40 °C
Hexyl formamide	0.896	0.890	0.883
Octyl formamide	0.880	0.876	0.874
Dibutyl formamide	0.886	0.883	0.879
Dihexyl formamide	-	-	0.875

3.1.1.5 Vapor pressure measurements

In order to avoid the decomposition risk of hexyl formamide, the temperature of the system was not increased above 180 °C in the experiments. The relation between temperature and vapor pressure was drawn and shown in Figure 3.3.

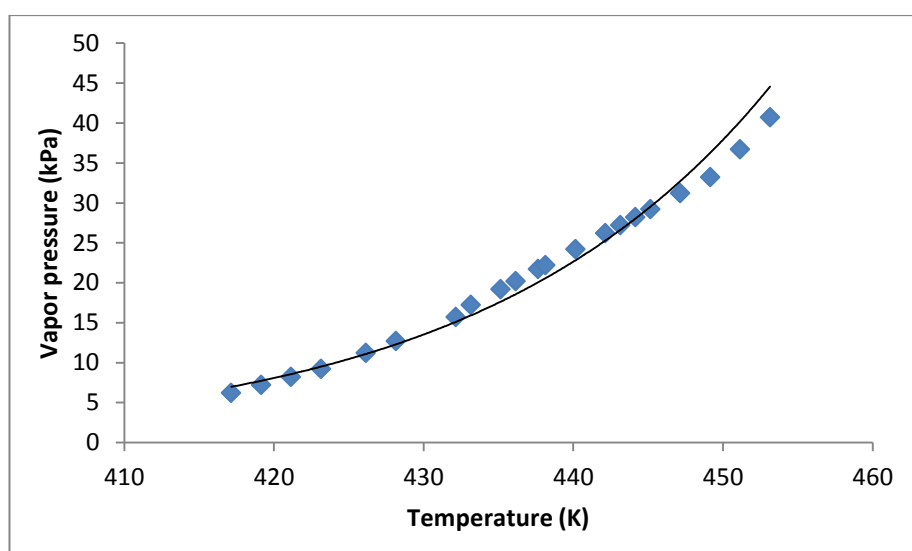


Figure 3.3 Temperature-vapor pressure relation for hexyl formamide

In general, vapor pressure of materials changes exponentially with respect to temperature. Therefore the data represented in Figure 3.3 was fitted to an exponential curve. The R^2 value was found as 0.98. The equation of the curve is given below;

$$P(kPa) = 3 * 10^{-9} * \exp(0.0515 * T (K)) \quad \text{Eqn. 1}$$

Equation 1 was used to estimate the vapor pressure of HeFo at room temperature and it was found as 0.016 kPa at 25 °C. With the same equation the normal boiling point of HeFo was estimated as 243 °C. This is such a high temperature that hexyl formamide will probably decompose before it evaporates even at vacuum conditions. This high boiling temperature also implies a high energy for evaporation of the solvent, which can be required in recovering the solvent after the extraction.

3.1.1.6 The solubility of lithium chloride and foreign ions in hexyl formamide

The solubilities of lithium chloride and foreign ions in hexyl formamide were measured in order to estimate and predict the selectivity of HeFo towards lithium. The concentration of ions in HeFo was found by dissolving and diluting HeFo mixture in water. The analysis was done by atomic absorption spectrophotometer. Results were given in Table 3.3.

Table 3.3 LiCl, NaCl and KCl solubilities in hexyl formamide

Salt	Solubility (g/100 ml HeFo)
Lithium chloride	6.94
Sodium chloride	0.47
Potassium chloride	0.19

3.1.2 Synthesis and characterization of lithium manganese oxide

Lithium manganese oxide adsorbents were synthesized with five different procedures having different precursors throughout the study in order to find the LiMnO with the highest capacity value. The methods used in the study can be generally grouped into two as hydrothermal and solid-solid synthesis methods. In hydrothermal method, the procedures of Chitrakar et al, Wang et al, and Zhang et al were studied [70], [84], [88]. The procedures were slightly modified and optimization of the resulting capacity values was done. In solid-solid synthesis, the methods based on Kitajou et al and Ooi et al were studied [79], [87]. Table 3.4

shows Li, Mn sources and oxidants employed in synthesis of lithium manganese oxide adsorbents throughout the study.

Table 3.4 Methods employed in synthesis of lithium manganese oxide adsorbents.

Method	Lithium source	Manganese source	Oxidant	Reference
Hydrothermal-1	LiOHH ₂ O	MnCl ₂	H ₂ O ₂	[84]
Hydrothermal-2	LiOH	MnO ₂	H ₂ O ₂	[70]
Hydrothermal-3	LiOHH ₂ O	Mn(NO ₃) ₂	H ₂ O ₂	[88]
Solid-Solid-1	LiOHH ₂ O	Mn ₃ O ₄	-	[79]
Solid-Solid-2	LiOHH ₂ O,	MnCO ₃ , MnO, MnO ₂	-	[87]

It is important to note that, there are additional procedures described with reflux method and spray pyrolysis method. Reflux method is an alternative method for hydrothermal method and spray pyrolysis method was employed only for once in a study made in Turkey [86].

3.1.2.1 Adsorbents synthesized by Hydrothermal-1 procedure

Among the hydrothermal methods, Hydrothermal-1 gave the adsorbent with the highest adsorption values and studied in detail. In this method LiOH and MnCl₂ were reacted to form a gel which was then transferred into an autoclave. The autoclave was taken to high temperature oven for reaction. After that, the precipitate was filtered and dried in room temperature and taken into high temperature oven to finalize the reaction. The whole process was divided in ten discrete steps in order to analyze the effect of each parameter on the resulting product efficiency as shown in Figure 3.4.

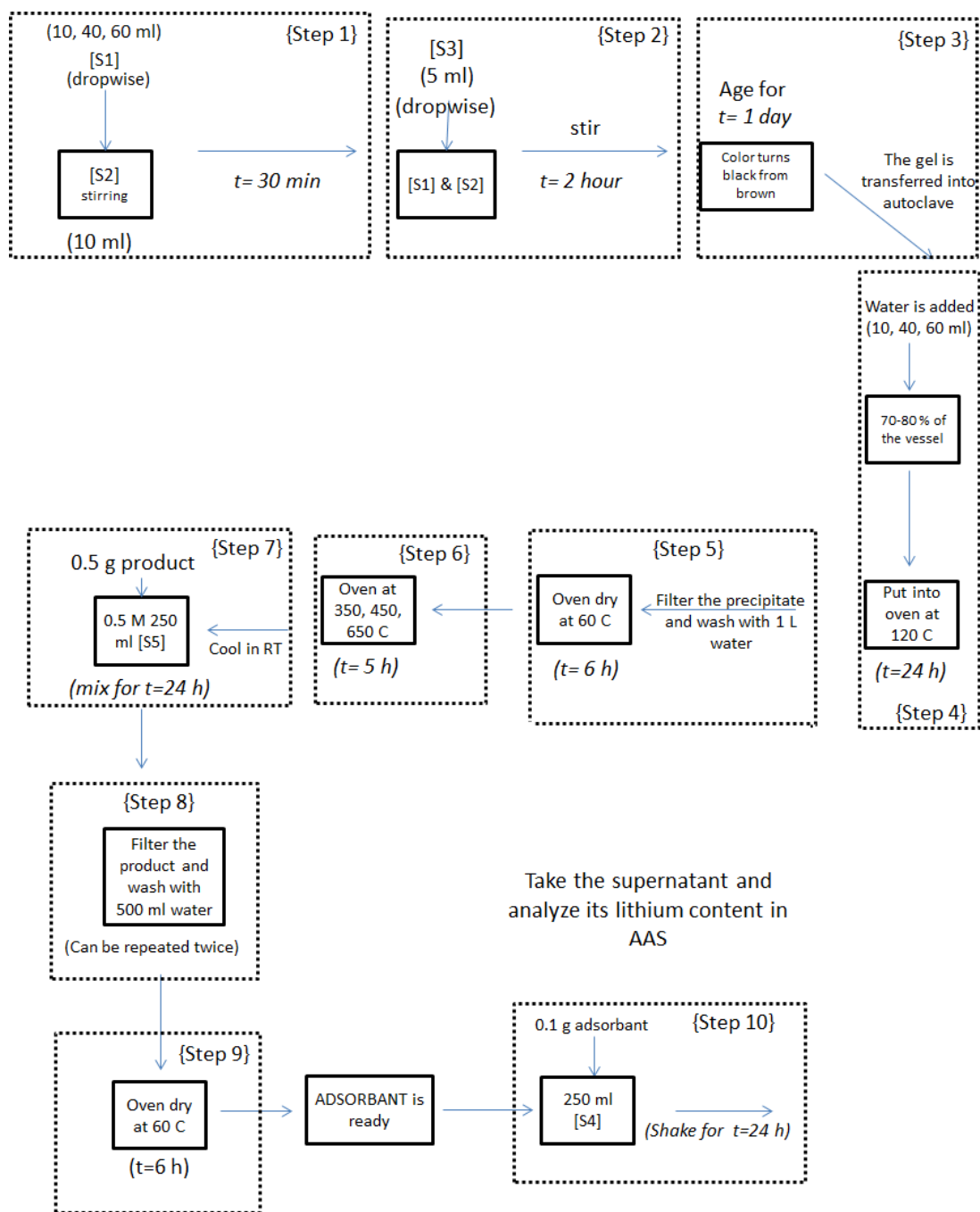


Figure 3.4 Hydrothermal-1 procedure in ten steps

([S1]: 2 M LiOH solution, [S2]: $\frac{3.96 \text{ g MnCl}_2 \cdot 4\text{H}_2\text{O}}{10 \text{ ml}}$ aq solution, [S3]: 30 % H_2O_2 (aq), [S4]: 5 ppm Li includes 4 ml desired pH buffer (aq), [S5]: 0.5 M HCl solution (aq))

Among those ten steps, critical variables were chosen that may affect the resulting adsorbent efficiency and the remaining variables were fixed. Critical variables were chosen as,

- Li/Mn ratio: 1, 2, 4 (STEP 1)
- Gel/water ratio in autoclave: 0.3, 0.6, 1.0 (STEP 4)
- Autoclave temperature: 120, 150, 180 °C (STEP 4)
- Oven temperature after autoclave: 350, 450, 650 °C (STEP 6)

In order to quantify the effect of each parameter, a factorial experimental design was done [93]. If three different variables were analyzed in each step, there comes out to be around $3^4=81$ experiments that should be performed. If repetitions were considered, there were 162 experiments that should be conducted which would be an excessive hard work. In order to reduce the number of experiments, the upper and lower limits for each variable were taken into account and $2^4=16$ experiments were performed. According to that plan, Table 3.5 was constructed and a set of 16 experiments were conducted.

Table 3.5 Optimization plan constructed by applying factorial design for the upper and lower limits of four variables versus acquired adsorbent capacity (response)

Sample no	Li/Mn fraction	Gel/water ratio	Autoclave temp. (°C)	Oven temp. (°C)	Adsorbent Capacity
<i>Limits</i>	<i>1-4</i>	<i>0.3-1.0</i>	<i>120-180</i>	<i>350-650</i>	<i>0-40 (mg Li/g ads)</i>
1	1	0.3	120	350	2.1
2	4	0.3	120	350	4.8
3	1	1	120	350	3.2
4	4	1	120	350	6.5
5	1	0.3	180	350	5.1
6	4	0.3	180	350	7.0
7	1	1	180	350	4.8
8	4	1	180	350	8.1
9	1	0.3	120	650	2.5
10	4	0.3	120	650	4.9
11	1	1	120	650	4.4
12	4	1	120	650	13.3
13	1	0.3	180	650	6.9
14	4	0.3	180	650	9.2
15	1	1	180	650	5.8
16	4	1	180	650	7.3

The data listed in Table 3.5 enlightens the effect of variables in lithium manganese oxide synthesis on adsorbent capacity. It can be deduced that the most effective variables are the oven temperature and Li/Mn ratio. The next effective variable is gel/water ratio in autoclave. The effect of autoclave temperature has the smallest effect on capacity values.

After the effect of each variable was roughly determined, a detailed experimental investigation was held to identify the effect of each individual variable by additional experiments.

First, the effect of oven temperature was examined as shown in Table 3.6.

Table 3.6 Effect of oven temperature on capacity of adsorbents synthesized by Hydrothermal-1 procedure

Adsorbent synthesis conditions				Adsorption process conditions			Capacity ($\frac{\text{mg Li}}{\text{g ads.}}$)
Oven temperature (°C)	Gel/water ratio	Autoclave temperature (°C)	Li/Mn fraction	Initial Li concentration (ppm)	Final Li concentration (ppm)	pH	
350	1	120	4	5	3.52	10.1	6.53
450	1	120	4	5	2.59	10.1	11.78
650	1	120	4	5	2.22	10.1	13.34
750	1	120	4	5	3.65	10.1	6.48

Table 3.6 shows that as oven temperature increases, the capacity value of the adsorbent also increases up to 650 °C. After that a lower capacity value was acquired at 750 °C. It is known that the thermodynamic equilibrium for spinel manganese oxide is established around 450-550 °C [94]. Therefore at 750 °C, the crystal structure may be distorted and the capacity values get decreased.

Second, the effect of gel water ratio in autoclave was investigated and the results were tabulated in Table 3.7.

Table 3.7 Effect of gel/water ratio on capacity of adsorbents synthesized by Hydrothermal-1 procedure

Adsorbent synthesis conditions				Adsorption process conditions			Capacity ($\frac{\text{mg Li}}{\text{g ads.}}$)
Gel/water ratio	Oven temperature (°C)	Autoclave temperature (°C)	Li/Mn fraction	Initial Li concentration (ppm)	Final Li concentration (ppm)	pH	
0.3	650	120	4	5	4.83	10.1	4.9
0.7	650	120	4	5	3.00	10.1	9.98
1	650	120	4	5	2.22	10.1	13.34

It can be shown from Table 3.7 that, as gel/water ratio in autoclave decreases, the capacity values of the adsorbents also decrease. The effect of water amount in autoclave on adsorption capacity of the resulting adsorbents can be explained by the concentration of the reactants in the medium. More concentrated mixtures give higher extent of reaction which result in higher amount of desired product.

Third, the effect of Li/Mn ratio was investigated in another set of experiments. The results were listed in Table 3.8.

Table 3.8 Effect of Li/Mn ratio on capacity of adsorbents synthesized by Hydrothermal-1 procedure

Adsorbent synthesis conditions				Adsorption process conditions			Capacity ($\frac{\text{mg Li}}{\text{g ads.}}$)
Li/Mn fraction	Oven temperature (°C)	Autoclave temperature (°C)	Gel/water ratio	Initial Li concentration (ppm)	Final Li concentration (ppm)	pH	
4	650	120	1	5	2.22	10.1	13.34
2	650	120	1	5	3.65	10.1	6.48
1	650	120	1	5	4.09	10.1	4.35

It is seen that the Li/Mn ratio has a remarkable effect on the resulting capacity values. The best result was acquired with Li/Mn=4 in which lithium ion presence in the crystal lattice has a highest value. It is also important to note that as lithium ion increases in the crystal lattice, the stability of the adsorbents tends to reduce in consecutive adsorption-desorption cycles.

Lastly, the effect of autoclave temperature was investigated and findings were tabulated in Table 3.9.

Table 3.9 Effect of autoclave temperature on capacity of adsorbents synthesized by Hydrothermal-1 procedure

Adsorbent synthesis conditions				Adsorption process conditions			Capacity ($\frac{\text{mg Li}}{\text{g ads.}}$)
Autoclave temperature (°C)	Gel/water ratio	Oven temperature (°C)	Li/Mn fraction	Initial Li concentration (ppm)	Final Li concentration (ppm)	pH	
110	1	650	4	5	2.84	10.1	11.78
120	1	650	4	5	2.22	10.1	13.34
130	1	650	4	5	3.00	10.1	9.98
140	1	650	4	5	2.84	10.1	11.78
150	1	650	4	5	3.52	10.1	6.79
180	1	650	4	5	3.48	10.1	7.34

Table 3.9 shows that lower autoclave temperatures result in higher capacity values. The temperature in an aqueous autoclave system can also affect the pressure of the media. The pressure of the system reaches to vapor pressure of water at specified temperature. The capacity loss at high temperature and pressures may be attributed to the nature of MnCl_2 and LiOH reaction but could not be identified explicitly.

Considering the experiments conducted to optimize the capacity of adsorbents synthesized by Hydrothermal-1 procedure, the highest capacity value of 13.3 mg Li/g ads. was acquired at gel/water ratio=1, oven temperature=650, Li/Mn fraction=4 and autoclave temperature=120. This value corresponds to 33 % of the maximum theoretical adsorption capacity (40 mg Li^+ /g adsorbent) of the lithium manganese oxide adsorbents. The value of 13.3 mg Li/g implies that one third of the active sites are available for lithium adsorption in LiMnO and the remaining sites were not reached by lithium ions due to mass transfer limitations or the synthesis was failed in some extent.

In order to get rid of mass transfer limitation in the particles and make the particles more porous, the lithium manganese oxide adsorbents was synthesized with Pluronics which was a polyethylene glycol-poly propylene glycol-polyethylene

glycol copolymer. The optimum synthesis conditions were chosen and 100 ml of 0.85 % Pluronics solution was added to the reaction mixture in autoclave stage instead of water. Unfortunately the resulting adsorbent gave a capacity value which was even smaller than the previous one as 2.53 mg Li/g adsorbent.

3.1.2.2 Adsorbents synthesized by solid-solid procedures

In solid-solid procedures, different manganese and lithium sources were mixed in a crucible and heated to certain temperatures where the reaction takes place.

In order to find the most efficient solid-solid method, several characterization techniques were employed. The characterization of the adsorbent synthesis was first done in DTA-TGA instrument in order to identify the behavior of the reactants during heating process.

- DTA-TGA measurements

Thermogravimetric analysis (TGA) and differential thermal analysis (DTA) were performed simultaneously in air at a heating rate of 10 °C min⁻¹. Four different reactants were used in the synthesis as manganese source which were, MnO, MnO₂, Mn₃O₄ and MnCO₃. The lithium source was fixed as LiOHH₂O.

As seen in Figure 3.5, MnO reacts with LiOH.H₂O under increasing temperature and given heat. It is seen that, at 85 °C, the water in medium evaporates. The endothermic peaks at around 428 °C and 476 °C are attributed to the conversion of β-MnO₂ to a more stable α-Mn₂O₃ with release of oxygen gas [82].

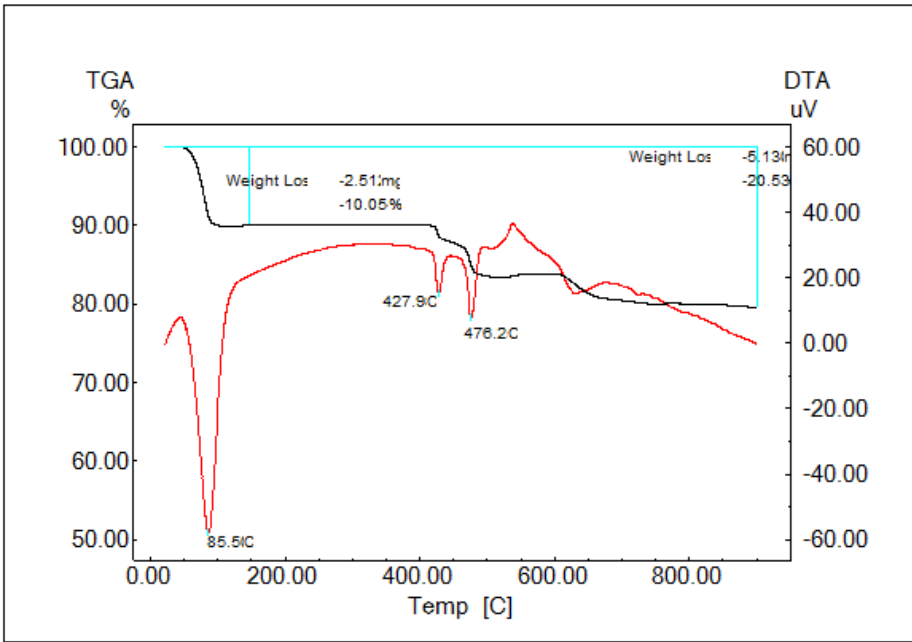


Figure 3.5 Heating curve for MnO and LiOH·H₂O reaction system

Figure 3.6 shows that, MnO₂ reacts with LiOH under increasing temperature and given heat. It is seen that, the behavior of the curve is very similar to the case in Figure 3.5. At 96 °C, the water in medium evaporates. The endothermic peak at around 428 °C and 467 °C are attributed to the conversion of β-MnO₂ to a more stable α-Mn₂O₃ with release of oxygen gas.

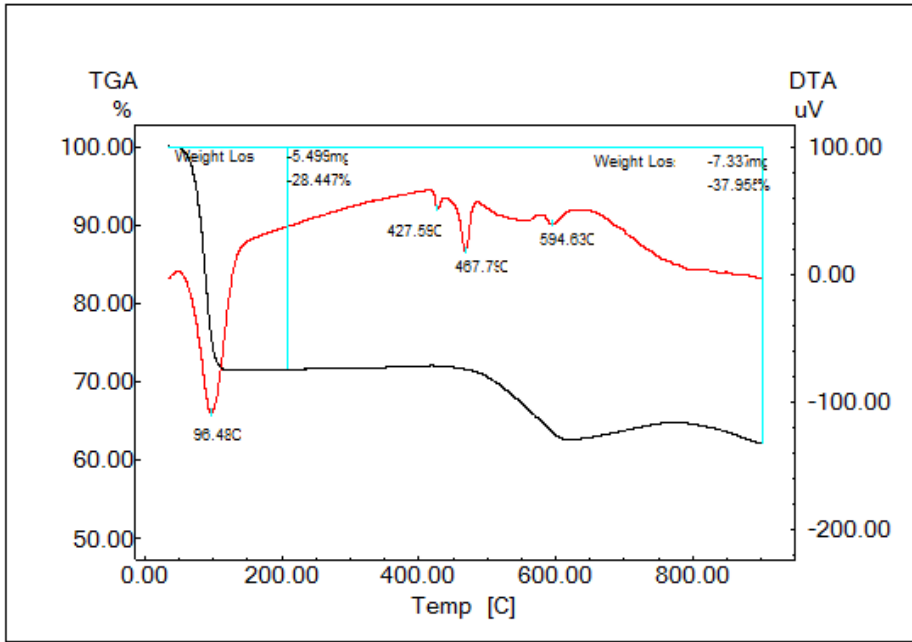


Figure 3.6 Heating curve for MnO₂ and LiOH·H₂O reaction system

In Figure 3.7, MnCO_3 reacts with $\text{LiOH}\cdot\text{H}_2\text{O}$ under increasing temperature and given heat, the weight loss around 78 °C implies the evaporation of water. The endothermic peak at 339 °C and weight loss can be ascribed to the decomposition of manganese carbonate to manganese oxide and carbon dioxide. The peak around 725 °C was attributed to transformation from Mn_2O_3 to Mn_3O_4 .

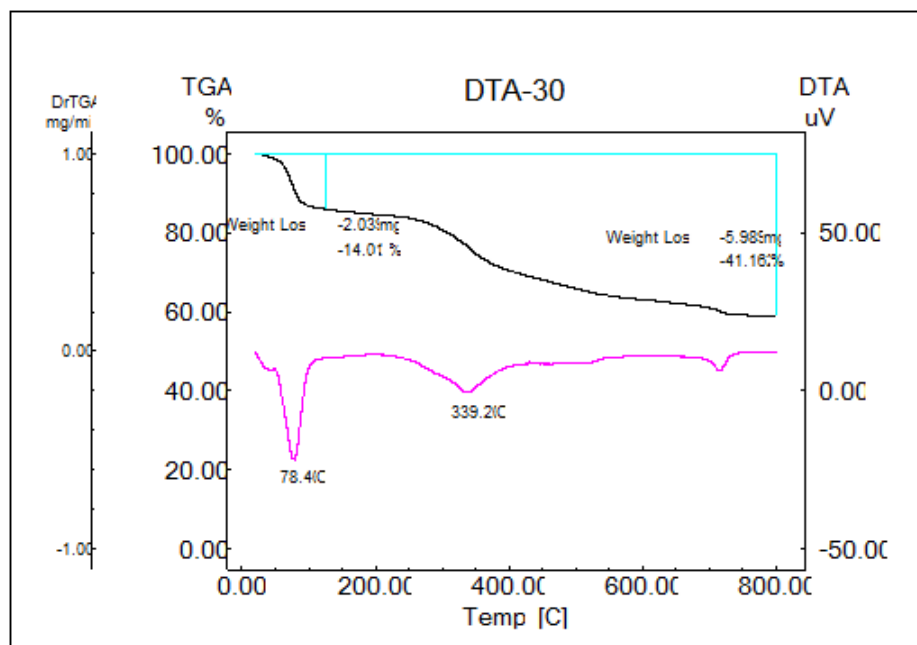


Figure 3.7 Heating curve for MnCO_3 and $\text{LiOH}\cdot\text{H}_2\text{O}$ reaction system

In Figure 3.8, Mn_3O_4 reacts with $\text{LiOH}\cdot\text{H}_2\text{O}$ under increasing temperature and given heat. It is seen that, the behavior of the curve is very similar to Figure 3.7. The weight loss around 79 °C implies the evaporation of water. The endothermic peak at around 428 °C and 471 °C are attributed to the conversion of $\beta\text{-MnO}_2$ to a more stable $\alpha\text{-Mn}_2\text{O}_3$ with release of oxygen gas.

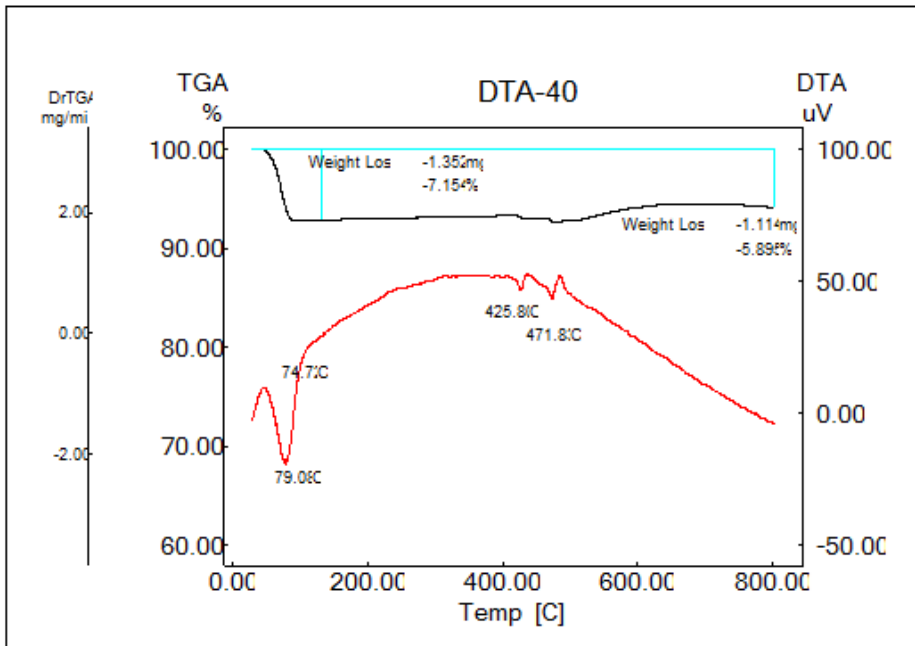


Figure 3.8 Heating curve for Mn₃O₄ and LiOHH₂O reaction system

After the synthesis of four different adsorbents by solid-solid synthesis method, it was seen that adsorbents synthesized by manganese carbonate and lithium hydroxide gave the highest uptake value which is 22.8 mg Li/g ads. The high performance of those adsorbents was attributed to the micron scale particle size. The carbonate group attached to manganese decomposes at around 340 °C and CO₂ evolves. Carbon dioxide evolution during synthesis results in a porous structure and decreases the particle size of the resulting products. Smaller particle size leads to increase in surface area which results in high capacity for the synthesized adsorbents.

- FTIR measurements

In order to identify the structure of synthesized adsorbents and investigate the effect of Li/Mn molar ratio on structure before and after acid leaching, FTIR measurements were carried out. Acid leaching was the last step in adsorbent preparation for all methods and function to exchange the hydrogen ions with lithium ions. Exchange of H⁺ and Li⁺ is a reversible process and do not distort the crystal structure. As seen in Figure 3.9, conservation of the structure after acid leaching is one of the fingerprints that validate successful synthesis. Acid leaching was done by dilute hydrochloric acid (0.5 M) solution for all adsorbents. The adsorbents before acid leaching were named as LMO and after acid leaching as HMO.

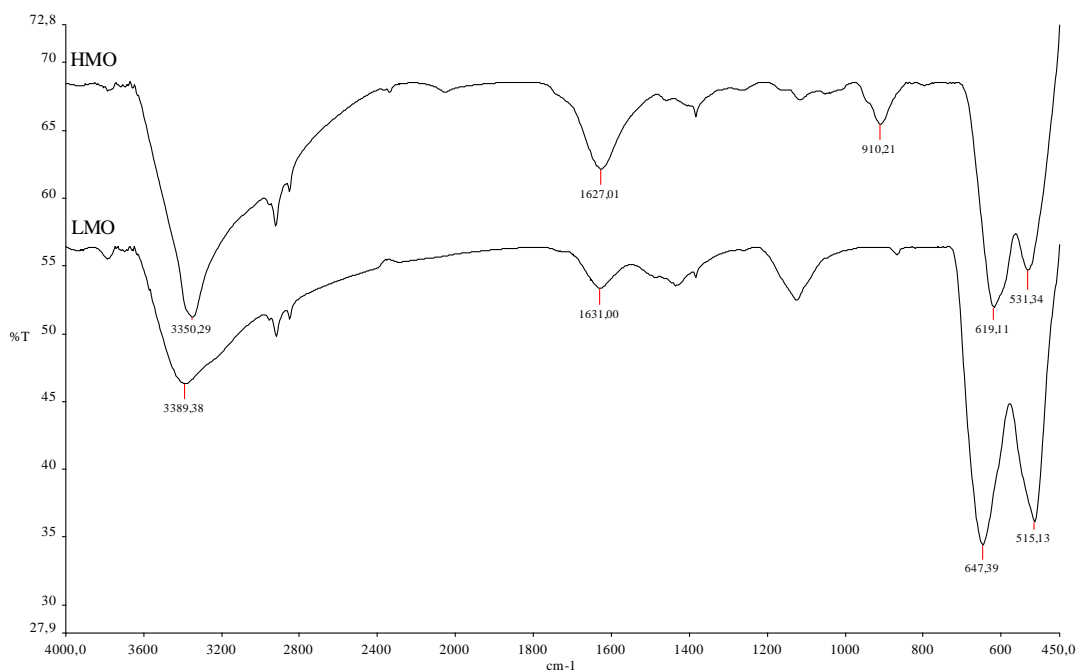


Figure 3.9 FTIR spectrum of spinel lithium manganese oxide synthesized by MnCO_3 and $\text{LiOH}\cdot\text{H}_2\text{O}$ (Li/Mn: 1/1) F30, before (LMO) and after (HMO) acid leaching

In the spectrum, spinel type lithium manganese oxide peaks can be identified as fingerprint of the adsorbents. The peaks around 3400 and 1600 cm^{-1} are belong to water in samples (stretching vibration of hydroxyl groups). The peaks around 630 and 500 cm^{-1} are belong to manganese-oxygen bonds. The peak around 910 cm^{-1} is ascribed to the coupled lattice vibration of protons which shows the completion of acid leaching process in the adsorbent. Peaks around 2900 cm^{-1} probably show the organic residue present in the FTIR cell or optic pathway in the instrument. The remaining peaks do not change much which imply that the lattice structure of the adsorbents is preserved before and after acid leaching which also validates the tapotactic extraction of lithium ions from crystal lattice.

In Figure 3.10, FTIR pattern of spinel lithium manganese oxide before and after acid leaching can be seen for Li/Mn:1/0.8 molar ratio.

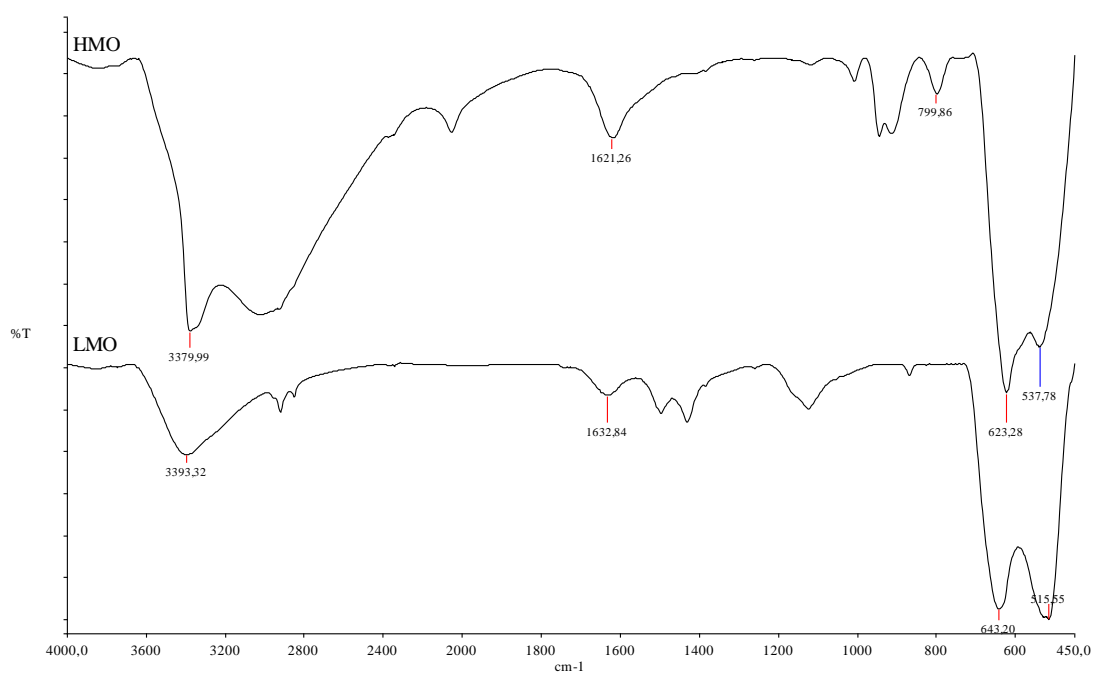


Figure 3.10 FTIR spectrum of spinel lithium manganese oxide synthesized by MnCO_3 and $\text{LiOH}\cdot\text{H}_2\text{O}$ (Li/Mn: 1/0.8 mole ratio) F31, before (LMO) and after (HMO) acid leaching

The spectrum shown in Figure 3.10 depicts the loss of structure after acid leaching. The water in the structure gives signals at 3400 cm^{-1} and 1600 cm^{-1} . Similarly, the characteristic peaks of Mn-O stretching are observed at 640 and 530 cm^{-1} . However the diversity in the rest of the spectrum implies the loss of crystal structure. The proton signal expected at 910 cm^{-1} is also distorted and additional signals appear. The brown color appears in the mixture of adsorbent and lithium chloride solution also validates the loss of structure. The brown color emerges by decomposition of Mn^{+3} to Mn^{+4} .

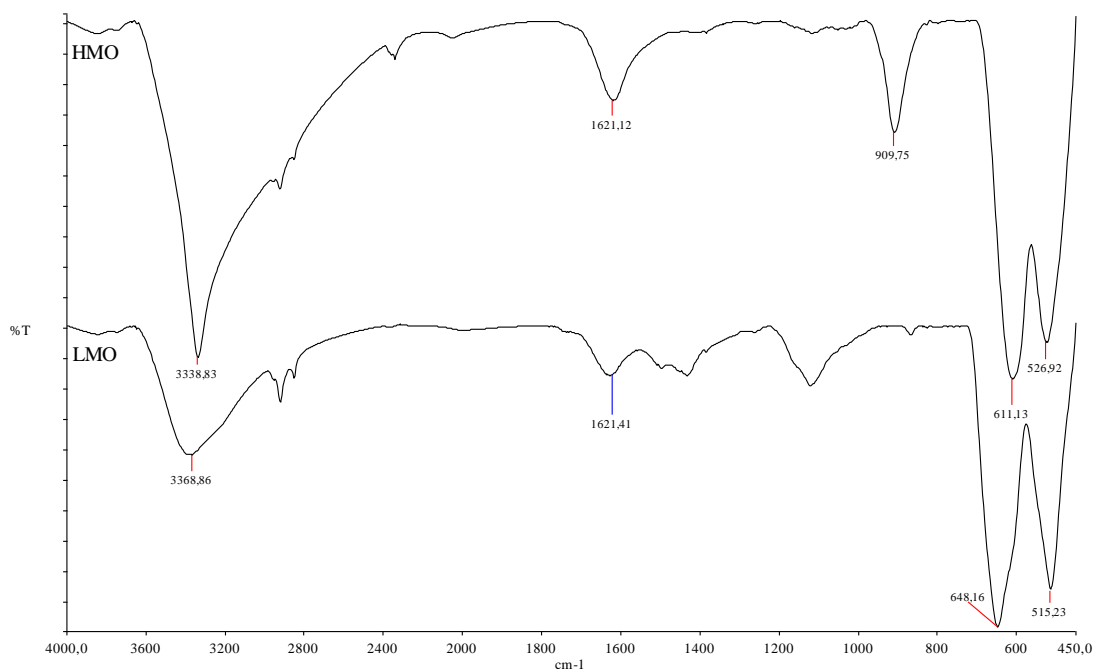


Figure 3.11 FTIR spectrum of spinel lithium manganese oxide synthesized via MnCO_3 and $\text{LiOH}\cdot\text{H}_2\text{O}$ (Li/Mn: 0.8/1 mole ratio) F32, before (LMO) and after (HMO) acid leaching

In Figure 3.11, Mn-O signals at 640 cm^{-1} and 530 cm^{-1} and water signals at 3400 cm^{-1} and 1600 cm^{-1} are clearly noticed. Two trends in spectrum before and after acid leaching are quite similar. Also proton signal around 910 cm^{-1} is much more obvious and sharp with respect to former adsorbents which implies higher hydrogen content. In fact, the strength of this signal implies a higher lithium capacity for the synthesized adsorbent. However the higher capacity comes in return for loosening the structure stability. The adsorbent capacity gets lost after two lithium adsorption-desorption cycle.

The adsorption experiments with the adsorbents synthesized with three different molar ratios showed that the highest capacity was acquired by the adsorbent having Li/Mn ratio of 0.8. However the stability of the adsorbent weakens after first adsorption-desorption cycle while the adsorbent having Li/Mn ratio of 1 lasts for several cycles.

The FTIR pattern for three adsorbents having different Li/Mn ratio (after acid leaching) were summarized in the same plot as shown in Figure 3.12.

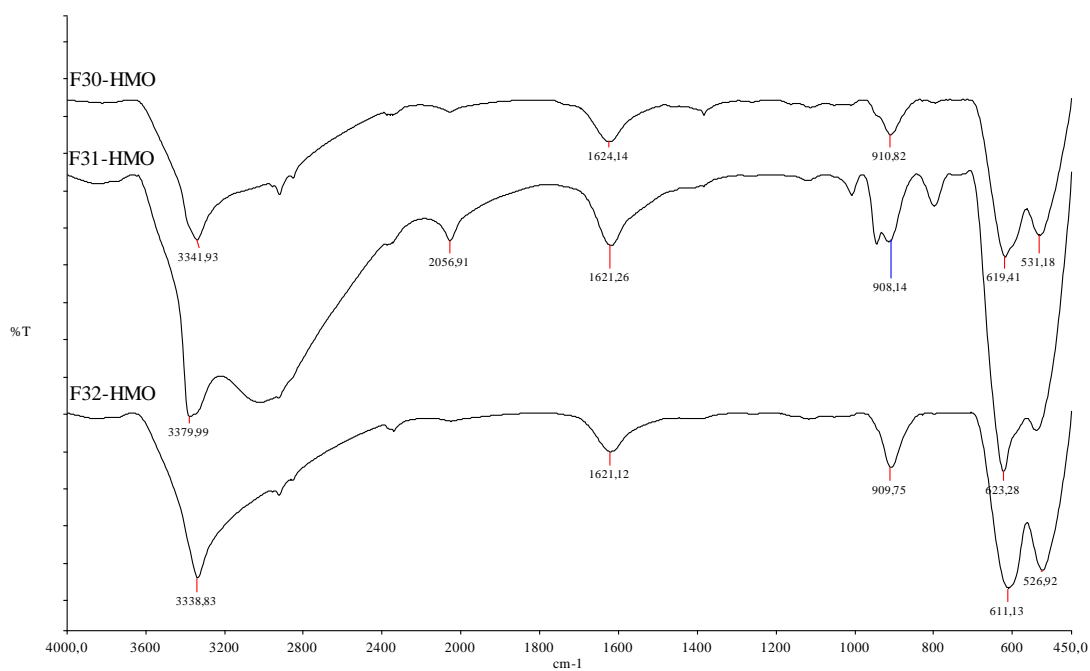


Figure 3.12 FTIR pattern for three different adsorbents (after acid leaching) having different Li/Mn molar ratios (F30-Li/Mn:1, F31-Li/Mn:1/0.8, F32-Li/Mn:0.8)

During the adsorption experiments, it was found out that, mixing the adsorbents with the acid leaching solution for a long time leads to an irreversible effect and the hydrogen atoms in the structure lose the position in lattice structure. This fact was proved by the FTIR measurements which can be seen in Figure 3.13. The signal at 905 cm⁻¹ slowly grows up to 4 hours. After that it disappears during acid leaching, which implies the integration of protons into lattice. After 24 hours the signal totally gets lost and the resulting adsorbent becomes useless to be employed in lithium separation. Therefore it was understood that, there is an optimum time of acid leaching process for the adsorbents synthesized by Hydrothermal-1 procedure.

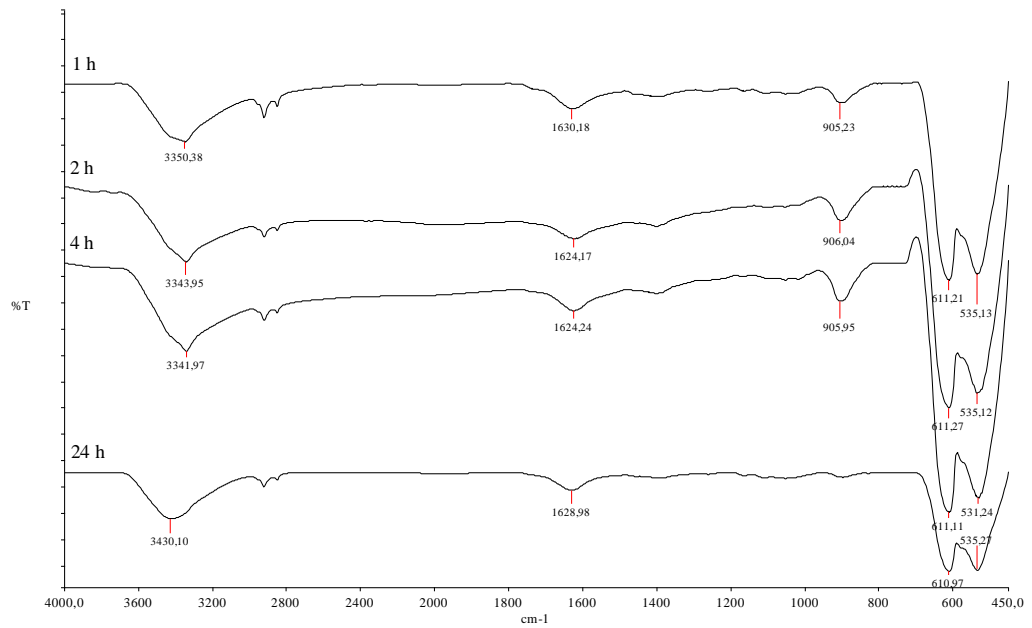


Figure 3.13 Effect of acid leaching process on lattice proton at different times for adsorbents synthesized by Hydrothermal-1 procedure

The FTIR pattern of adsorbents synthesized by procedures Solid-Solid-2, Hydrothermal-1 and Hydrothermal-3 are given in Figure 3.14.

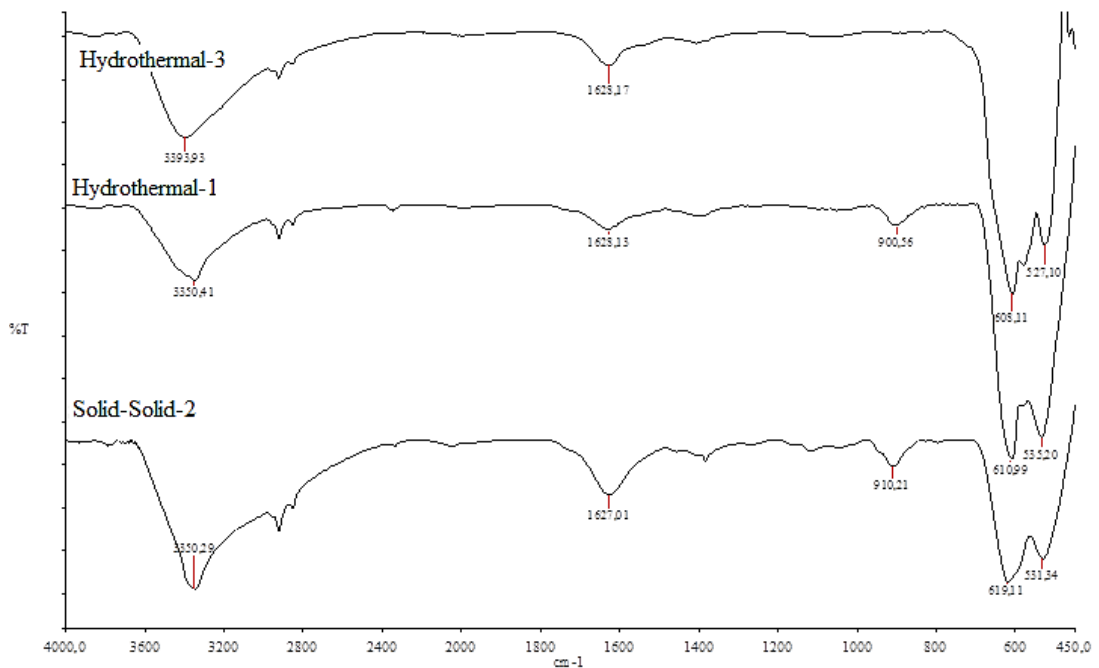


Figure 3.14 The adsorbents synthesized with three different methods

As it was observed from Figure 3.14, the three spectra for three different adsorbents were very similar. Mn-O signals were observed at the same wavelength. The signal

at 910 cm^{-1} , which shows the coupled lattice vibrations of protons in the structure, Hydrothermal-3 adsorbents differ from others. This also explains why these adsorbents generally have very low adsorption capacities, around 3-4 mg/g. Hydrothermal-1 (Capacity: 13.3 mg Li/g) and Solid-Solid-2 (Capacity: 21.1 mg Li/g) procedures give nearly exact spectrum which implies the similar structure. At that point, the difference of the capacity values between two adsorbents was explained with the particle size and the porosity difference between the adsorbents. In solid-solid synthesis, manganese carbonate decomposition into carbon dioxide leads to a more porous structure and smaller particle size in microns which produce higher surface area and increasing capacity. The detailed capacity values of the adsorbents synthesized by Solid-Solid-2 method are given in Chapter 3.3.

- XRD measurements

After the analysis of the adsorbent synthesis procedures listed in Table 3.4, Solid-Solid-2 method was found as the most efficient method which leads to adsorbents with highest lithium uptake value. In order to increase the performance of the adsorbents, a set of experiments were conducted under different synthesis temperatures and Li/Mn molar ratios. 350, 450, 550 and 650 °C were chosen as reaction temperatures and 0.8, 1 and 1.25 were chosen as Li/Mn ratios. The XRD pattern for the synthesized adsorbents were taken both in lithium manganese oxide (LMO) and hydrogen manganese oxide (HMO) forms. It was found out that, Li/Mn ratio of 1 and 450 °C synthesis temperature gave the most efficient adsorbents.

The XRD pattern of the selected adsorbents are shown in Figure 3.15 and Figure 3.16 for LMO and HMO forms respectively. The permanent signals before and after acid leaching show the stability of crystal structure which implies tapotactic exchange of lithium and protons in crystal lattice.

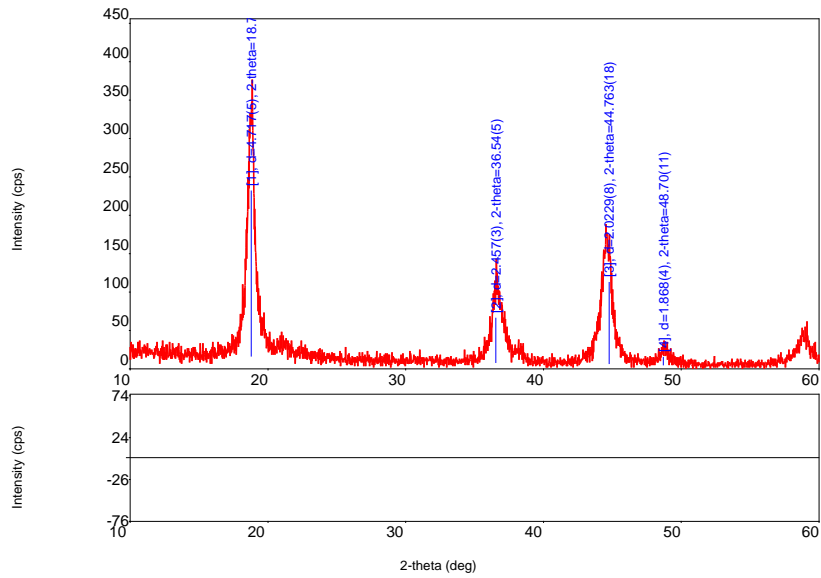


Figure 3.15 XRD spectrum of the spinel lithium manganese oxide LMO (450 °C, Li/Mn=1)

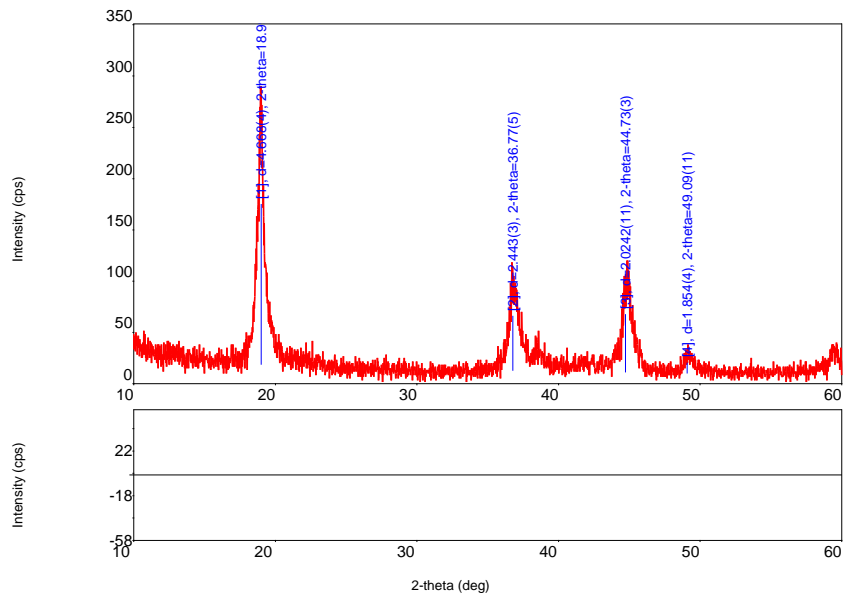


Figure 3.16 XRD spectrum of the spinel lithium manganese oxide HMO (450 °C, Li/Mn=1)

The crystal system and lattice constant of the selected lithium manganese oxide was found by applying Sadoway's method. There are two equations that was used in calculations.

First equation is Braggs' Law,

$$\lambda = 2d\sin\theta \quad \text{Eqn. 2}$$

λ : Wavelength of the copper target

d : Spacing between the planes in the atomic lattice

θ : Angle between the incident ray and the scattering planes

Second equation relates lattice constant with d ,

$$d = \frac{a}{\sqrt{h^2+k^2+l^2}} \quad \text{Eqn. 3}$$

From those two equations, following equation is acquired,

$$\frac{\lambda^2}{4a^2} = \frac{\sin^2 \theta}{h^2+k^2+l^2} \quad \text{Eqn. 4}$$

Here the left side of the equation is constant, which means that the right side of the equation must be a constant value too.

Wavelength of the copper target is known as 1.5418 Å.

The calculations to find the crystal system of manganese oxide and lattice constant are given in Table 3.10.

Table 3.10 Finding crystal system and lattice constant of LiMnO

2θ	Sin ² θ	Normalize values with first value	Clear	(hkl)	Compute	Compute a
			fractions by multiplying with 3 (for this case)		$\frac{\sin^2\theta}{h^2 + k^2 + l^2}$	$\frac{\lambda^2}{4a^2} = \frac{\sin^2\theta}{h^2 + k^2 + l^2}$
18.7	0.0264	1	3	(111)	0.0088	8.22
36.5	0.098	3.712	11.136	(311)	0.0089	8.17
44.7	0.145	5.492	16.477	(400)	0.0088	8.22
48.7	0.17	6.439	19.318	(331)	0.0088	8.22
58.5	0.239	9.053	27.159	(333)	0.0088	8.22

The planes of (111), (311), (400), (331) and (333) listed in Table 3.10, imply a FCC crystal system, with a lattice constant of 8.21 Å. These results coincide with the XRD data given in the literature [74] in which lithium at tetrahedral sites, manganese (III) and manganese (IV) at octahedral sites of a face centered cubic crystal system with 8.21 Å lattice constant.

The XRD pattern of adsorbents having Li/Mn ratio different than 1 also gives similar pattern and it was found that, the molar ratio changes of Li/Mn does not affect the crystal structure significantly. In that manner adsorbents having Li/Mn ratio higher than 1 can give higher lithium content in the adsorbent and increase the capacity of lithium uptake. Unfortunately, in that case the stability of the adsorbent was found insufficient which was indicated by the blurred solutions due to dissolved manganese ions during adsorption process.

The adsorbents synthesized at 650 and 750 °C give almost the same peaks in pattern. However peaks have high amount of noise and red colored impurities in crucible were observed after the synthesis. At temperatures 450 and 550 °C, the synthesis of manganese oxides give almost the same peaks. However peaks for 550 °C have less amount of noise. It is concluded that both temperatures are suitable for synthesis. In terms of lower energy consumption, 450 °C was used in the final adsorbents. The XRD pattern for the adsorbents synthesized at different temperature and molar ratios are given in APPENDIX B.

3.1.3 Synthesis and characterization of lithium manganese oxide-polymer beads

In order to employ the synthesized lithium manganese oxide adsorbents in an adsorption column, the size of particles must be increased from microns to millimeters to overcome the large pressure drop. Inorganic supporting materials like silica and alumina are used to address this problem. In general, the active material was mixed with supporting material in a mixture and impregnated or coated on the supporting material by various methods [95]. In this study these methods were found insufficient in impregnating the lithium manganese oxide onto silica or alumina. Even the synthesis of lithium manganese oxides were done on targeted surfaces, but the expected adhesion could not be observed.

A suspension polymerization technique was used in order to overcome this problem and lithium manganese oxide particles are tried to be covered by a polymeric matrix. In this technique, an organic phase and aqueous phase were prepared separately. In organic phase, glycidyl methacrylate (GMA), methyl methacrylate, ethylene glycol dimethacrylate and AIBN were dissolved in toluene. In aqueous phase, water, sodium sulfate, polyvinyl pyrrolidone were dissolved. Lithium manganese oxide particles were added to organic phase and then dripped into aqueous phase slowly at 65 °C.

After polymerization reaction was completed, lithium manganese oxides were weighed and it was found as 0.85 g of polymer covers 1 g of lithium manganese oxides, which shows that the polymerization reaction works and covers the LiMnO particles. Unfortunately the size of the manganese oxide-polymer particles at the end of the reaction was still in micron level. In order to increase the polymer content around the particles, an additional synthesis was done where the monomer amount was increased by five folds. But the polymer around manganese oxides was found as 1.5 g per 1 g of MnO₂ and the size of the particles were still in microns. Therefore this method was found insufficient to increase the particle size of the lithium manganese oxides.

As an alternative, a precipitation method was used. In this method, a polymer binder, targeted material and solvent were mixed to form a slurry of suspended particles in

the mixture. Then, this mixture was dripped into a non-solvent liquid to form the desired beads. In this method, various couples of solvent-polymer were used to find out the optimum combination for bead formation. Different solvent-polymer pairs and the observations on the resulting beads were listed in Table 3.11.

Table 3.11 Different solvent-polymer couples utilized for LiMnO bead synthesis by precipitation method

Polymer	Solvent	Result
Poly vinyl alcohol	NMP	Beads dissolve in water
Poly MMA-co-BA	NMP	Does not give ordinary spheres
Poly MMA-co-BA	THF	Does not give ordinary spheres
Poly MMA-co-BA	DMF	Does not give ordinary spheres
Poly MMA-co-BA	Dioxane	Does not give ordinary spheres
Poly MMA-co-BA	DMSO	Does not give ordinary spheres
PET	NMP	Polymer is not dissolved
PET	THF	Polymer is not dissolved
PE	NMP-THF-DMF- Dioxane-DMSO	Polymer is not dissolved
PS	NMP	Beads are formed but does not show stability
PS-Br	NMP	Beads are formed but does not show stability
Poly urethane	NMP	Does not give ordinary spheres
Poly vinyl acetate	NMP	Beads are formed but does not show stability
Poly (styrene-maleic anhydride)	NMP	Beads are formed and show stability in water, but lose their shape in air. In water high pH dissolves beads.

Among the polymer-solvent couples listed in Table 3.11, most promising results were acquired for poly (styrene-maleic anhydride). However, beads lost their form in air and high pHs (above 8). In order to enhance the bead stability, poly glycidyl methacrylate polymer was synthesized and added to poly (styrene-maleic anhydride) before mixing with LiMnO. The idea behind that is to introduce an epoxy group to polymeric medium and form crosslinkings which will increase the stability of the beads. The epoxide groups are known to open at high temperature and acidic medium. Therefore the slurry was dripped into 0.5 M HCl at 90 °C. At first, the beads changed color from black to white and gain stability in atmosphere. However,

they were still unstable in high pH aqueous solution. They swell and lose their stability. In order to overcome this problem, terpolymerization of maleic anhydride, styrene and glycidyl methacrylate were done. The logic is to introduce epoxy groups into the polymeric backbone and finally increase stability and strength.

3.1.3.1 Synthesis of poly (styrene-maleic anhydride-glycidyl methacrylate)-lithium manganese oxide beads

Poly (styrene-maleic anhydride-glycidyl methacrylate) was first synthesized in 1999 by a visiting professor from Azerbaijan Academy of Sciences in METU Chemistry department. The product was proposed to be used in films and coatings owing to its good mechanical and dielectric properties. In the polymerization reaction, all monomers were dissolved in ethyl methyl ketone and put into a reaction balloon to polymerize by benzoyl peroxide initiator [90]. Styrene and maleic anhydride monomers are known to lead to an alternating polymer which is called SMA, and it is used in paper sizing, powder coating, pigment dispersions etc. [96]. It also shows strong rubbery behavior and high elasticity. In order to sustain rubbery property of the polymer, styrene and maleic anhydride were used in equal molar proportions and GMA ratio was changed from 5 to 20 % in this study. After the polymerization reaction, poly maleic anhydride-styrene-glycidyl methacrylate (PSMA), MnO₂ and NMP was mixed in certain proportion and spherical beads were acquired by dripping the slurry into water. Water which was used as a non-solvent was also mixed with cetyl tert butyl ammonium bromide (CTAB) which was a well-known surfactant, in order to decrease the surface tension of the water and ease the formation of the spherical beads. The epoxy groups in resulting beads were known to form crosslinks with maleic anhydride groups even by the humid in the air at 125 °C or UV light [90]. The resulting beads were first dried and then exposed to UV light for 24 hours. Another set of beads were put into an oven at 125 °C for 40 minutes directly. The beads which were heat treated gave more consistent results; therefore heat treatment of beads was preferred rather than UV treatment to have a crosslinked product. The resulting PSMA polymer has a structure shown in Figure 3.17.

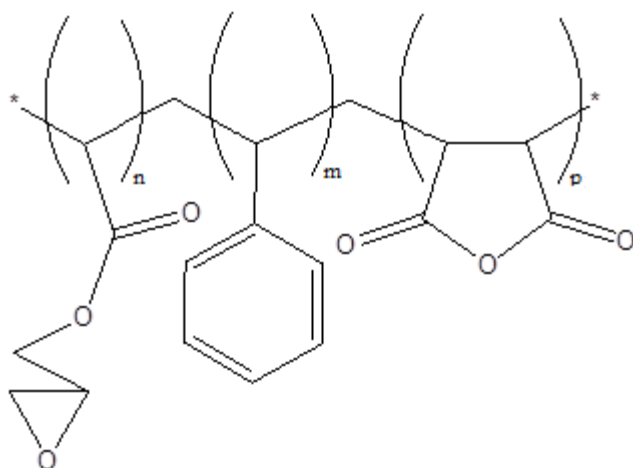


Figure 3.17 Structure of poly maleic anhydride-styrene-glycidyl methacrylate (PSMA)

Optimization of GMA ratio in PSMA to have a more rigid and stable beads, a set of polymerization reactions were carried out. The molar ratio of the monomers and the properties of the synthesized beads are given in Table 3.12.

Table 3.12 PSMA beads synthesized with different GMA content at 70 °C (Benzyl peroxide molar ratio:0.01, monomer/solvent ratio: 0.33)

Styrene (mol. %)	Maleic anhydride (mol. %)	GMA (mol. %)	Properties of the resulting beads	
			Rigidity	Swelling at pH:9
47.5	47.5	5	Low	High
45	45	10	Medium	High
44	44	12	Medium	Medium
42.5	42.5	15	High	Low
42	42	16	High	Low
41.5	41.5	17	Form crosslinks before bead formation	
40	40	20	Form crosslinks before bead formation	

Table 3.12 shows that as GMA ratio increases in the polymer, the rigidity of the resulting bead increases and its swelling amount decreases up to 16 % molar ratio. At higher GMA content, polymer forms crosslinks during bead preparation which disrupts the spherical shape of the beads. Therefore 16 percent GMA molar ratio was chosen to be an optimum value to prepare manganese oxide-PSMA beads. The volume of the beads increases by 4 % at pH 9 while keeping their form and stability.

In bead preparation process, manganese oxide/PSMA ratio, NMP/PSMA ratio and the mixing time for the beads in water were assumed to be critical variables in order to get optimum bead strength, lithium adsorption capacity and stability. The effect of water temperature, in which the beads are dripped into and CTAB concentration in water have minor contribution to the resulting form of the beads. The mixing time of 24 hours was fixed and used for all bead synthesis. Manganese oxide/PSMA ratio affects the final manganese oxide content of the beads, which directly affect the lithium adsorption capacity. In order to have the largest manganese oxide ratio in the resulting beads, the amount of the manganese oxide in the slurry was kept at maximum and the slurry was saturated with MnO_2 . NMP/PSMA ratio affects the viscosity of the slurry, shape and MnO_2 content of the resulting beads. When NMP amount is high, the beads are formed perfectly in spherical shape but the MnO_2 content of the beads decreases. When NMP amount is low, the viscosity becomes too high and it becomes difficult to form spherically shaped beads while dripping. Therefore a value of 2 was found as optimum PSMA/NMP ratio after series of trials. The resulting beads contain 51 % by weight manganese oxide.

PSMA polymer has never been used as a polymeric support material for any metal oxide bead preparation before. So this is the first study which examines the bead preparation by PSMA and its usage in lithium separation. In the previous methods, researchers use PVC [97], chitin [79], polyurethane [98] and water glass [99] as a binder, but there are two problems with those materials.

First problem was the weak strength (rigidity) of the resulting beads. The polymers do not crosslink in those studies, which results in weak mechanical properties and stability. On the other hand, eventual self-crosslinking property of PSMA in water during bead formation makes it unique as a metal oxide support material.

Second problem is the hydrophobic structure of the beads, which limit the diffusion of water into the beads and slow down the overall separation. On the contrary, PSMA beads swell in alkaline medium which increases the diffusion of water and ions into the beads and enhance the overall separation process. Self-crosslinking and swelling properties of the PSMA make it superior than any polymer binder employed up to now.

3.1.3.2 Characterization of PSMA content

The characterization of PSMA was done by FTIR and C-NMR techniques. FTIR spectrum of PSMA polymer is shown in Figure 3.18. At 950 cm^{-1} , O-H bending signal is observed. At 1770 cm^{-1} , C=O stretching and at 1450 cm^{-1} , C-H bending signals are observed. The results coincide with the literature findings [90]. FTIR spectrum is not enough to prove the structure of the polymer alone. It designates the presence of some characteristic bonds in the structure. However, spectrum is accepted as a fingerprint.

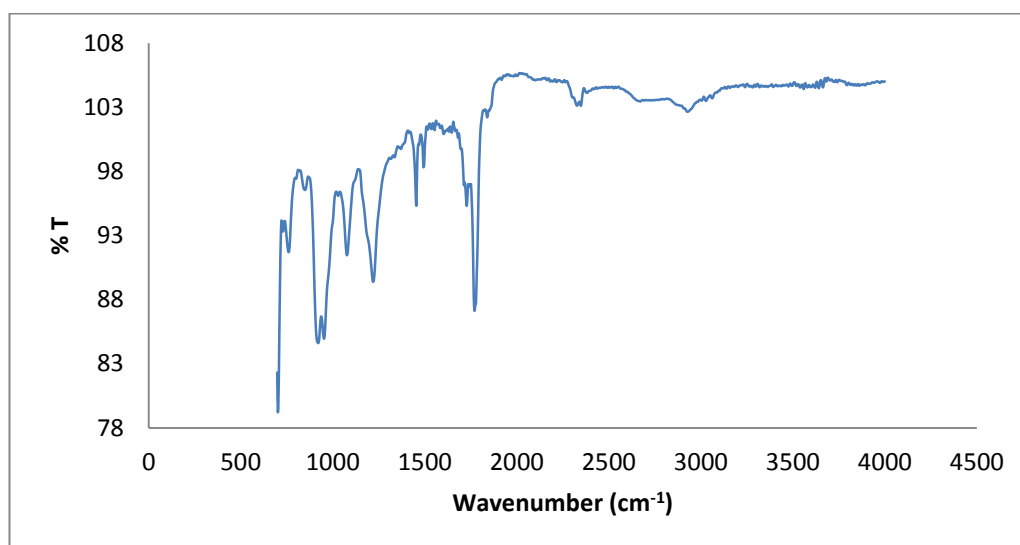


Figure 3.18 FTIR spectrum of poly (styrene-maleic anhydrid-glycidyl methacrylate) terpolymer (PSMA)

^{13}C -NMR spectrum of PSMA is shown in Figure 3.19. The signal at 165 ppm designates esteric carbonyl carbon in glycidyl methacrylate and maleic anydhride. The large signal at 125 ppm belongs to aromatic carbons in styrene. Wide signal between 5 and 60 ppm represents aliphatic carbons. Signal at 235 ppm shows the remaining ethyl methyl ketone carbonyl carbons.

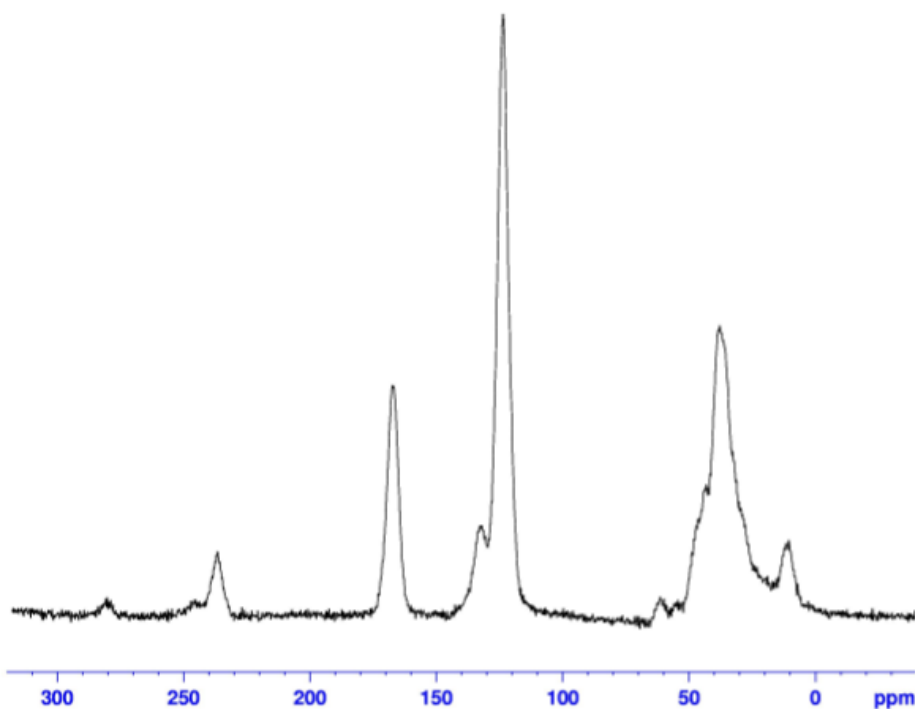


Figure 3.19 ¹³C-NMR spectrum of PSMA

3.1.3.3 Characterization of the PSMA-LiMnO beads

3.1.3.3.1 SEM characterization

In order to observe the effect of contents in PSMA-LiMnO bead morphology, a set of experiment was performed and the ingredients were changed according to Table 3.13.

Table 3.13 The amount of the components used in bead synthesis

Bead #	PSMA (g)	EMK (g)	NMP (g)	LiMnO (g)	% LiMnO in resulting bead
T14	2.62	0.5	3	1.1	52
T15	3	2	1	1	51
T16	3	-	1.5	1	51
T17	3.52	2	3.52	6	81
T18	3.4	2.68	2.26	6	82
T19	3.1	4.12	1.03	6	83
T20	3.38	2.68	2.26	1.5	58
T21	2.67	1.92	1.78	3	74
T22	3.1	4.12	4.12	6	84

After the synthesized beads were analyzed physically, it was seen that T17 and T18 lose their sphere shapes and become lentil shaped. The high manganese oxide content may induce that result. Bead T19 was precipitated like needles. Thin and long particles were formed. This behavior was attributed to the lack of NMP in slurry. Bead T20 was precipitated in leaf form rather than a sphere. The reason for that behavior was probably the lack of manganese oxide content in mixture. Bead T21 gave perfect sphere shapes. But unfortunately they coagulate in filter paper and could not retain their shapes. Bead T22 look similar to lentil shape. But the lentils were distracted. Bead T16 was the perfect ratio that we acquired in bead synthesis so far. Well-shaped spheres were acquired with high stability.

The SEM photographs of selected beads are shown below for T16, T18, T21 and T22. The remaining SEM photos are given in APPENDIX C.

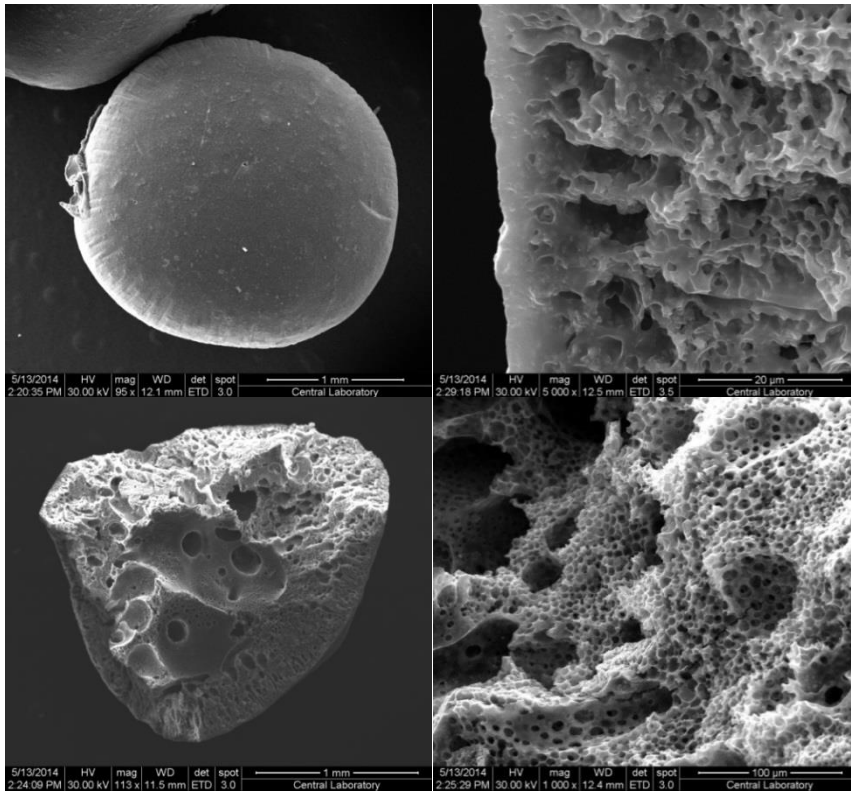


Figure 3.20 SEM photographs for Bead T16

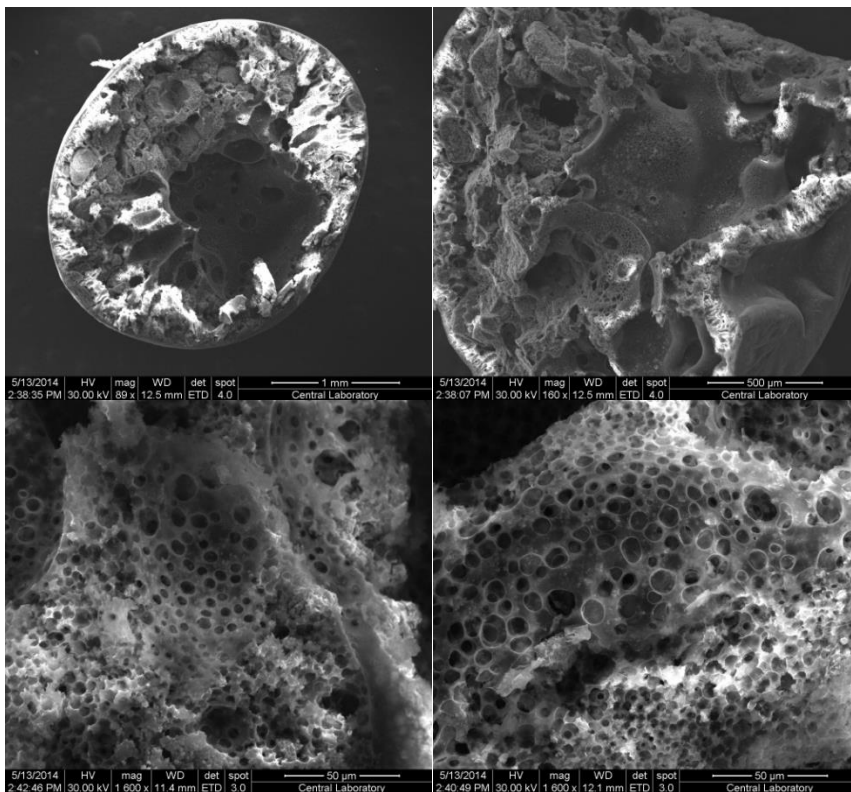


Figure 3.21 SEM photographs for Bead T16 after acid leaching

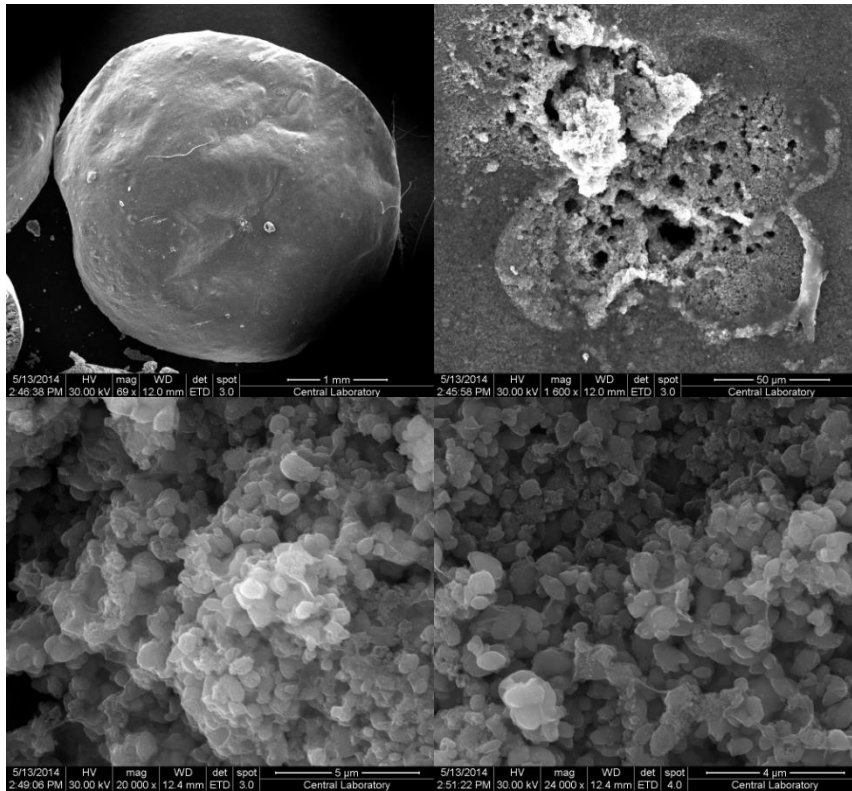


Figure 3.22 SEM photographs for Bead T18

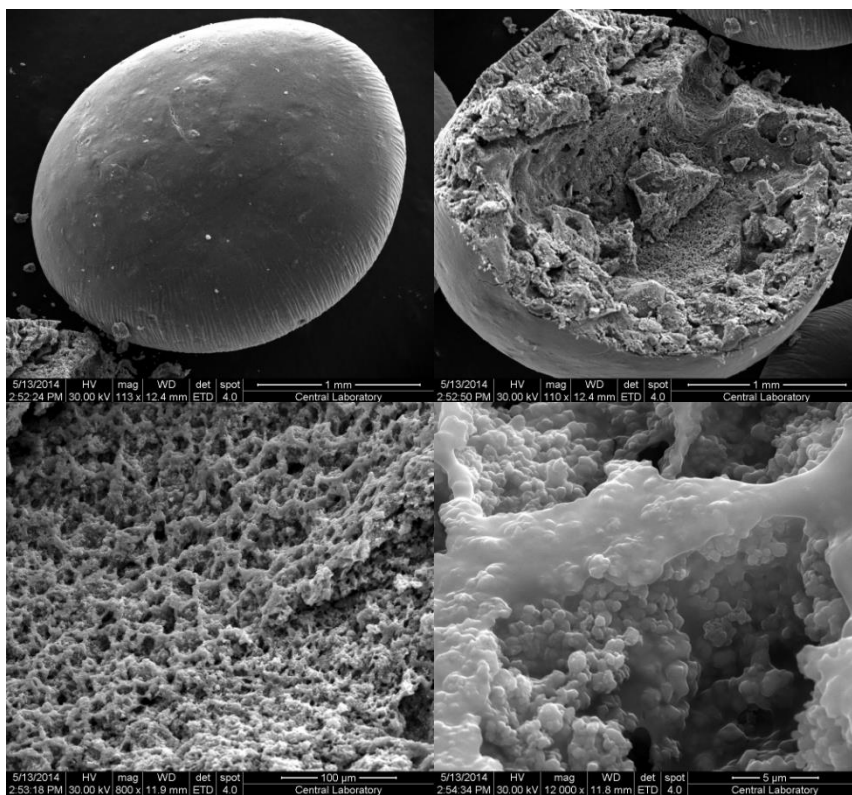


Figure 3.23 SEM photographs for Bead T21

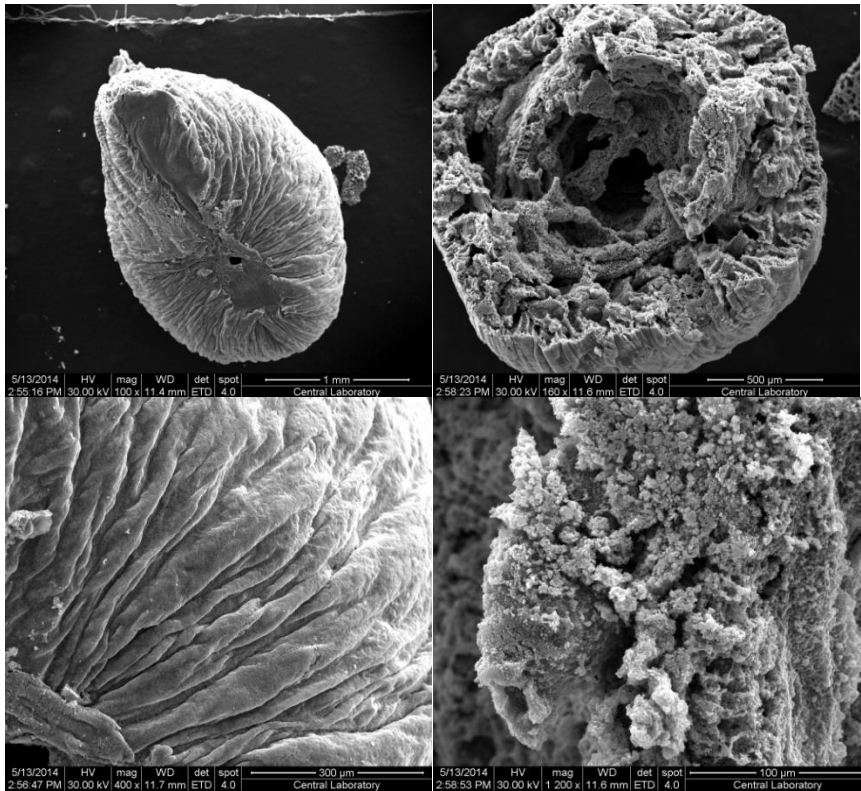


Figure 3.24 SEM photographs for Bead T22

SEM photographs describe that the beads have highly porous structure. The outer surface of the beads seemed to be covered by a smooth polymer layer. This layer holds the LiMnO particles inside the bead and let the diffusion of water and metal ions inside and outside of the particle. The bead morphology before and after acid leaching remains nearly same which designates the stability of bead structure towards acidic and basic conditions. When the beads absorb water especially in basic conditions by swelling, the porous structure inside the beads provide large surface area for adsorption.

3.1.3.3.2 BET measurements

BET measurements were done with beads T14, T15, T16, T16 after acid leaching, T18 and T21. The results were tabulated in Table 3.14

Table 3.14 BET results of PSMA-LiMnO beads

Bead #	Multipoint BET (m ² /g)	Cumulative Adsorption Pore Volume (ml/g)	Adsorption Pore Diameter (Å)
T 16	22.7	0.030	25.2
T 16 after acid leaching	35.14	0.104	10.7
T18	27.2	0.057	10.6
T21	21.9	0.037	10.9
T 22	10.95	0.023	34.9

* *BJH method was used in calculations of pore volume and diameter*

Table 3.14 shows that, the surface area of the beads changes between 10 to 35 m²/g. The maximum surface area was found as 35.14 m²/g for T16. It was also seen that after acid leaching the surface area, pore volume and pore diameter increases which produces additional mass transfer area.

After analyzing the visual observations during bead preparation and the results acquired in SEM and BET, Bead T16 was chosen to be employed in column experiments as it provides the perfect spherical shape, highest porosity, surface area, strength and stability.

3.1.4 Acquisition of lithium containing brines from nature

In addition to artificial lithium solutions prepared, following lithium containing aqueous solutions were obtained from nature.

3.1.4.1 Concentrated brine from Çamaltı Salina, İzmir

In Çamaltı Salina, 3.5 bome sea water is concentrated to approximately 30 bome in large ponds by utilizing solar energy. Corresponding plant is harvesting halite (NaCl) from the ponds for 3 months starting with September in every year. The samples of concentrated sea water were taken from the last pond where the water is finally pumped back to sea (it is the water with the highest salt concentration in Salina). The water samples are pink in color due to a halophilic algae which lives in

it. The algae is the dominant species in the water, and does not allow growing any other organic content. It was deduced that, calcium was absent in concentrated sea water. It is because of the precipitation of calcium ions in the form of calcium carbonate and sulfate during the evaporation in the ponds. The composition of the concentrated brine in Çamaltı Salina is tabulated in Table 3.15.

Table 3.15 The composition of the concentrated brine in Çamaltı Salina

Metal ion	Concentration (ppm) (mg/L)
Sodium	76750
Magnesium	21000
Calcium	-
Potassium	11023
Lithium	1.25

3.1.4.2 Preparation of boron clay extract from Bigadiç

Bigadiç has the largest boron reserves in the world. After boron is produced in mine, remaining residue (clay) is disposed to nature. The clay is called as ulexite and there is around 3000 ppm lithium content in the clay, mostly bounded to silicates ($\text{Li}_2\text{Si}_2\text{O}_5$). The conventional process to extract lithium from the clay needs hot temperature (900-1100 °C) roasting of clay with sodium sulfate which makes the process expensive and brings alternative economical methods into consideration. In order to take lithium into the solution directly, acid treatment is required. Mostly hydrochloric acid and sulfuric acid are used. In this study, the acid quantity and type used for leaching of lithium from the clays were optimized. In order to do that optimization, different volumes of different acids were mixed with clay under varying water content and time. The results were summarized in Table 3.16.

Table 3.16 Leaching of lithium ions from boron clay

Exp #	Acid type	Clay amount (g)	Acid/water (v/v)	Rxn. Time (h)	Li content in clay (g)	Li content in solution (ppm)	Li content in solution (g)	Extracted Li (%)
1	H ₂ SO ₄	50	15 /250	0.25	0.15	55	0.0275	18
2	H ₂ SO ₄	50	30 /300	0.50	0.15	242	0.121	81
3	H ₂ SO ₄	50	30/300	2	0.15	250	0.125	83
4	H ₂ SO ₄	50	30/300	43	0.15	279	0.1395	93
5	H ₂ SO ₄	50	45/250	2	0.15	283	0.1415	94
6	H ₂ SO ₄	50	60/300	2	0.15	287	0.1435	96
7	HCl	50	100/120	2	0.15	267	0.1335	89
8	HCl	50	100/120	20	0.15	284	0.142	95

After Table 3.16 is analyzed, it is seen that above 90 % of lithium can be extracted from clay. The remaining acid in the solution was found by 0.1 M NaOH titration and it was decided that, maximum amount of lithium leached by using minimum amount of acid was in the case of 30 ml H₂SO₄ and 300 ml water couple (Exp. 3).

The lithium solution acquired after filtering the solid content in the clay was very acidic. In order to use the solution in adsorption experiments NH₃ was added into the solution. After addition of ammonia, a white precipitate formed which was filtered afterwards. In this study the clay was treated with sulfuric acid prior to process in the column in order to take lithium ions into the aqueous phase. The final concentration of the clay extract is shown in Table 3.17

Table 3.17 The composition of the clay extract taken from Bigadiç

Metal ion	Concentration (ppm)
Sodium	4880
Magnesium	15110
Potassium	530
Lithium	388

3.2 Liquid-liquid extraction by N-alkyl formamides

Lithium chloride extraction experiments were carried out using either lithium chloride solutions in the absence or presence of foreign ions namely Na, K, Mg and Ca. The distribution factor, k was used for comparison of their extractabilities and the selectivities. The distribution factor (Nernst distribution coefficient) is defined as follows,

$$\text{Distribution coefficient } (k) = \frac{\frac{\text{Solute amount in extract phase } (E)}{\text{Amount of phase } E}}{\frac{\text{Solute amount in raffinate phase } (R)}{\text{Amount of phase } R}}$$

Equal volume of water and formamide (10 mL of each) were used in all experiments for the sake of simplicity.

In order to make precise estimation for the extractability from pure lithium chloride solutions, the extraction experiments were performed at various pH and temperature conditions.

Table 3.18 shows LiCl distribution coefficients of the formamides at pH: 4.0, 7.0 and 10.0. The results tabulated, imply that hexyl formamide is the best for the extraction of LiCl at pH 4 and 10. The results also show that the formamides exhibit very little changes of LiCl extraction in between pH 4 and 10.

The low pH dependency observed is somewhat surprising, because if the polar formamide group involves in dipole-dipole interaction with lithium ion, one must observe pH dependency for the extraction due to blocking of non-bonding electrons of oxygen with proton. The reverse situation might be due to nearly equal affinity of Li^+ and protons towards formamide group.

The highest extraction capability of hexyl formamide is most probably due to its low molecular weight which means maximum formamide content per unit mass.

Table 3.18 The effect of pH on distribution coefficient of LiCl for the formamides at 25 °C, 10 ml water/10 ml formamide ratio (The initial LiCl concentration was 1.4 M)

Formamide	pH	Distribution coefficient
Hexyl formamide	4	0.14
	7	0.12
	10	0.14
Octyl formamide	4	0.08
	7	0.05
	10	0.06
Dibutyl formamide	4	0.04
	7	0.04
	10	0.06

(1.4 M Li solution preparation: Dissolve 5.95 g of LiCl in 100 ml volumetric flask)

Table 3.19 represents LiCl distribution coefficients of the formamides at different temperatures namely 10, 25, 40 °C. The results show that, distribution coefficients increases with decreasing temperature. The extraction experiments could only performed with dihexyl formamide at 40 °C.

Table 3.19 The effect of temperature on distribution coefficient values for different formamides at pH:4, 10 ml water/10 ml formamide ratio, initial lithium concentration of 1.4 M Li.

Formamide	Temperature (°C)	Distribution coefficient
Hexyl formamide	10	0.16
	25	0.14
	40	0.11
Octyl formamide	10	0.09
	25	0.08
	40	0.07
Dibutyl formamide	10	0.04
	25	0.04
	40	0.03
Dihexyl formamide	40	0

In order to understand the effect of temperature on extraction process, standard enthalpy change (ΔH^0) and standard entropy change (ΔS^0) can be predicted using the Van't Hoff equation:

$$\ln k = -\frac{\Delta H^0}{RT} + \frac{\Delta S^0}{R} \quad \text{Eqn. 5}$$

The values of standard enthalpy change and entropy change were calculated from the slope and intercept of Von't Hoff plot respectively (See Figure 3.25). In the equation k is the distribution coefficient, R is the universal gas constant and T is the absolute temperature. The R^2 values calculated in linear regression are 0.9631, 0.9958 and 0.7244 for hexyl formamide, octyl formamide and dibutyl formamide respectively.

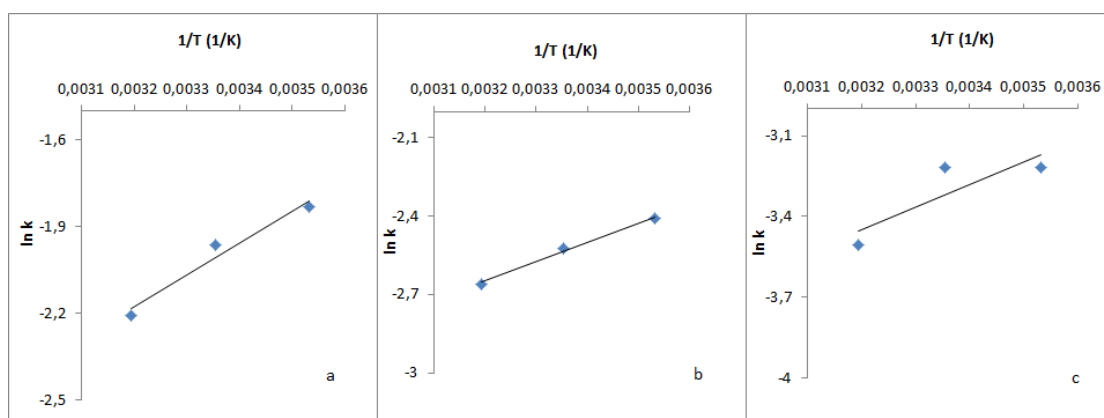


Figure 3.25 Van't Hoff Plots for hexyl formamide (a), octyl formamide (b), dibutyl formamide (c)

The calculated values of ΔH^0 and ΔS^0 were tabulated in Table 3.20. The change in enthalpy values in extraction was found negative which implies the process is exothermic in nature. The increase in distribution coefficients with respect to decreasing temperature confirms the findings. The negative values of ΔS^0 indicates decrease in disorder in the system during extraction. Therefore the extraction of LiCl with formamides is enthalpy driven process.

Table 3.20 ΔH° and ΔS° values calculated from Van't Hoff plots

Formamide	ΔH° (kJ/mol)	ΔS° (J/mol.K)
Hexyl formamide	-9.16	-47.40
Octyl formamide	-6.16	-41.75
Dibutyl formamide	-6.94	-50.89

The effects of initial lithium concentration and volume ratio of water to formamide towards distribution coefficients were represented in Figure 3.26. The extracted lithium was plotted against initial concentration at different formamide/water volume ratios as depicted in Figure 3.26. It is clearly seen that the distribution coefficients do not change with the volume ratios indicating typical Nernst extraction behavior. The initial LiCl concentration however greatly effects on the distribution coefficient so that when concentration is increased from 100 ppm to 10000 ppm, the extracted lithium increases 80 percent. This can be explained in terms of high ionic strength effect.

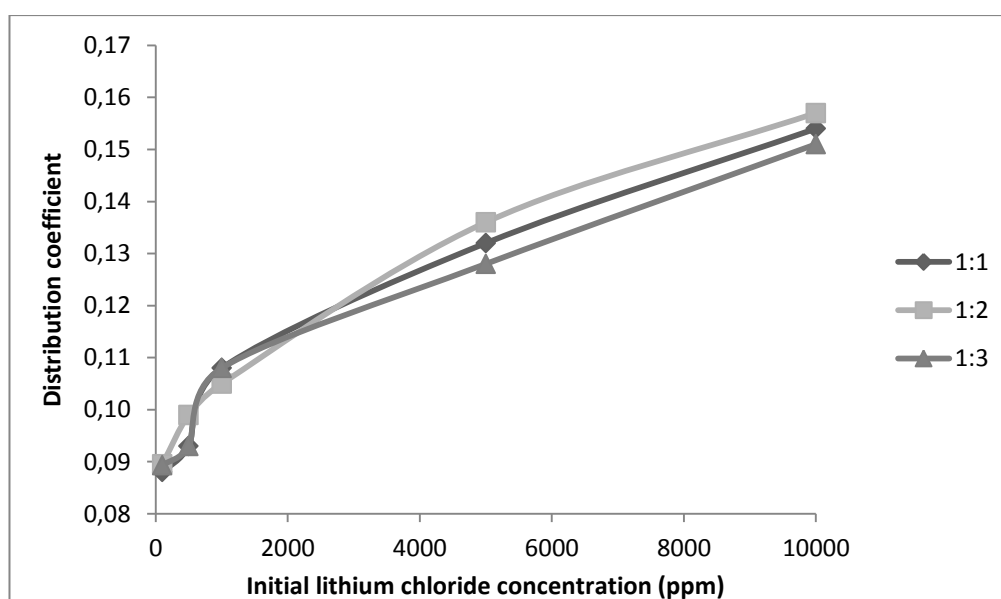


Figure 3.26 Effect of initial LiCl concentration on k of hexyl formamide at pH:4. The plots were drawn for three different water/formamide volume ratios (1:1, 1:2, 1:3) at 10 °C.

The high concentration range (100-10000 ppm Li) covered here was considered to be insufficient for the extraction of low concentrated solutions. For a better

understanding of the extraction from dilute solutions, a series of experiment were carried out in which initial Li concentration was varied from 10 to 100 ppm. The results obtained are given in Table 3.21.

Table 3.21 Equilibrium data between extract and raffinate phase for the formamide-water-lithium chloride system at 25 °C, pH: 4 and 10 ml water/10 ml hexyl formamide

Water phase			Formamide phase		
Li (ppm)	Water (%)	Formamide (%)	Li (ppm)	Water (%)	Formamide (%)
11.250	98.467	1.533	0.749	15.870	84.129
21.940	98.459	1.541	1.488	15.953	84.047
32.967	98.462	1.538	2.915	15.747	84.253
41.073	98.453	1.547	3.825	15.755	84.245
52.246	98.463	1.537	5.738	15.804	84.195
61.022	98.477	1.523	7.160	16.218	83.781
73.369	98.478	1.522	8.043	14.995	85.005
81.611	98.472	1.528	8.412	15.396	84.603
90.126	98.468	1.532	8.619	15.596	84.403
103.312	98.508	1.492	10.763	16.053	83.946

The data tabulated in Table 3.21 helps to identify the extraction equilibria more precisely and construct a guide to a possible extraction column design.

Ternary system of hexyl formamide-water-lithium chloride is drawn in dilute lithium chloride region. It is deduced that the formamide fraction in water phase and water fraction in formamide phase do not vary much with respect to lithium concentration. Therefore the resulting data was fitted to a two dimensional chart rather than a ternary diagram and shown in Figure 3.27.

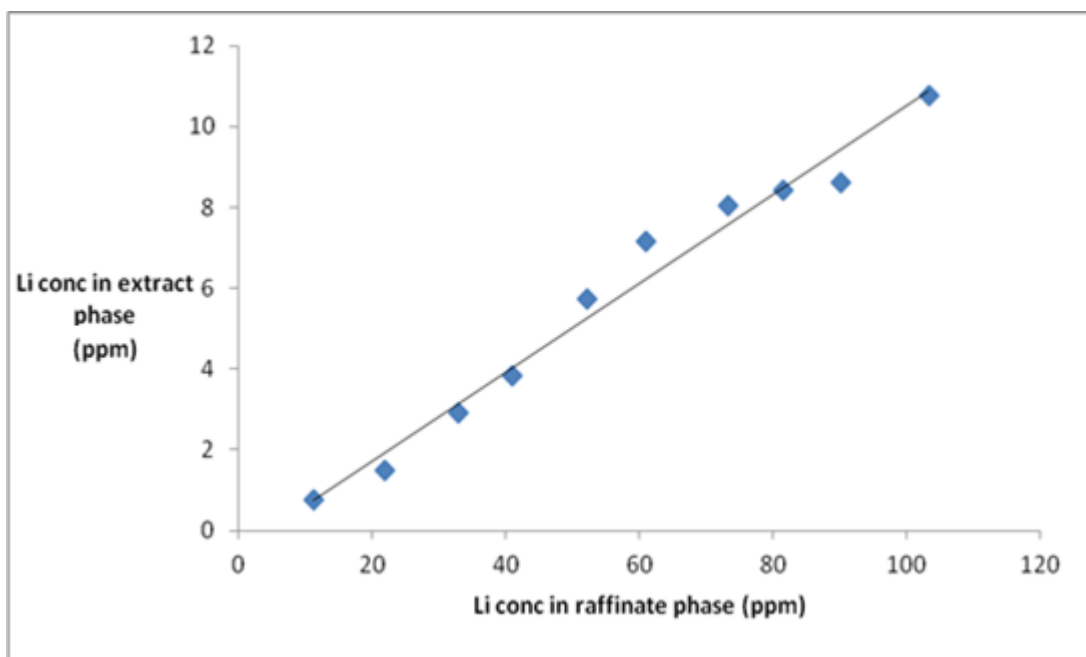


Figure 3.27 The lithium concentration in extract (formamide) and raffinate (water) phases at 25 °C and pH:4 for 10 ml water/10 ml hexyl formamide

The lithium concentration in extract phase and raffinate phase can be fitted in a linear equation with an R^2 value of 0.978 in below.

$$y = 0.11x - 0.48 \quad \text{Eqn. 6}$$

Where y is lithium concentration in formamide phase and x is the lithium concentration in water phase, in ppm..

The behavior of the lithium uptake by hexyl formamide remains constant while lithium concentration changes in dilute regime.

Selectivity:

Selectivity of hexyl formamide towards lithium ion in the presence of sodium, potassium, calcium and magnesium ions was investigated with an artificially concentrated sea water. The artificial sea water was prepared by following the

procedure in ASTM D1141. In seawater sample, sodium, potassium, magnesium and calcium ions have the highest concentration with 10770, 380, 1290, 412 ppm respectively. The lithium ion concentration is so small as around 0.17 ppm. In Salinas, seawater is concentrated for ten times larger than its initial concentration. Therefore, the artificial seawater used in selectivity measurements was evaporated at 25 °C until its weight gets 10 % of its initial weight. In the selectivity experiments, temperature was kept constant at 25 °C and 10 ml hexyl formamide/ 10 ml water was used. The experiments were repeated for acidic (pH:4) and basic (pH:10) conditions. The distribution coefficient of HeFo towards lithium and foreign ions (Na, K, Mg, Ca) with the final composition of artificially concentrated seawater were listed in Table 3.22.

Table 3.22 Artificial concentrated seawater composition and the resulting distribution coefficient values in selectivity experiments.

Metal ion	Artificial concentrated sea water composition (mg/L)	Distribution coefficient (pH:4)	Distribution coefficient (pH:10)
Sodium	62810	0.058	0.048
Magnesium	6940	0.21	0.16
Calcium	3523	0.4	0.43
Potassium	5270	0.06	0.07
Lithium	2.1	0.12	0.11

The selectivity values which were found by dividing distribution coefficients into each other were listed in Table 3.23.

Table 3.23 The selectivity values of hexyl formamide for lithium near foreign (Na, K, Mg, Ca) ions in sea water.

	pH:4				pH:9			
	$S_{Li/Na}$	$S_{Li/Mg}$	$S_{Li/K}$	$S_{Li/Ca}$	$S_{Li/Na}$	$S_{Li/Mg}$	$S_{Li/K}$	$S_{Li/Ca}$
Selectivity	2.07	0.57	2.00	0.30	2.29	0.69	1.57	0.26

Table 3.22 and Table 3.23 imply that the selectivity of HeFo towards lithium compared to potassium and sodium are higher than 1 but lower than 1 for calcium and magnesium ions. The selectivity values do not change very much with respect to changes in pH like in the case of distribution coefficients. Following the calculation of the selectivity values for artificial sea water, selectivity experiments were conducted by the real concentrated brine samples taken from Çamaltı Salina, İzmir. The initial solution composition and acquired distribution coefficients were listed in Table 3.24.

Table 3.24 Composition of the concentrated sea water taken from Çamaltı Salina and resulting distribution coefficients (25 °C, 10 ml HeFo/10 ml water, pH:7.4)

Metal ion	Concentration (ppm) (mg/L)	Distribution coefficient	Selectivity values ($k_{lithium}/k_{metal}$)
Sodium	76750	0.01	7.8
Magnesium	21000	0.09	0.86
Calcium	-	-	-
Potassium	11023	0.01	7.8
Lithium	1.25	0.078	1

Table 3.24 shows that the distribution coefficient values are lower than the values in the experiments conducted for the artificial sea water. The reason of decrease in the values may be additional foreign ions present in sea water, which may compete with lithium ions and reduce the extraction amount. Eventually the distribution coefficient value was found as 0.078 for hexyl formamide, still larger than n-butanol, which shows the solvation power of hexyl formamide.

Regeneration of formamides:

The regeneration of formamides was done by using hydrochloric acid solution at different pH. After the extraction process, the resulting formamides were taken in a separate flask and mixed with acid solution. Following the vigorous shaking at 25 °C in a separation funnel, 1 hour was allowed in order to have phase separation completely. The results were tabulated in Table 3.25.

Table 3.25 The effect of pH on recovery of lithium from hexyl formamide

Hexyl formamide amount (g)	C _o ^(a) (ppm)	Acid volume (ml)	C ^(b) (ppm)	pH of the solution	The percent recovery of LiCl (%)
10	1.6	10	0.15	1	91
10	1.6	10	0.16	2	90
10	1.6	10	0.19	3	88
10	1.6	10	0.14	4	92

(a) Initial Li concentration in hexyl formamide, (b): Final Li concentration in hexyl formamide.

It is seen that the pH of the acidic solution used to recover lithium from hexyl formamide does not affect the percent recovery amount which is around 90 %.

The recovery of lithium ions from hexyl formamide can be further repeated by addition of acidic solutions into remaining hexyl formamides. The recovery amount is again observed as 90 % as shown in Table 3.26.

Table 3.26 The effect of pH on recovery of lithium from hexyl formamide (Second recovery)

Hexyl formamide (g)	C _o ^(a) (ppm)	Acid volume (ml)	C ^(b) (ppm)	pH solution	The recovery of LiCl (%)
10	0.15	10	0.015	1	90
10	0.16	10	0.016	2	90
10	0.19	10	0.02	3	89
10	0.14	10	0.013	4	91

(a): Initial Li concentration in hexyl formamide, (b): Final Li concentration in hexyl formamide

The recovery of lithium chloride from hexyl formamide was done also by using 1 M hydrochloric acid solution. In that case 93 % of lithium can be recovered from hexyl formamide phase. The recovered lithium can be further precipitated as lithium carbonate by adding equal molar soda ash.

3.3 Adsorption via lithium manganese oxide adsorbents

Among the various synthesis methods and reactants, lithium manganese oxide with the maximum capacity value was synthesized by Solid-Solid-2 procedure in which employs manganese carbonate and lithium hydroxide monohydrate was employed as precursors. The performance of the adsorbents was evaluated by the experiments conducted with variable pH and initial lithium chloride concentration.

3.3.1 Effect of pH on adsorption

In order to investigate the effect of pH on capacity values of LiMnO adsorbents, a series of experiments were conducted under varying pHs.

Table 3.27 Capacity values of adsorbents at different pHs (Total volume: 100 ml, Adsorbent amount: 0.02 g)

pH	Initial Li conc. (ppm)	Final Li conc. (ppm)	Capacity (mg Li/g adsorbent)
6.3	9.02	7.98	5.2
7.3	9.02	7.66	6.8
8.2	9.02	7.51	7.6
9.3	9.02	6.12	14.5
10.2	9.02	4.46	22.8

Table 3.27 shows that, pH of the adsorption medium strictly affects the performance of the adsorbents. As pH increases from 6.3 to 10.2, the capacity values increases from 5.2 to 22.8 mg Li/g adsorbent. This effect is mainly caused by the competition between the lithium ions and hydrogen ions due to the nature of ion exchange/adsorption process. When hydrogen ion concentration is high (i.e., at low pH), H^+ ions have a high chance to replace Li^+ ions. At high pH range, H^+ concentration is low, then lithium ions have higher chance for attachment to the adsorbent. Therefore, the capacity of the adsorbents increases with increasing pH values.

3.3.2 Effect of initial lithium concentration on adsorption

Similar to pH, the effect of initial lithium concentration on capacity values of the adsorbents were investigated by performing a set of experiments under varying initial lithium chloride concentrations.

Table 3.28 Capacity value of the adsorbents at different initial lithium concentrations (pH:10.2 and adsorbent amount: 0.02 g)

Initial Li conc. (ppm)	Final Li conc. (ppm)	Capacity (mg Li/g)
4.73	0.14	22.8
8.36	3.99	21.6
44.89	40.4	22.9

Table 3.28 shows that the initial lithium concentration does not affect the capacity value of the adsorbents. In other words the lithium concentration in the medium does not affect the total lithium amount adsorbed on the particle. This behavior implies that the mass transfer limitations around the particle and inside the particle are not significant to affect the thermodynamic limits of the adsorption process within given time (24 h). The small particle size and high porosity of the adsorbents reduces the mass transfer resistance.

3.3.3 Kinetics of the adsorption process

The kinetics of the adsorption process was studied with five identically prepared mixtures by measuring the uptake amount of lithium at different times. The initial lithium concentration was 10 ppm, pH was 10.2 and 0.02 g of adsorbent was used for each parallel experiment.

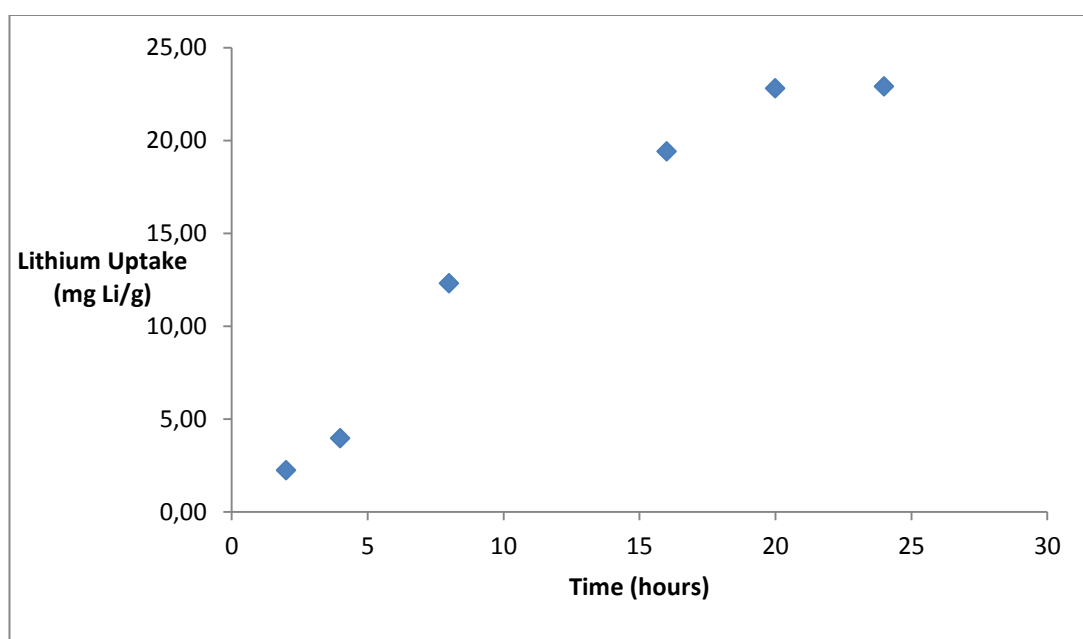


Figure 3.28 The kinetics of adsorption process

It is seen in Figure 3.28 that, the adsorption process is completed in 20 hours with the maximum lithium uptake value of 22 mg Li/g adsorbent. When the results in Table 3.28 and Figure 3.28 were evaluated together, it was seen that the same uptake value of 22 mg Li/g was acquired for both the experiments having initial lithium concentration of 4.73 and 10.0 ppm Li in 24 h. If the mass transfer limitations

govern the kinetics of the process, one must find a lower value for initial lithium concentration of 4.73 ppm Li. The equal values of uptake ratio for different initial lithium concentrations, at equal adsorption times validate the negligible mass transfer limitation in the process.

3.3.4 Equilibrium Isotherms

Equilibrium isotherm calculations were done with solutions containing different initial lithium concentrations between 1 and 5 ppm.

Equilibrium concentration of lithium in solution with respect to uptake value is shown in Figure 3.29.

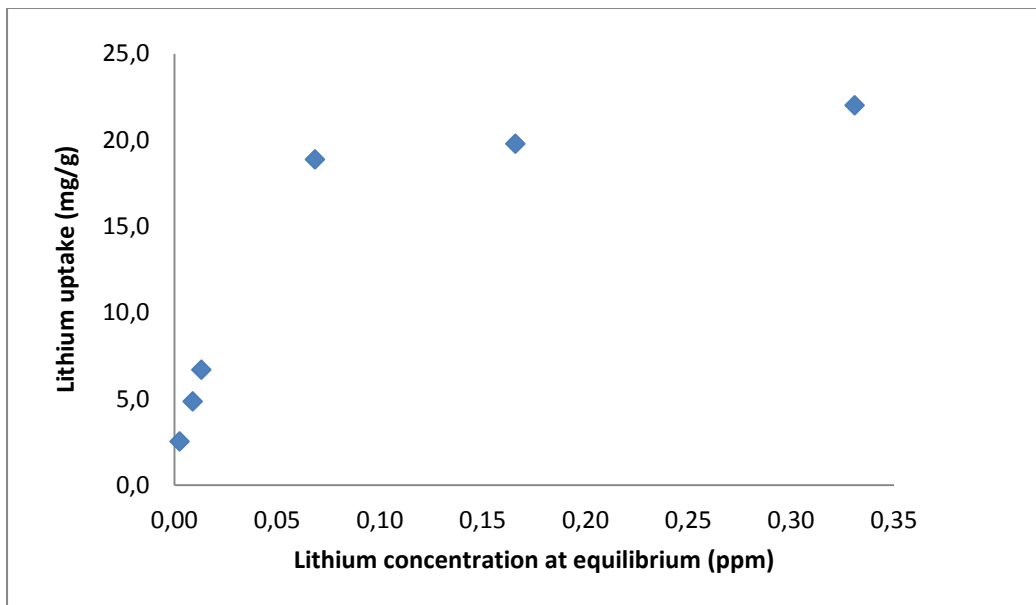


Figure 3.29 The equilibrium concentration of lithium in solution vs uptake of lithium ions

- Langmuir Isotherm

The general Langmuir isotherm equation is shown below;

$$\frac{C_e}{Q_e} = \frac{1}{K_{ads} \cdot Q_m} + \frac{C_e}{Q_m} \quad \text{Eqn. 7}$$

Here,

C_e : Lithium concentration in solution at equilibrium (mg/L)

Q_e : Uptake amount of lithium at equilibrium (mg/g)

K_{ads} : Empirical equilibrium constant (L/mg)

Q_m : Theoretical maximum adsorption capacity (mg/g)

According to the data labeled in Figure 3.29, the Langmuir isotherm curve is drawn and shown in Figure 3.30 with a best line having R^2 value of 0.997.

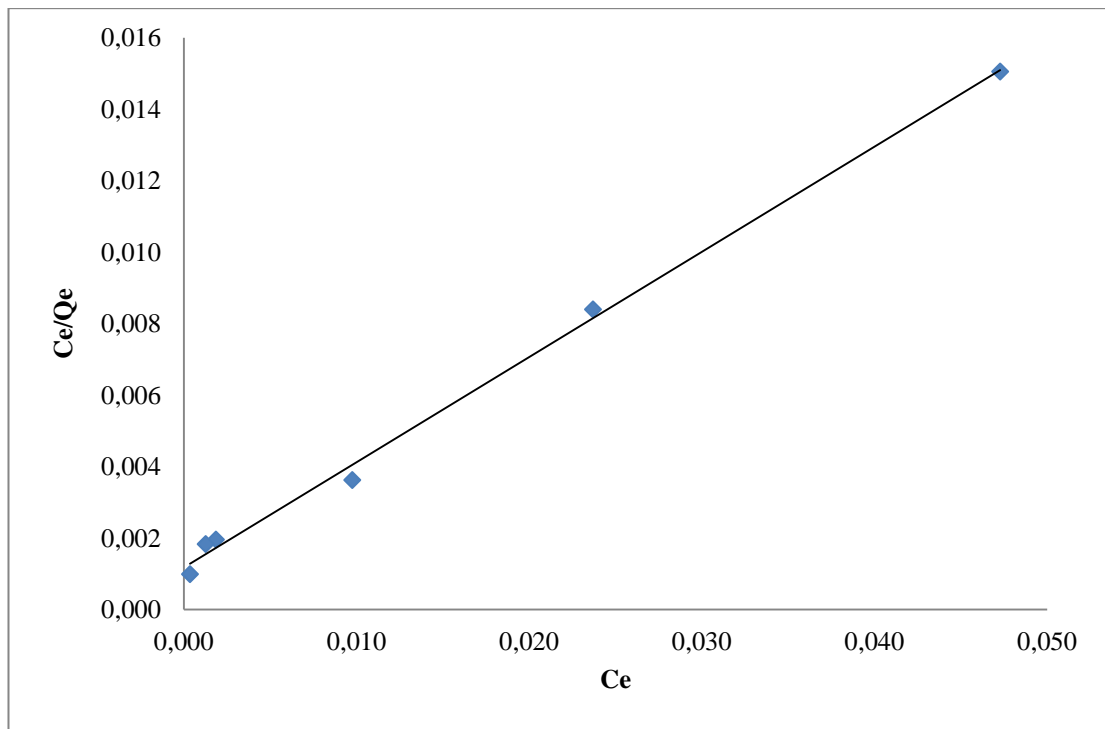


Figure 3.30 Langmuir isotherm curve for LiMnO at 25 °C.

The equation of the best line is,

$$\frac{C_e}{Q_e} = 0.2944C_e + 0.0012 \quad \text{Eqn. 8}$$

Q_m value was found as 3.4 mg/g and K_{ads} was found as 184.8 L/mg. K_{ads} value was higher than values cited in the literature, but there is a contradiction in the K_{ads} values at different studies [83], [85], [100]. This difference in K_{ads} values may result in insufficiency of Langmuir isotherm to explain what is happening in separation process. The ion exchange mechanism and surface adsorption mechanism are two possible mechanisms taking place simultaneously in the process. The maximum uptake value was found as 3.37 mg Li/g, which should be around 20 mg Li/g according to the previous experiments.

- Freundlich isotherm

Freundlich isotherm equation is shown below,

$$Q_e = K_f \cdot C_e^{1/n} \quad \text{Eqn. 9}$$

Where, K_f indicates relative capacity and n indicates adsorption intensity.

By taking the logarithm of both sides, the equation shown below is acquired,

$$\log Q_e = \log K_f + \frac{1}{n} \cdot \log C_e \quad \text{Eqn. 10}$$

The log Q_e vs log C_e plot is shown in Figure 3.31 with a best line having R^2 value of 0.9504.

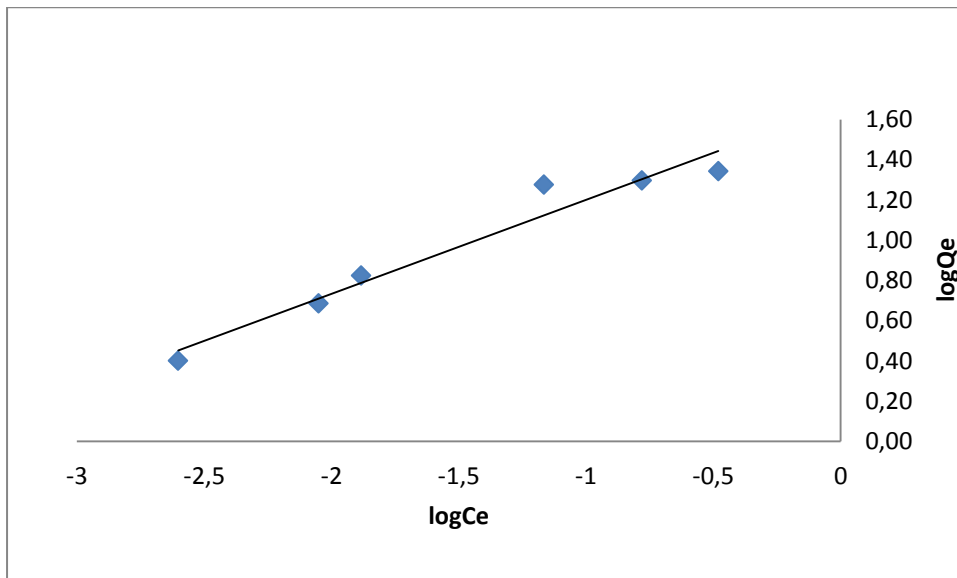


Figure 3.31 Freundlich isotherm curve for LiMnO at 25 °C.

The slope gives $1/n$, n value was found as 2.14, which means high tendency of lithium ions towards manganese oxide particles. The intercept value was equal to $\log(K_f)$ which gives K_f as 45.7 L/mg. The Freundlich isotherm actually works for dilute systems, thus fits to the concerning system with R^2 value of 0.95.

3.3.5 Stability experiments

In order to understand the stability of lithium manganese oxides, a cycle of adsorption and desorption with lithium chloride feed solution and hydrochloric acid leaching solution was repeated. The experiment was started with the adsorption of 5 ppm lithium chloride following by the desorption with 0.5 M HCl and continues with the adsorption of lithium chloride. This cycle was repeated for six times and the loss of capacity in the adsorbents was tabulated in Table 3.29.

Table 3.29 The stability of lithium manganese oxide particles in lithium recovery

Cycle no	Capacity (mg Li/g ads.)	Capacity change with respect to first cycle (%)
1	21.1	100
2	20.7	98.1
3	20.1	95.3
4	19.8	93.8
5	19.6	92.9
6	19.4	92

As it can be deduced from Table 3.29, the capacity of the adsorbents was decreased by around 1 % in each additional cycle. If these values were extrapolated linearly, the half-life of the adsorbents was found at 50th. adsorption-desorption cycle. The mechanism of adsorption in lithium manganese oxides is explained by ion exchange or redox reactions occurring in crystal structure. The exchange of ions in the crystal is happening in tapotactic way which means there is no distortion of the crystal lattice due to interchange of the ions. Treatment of LiMnO with acid causes the removal of nearly all the lithium from the tetrahedral sites while maintaining a spinel-type structure stable. However it is also known that, Mn (IV) atoms are placed in octahedral sites of the adsorbent crystal and transition metal atoms at octahedral

position may result in Jahn-Teller distortion [72], [87]. This distortion leads the crystal to lower its energy which is favorable. In lithium manganese oxide, this type of distortion may cause tiny distractions in crystal lattice and result in a loss of capacity of the adsorbent.

3.3.6 Selectivity experiments

The selectivity experiments were conducted by a feed solution which consists of equal concentration of lithium, sodium, potassium and magnesium ions at pH:10. The results and conditions of the experiments were tabulated in Table 3.30.

Table 3.30 Selectivity of lithium manganese oxides with respect to Na, K and Mg.

Metal ion	Feed solution (ml)	Initial Conc. (ppm)	Final Conc. (ppm)	Adsorbent amount (g)	Capacity (mg ion/g adsorbent)	Selectivity with respect to lithium
Li	100	9.60	0.77	0.051	17.31	1
Na	100	9.68	9.35	0.051	0.64	0.037
K	100	10.37	9.57	0.051	1.38	0.08
Mg	100	9.40	8.75	0.051	1.30	0.075

Table 3.30 shows that, lithium manganese oxide adsorbent has strong selectivity towards lithium; 27 times higher than sodium, 12.5 times higher than potassium and 13.3 times higher than magnesium ions. The relatively high selectivity for Li^+ can be explained by the ion-sieve effect of the spinel lattice with a three-dimensional (1×3) tunnel, suitable in size for fixing Li^+ in cubic phase MnO_2 ion sieves obtained from LiMnO precursors, yet other metal ions can only adsorb on the adsorbent surface sites because of their large ionic radii, similar to the cases of the MnO_2 ion-sieves in other studies [77], [87]. Moreover the tapotactic insertion-desertion mechanism of Li^+ ions in the crystal lattice does not let other ions to take place of the lithium ions. This ability of the adsorbent makes it unique for selective lithium separation operations compared to other candidate chemicals.

3.4 Separation of lithium by PSMA-LiMnO beads in an adsorption column

Column experiments with PSMA-manganese oxide adsorbents were first done with artificial brine solutions in order to quantify the column performance. The main parameters that affect the performance of the column are pH, feed concentration, flow rate and particle size of the beads. The column dimensions and adsorbent amount was fixed for all experiments.

All the experiments were performed with the same bead which was labeled as T16. The MnO₂ content of T16 is 51 %. The column diameter is 20 mm, the column height is 385 mm and total weight of the beads is 38.5 g. Bead size is 3mm in size unless otherwise stated.

3.4.1 The breakthrough plots for solutions containing lithium chloride only

3.4.1.1 Effect of pH

The most critical parameter that affects the behavior of adsorption process is pH. As explained in Section 3.3.1, increase in pH strictly improves the capacity of LiMnO particles. On the other hand, the swelling ratio of PSMA content in the beads increases at high pH. Swelling of the beads increases the transfer rate of lithium ions in and out, however reduces the flow rate in the column. At pH values higher than 9, flow in the column was even cut down by the expansion of the beads. Therefore the maximum pH value was determined as pH:9.0 by the restriction of swelling behavior of the beads. The minimum pH value was chosen as 7.5, where the activity of LiMnO particles becomes significant.

Three experiments were performed at pH: 7.5, 8.2 and 9.0. The column conditions were tabulated in Table 3.31.

Table 3.31 The column operating conditions for the pH dependency of adsorption process

Run #	Feed Li conc. (ppm)	Feed buffer content*	Feed pH	Average flow rate (ml/min)	Total processed solution (ml)	Outlet initial and final pH
1	20	0.23/1.65	7.5	15	14440	2.25 - 2.98
2	20	0.33/1.65	8.2	15	14440	2.25 - 3.21
3	20	0.48/1.65	9.0	15	16350	2.25 - 3.45

*($m\text{LiNH}_3(25\%)/g\text{NH}_4\text{Cl}$)

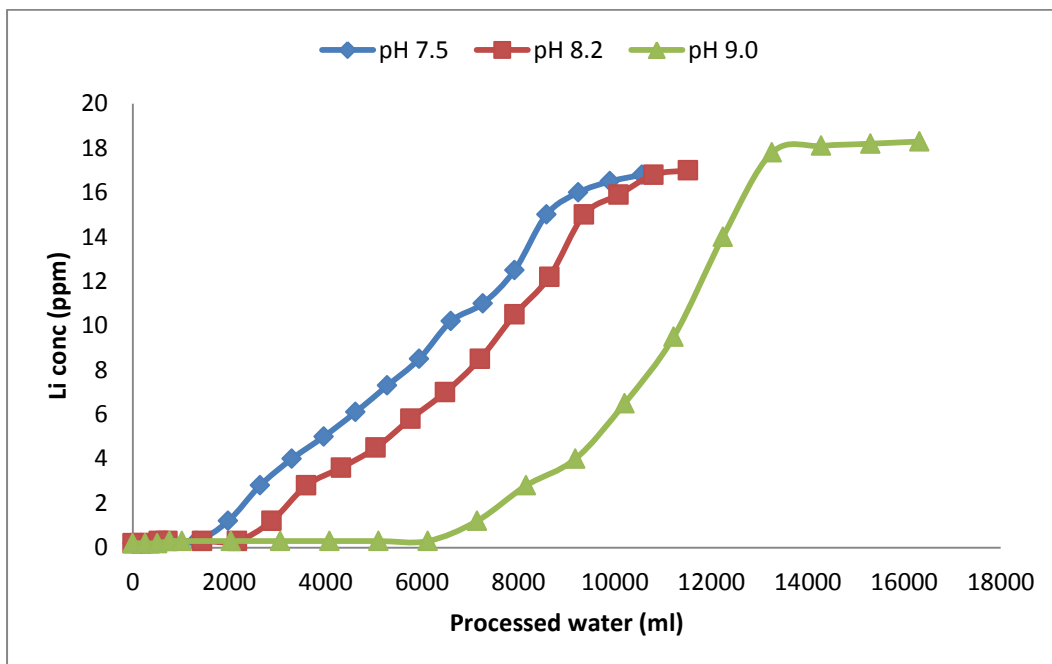


Figure 3.32 The breakthrough curves at different pH values

Figure 3.32 shows the behavior of the breakthrough curves at different pH values. As pH increases, curves shift to the right and become steeper. The higher capacity of LiMnO at higher pH values leads to this behavior. The capacity values were calculated as 128.8, 148.8 and 221.2 mg Li for pH 7.5, 8.2 and 9.0 respectively while the theoretical capacity values were 137.5, 153.2 and 235.6. The capacity values increase according to theoretical capacity values which implies that the process has low/negligible mass transfer limitation.

3.4.1.2 Effect of initial lithium concentration

The lithium concentration in brines as natural lithium sources varies from 0.17 ppm (sea water) to 1500 ppm (Salar de Atacama, Chile). The lithium concentration in feed solutions does not change the performance of the column but affects the shape of the breakthrough curves. In order to observe this effect, three runs were carried out by changing the concentration in feed solution. The conditions are shown in Table 3.32.

Table 3.32 The column operating conditions for different initial lithium concentration in adsorption process

Run #	Feed Li conc. (ppm)	Feed buffer content*	Feed pH	Average flow rate (ml/min)	Total processed solution (ml)	Outlet initial and final pH
4	5	0.48/1.65	9	15	14440	2.25 – 3.45
3	20	0.48/1.65	9	15	16350	2.25 – 3.45
5	120	0.48/1.65	9	15	21110	2.25 – 3.45

*($mlNH_3(25\%)/gNH_4Cl$)

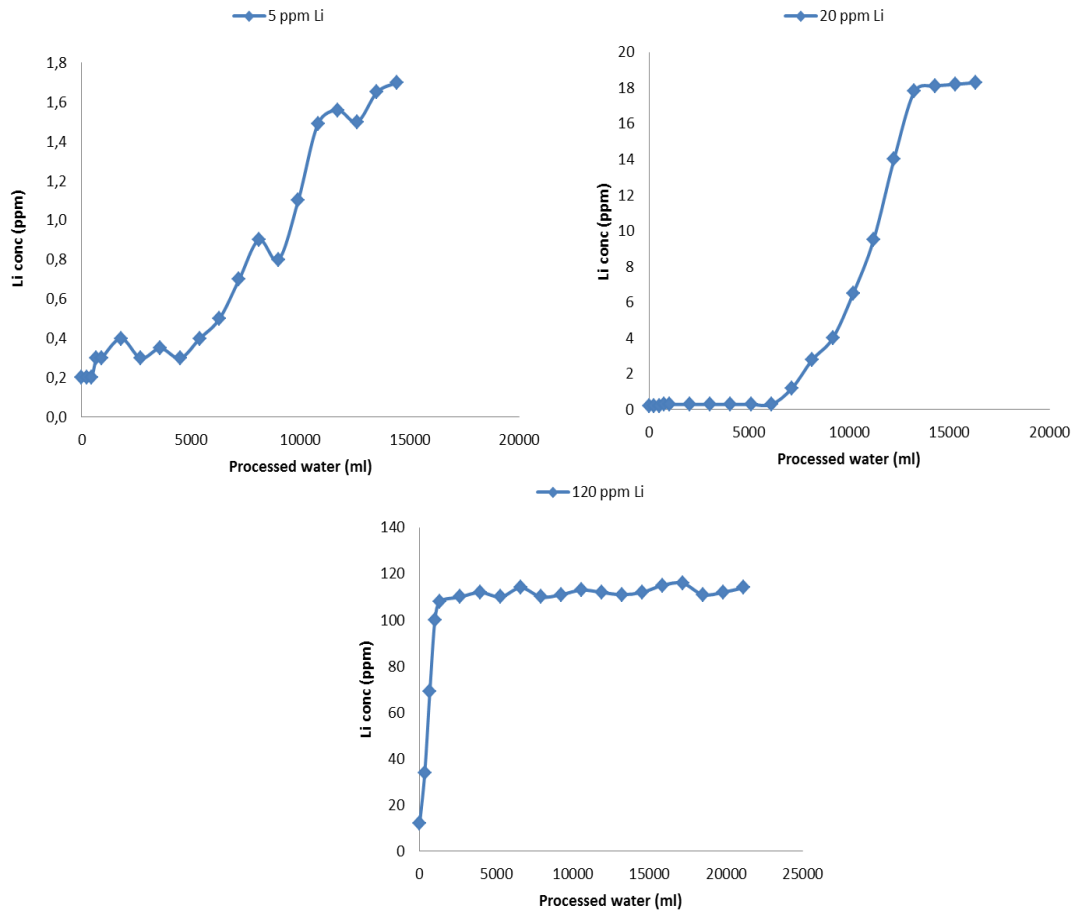


Figure 3.33 The breakthrough curves at different initial lithium concentrations.

Figure 3.33 shows the change in shapes of the breakthrough curves with respect to change in initial lithium concentration. At 5 ppm, the curve has many small fluctuations and cannot reach the saturation in the end. The capacity of the column was found as 60.1 mg Li which is 26 % of the theoretical capacity. At 20 ppm initial concentration, a smooth breakthrough curve is observed and the capacity is found as 212.2 mg Li (94 % of the theoretical capacity). At 120 ppm, the curve has a sharp increment at the beginning of the process and reaches to its final concentration. The breakthrough behavior cannot be observed. The capacity value was found as 230.0 mg Li which is 98 % of the theoretical capacity. The column capacity reaches near to its saturation point in fast and effective way. As the initial lithium concentration increases from 5 to 120 ppm, the curves get steeper as expected. In the scope of

lithium recovery, in order to separate more lithium from brines, feeding the column until its saturation becomes important.

3.4.1.3 Effect of flow rate

In order to show the effect of flow rate on breakthrough curves, a series of experiments were conducted. The operating conditions for the experiments are listed in Table 3.33.

Table 3.33 The column operating conditions for different flow rates in adsorption process

Run #	Feed Li conc. (ppm)	Feed buffer content	Feed pH	Average flow rate (ml/min)	Total processed solution (ml)	Outlet initial and final pH
6	20	0.48/1.65	9	5	4800	2.25 – 3.15
3	20	0.48/1.65	9	15	16350	2.25 – 3.45
7	20	0.48/1.65	9	30	28800	2.25 – 4.10

*(mlNH₃(25%)/gNH₄Cl)

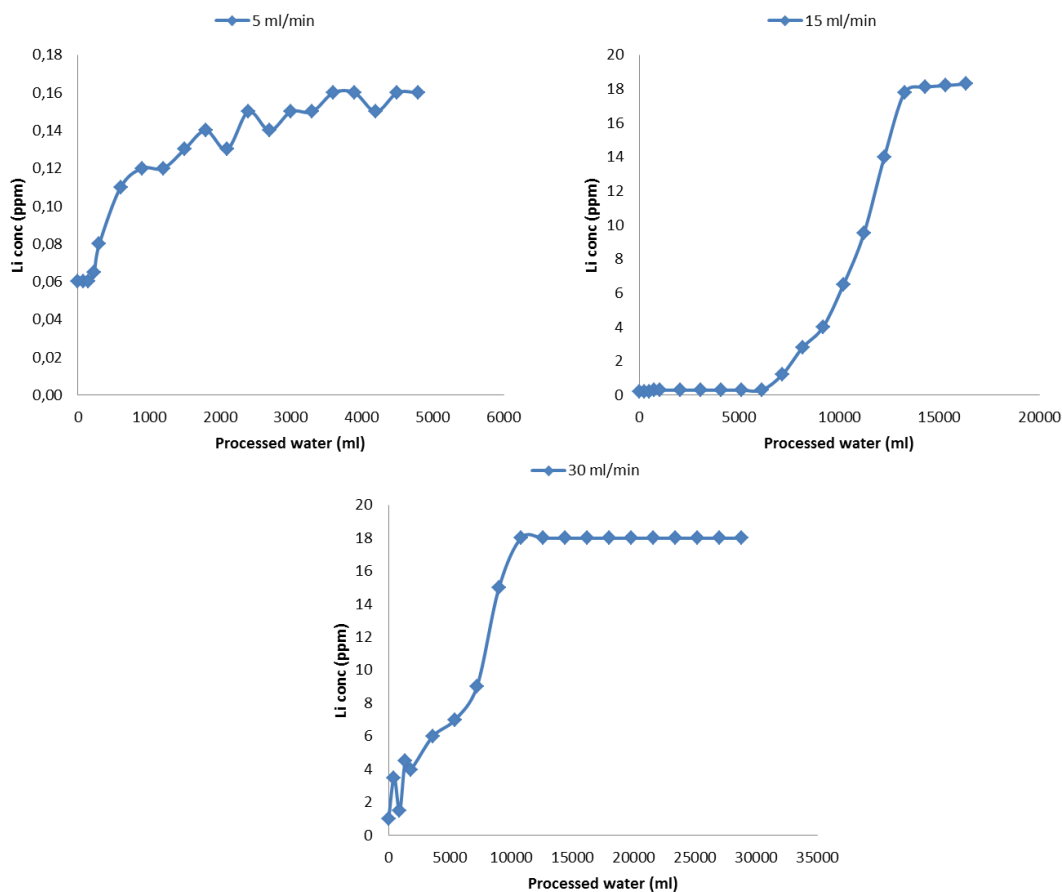


Figure 3.34 The breakthrough curves at different flow rates.

Figure 3.34 shows the effect of increasing flow rates on breakthrough behavior. Under 5 ml/min flow rate, the breakthrough cannot be reached similar to the case in 5 ppm Li feed. Lithium concentration in the effluent of the column is below 0.16 ppm during the process and the column capacity was calculated as 95.35 mg Li. The low lithium concentration in the effluent is due to the increasing space time of the lithium solution in the column. As flow rate increases to 30 ml/min, the space time decreases hence, curves become steeper. The oscillations observed in initial stages of the process are attributed to the channeling or dead volume effect. The column capacity is calculated as 160.2 mg Li, which is 68 % percent of the total theoretical capacity. The percent saturation of the column is smaller than expected, probably due to the low space time in the process. The breakthrough curve at 15 ml/min seemed to be the ideal one to observe the breakthrough point and the general characteristics of the adsorption column.

3.4.1.4 Effect of bead size

The size of the beads in the column may change the performance of the system due to mass transfer effects. In order to investigate the effect of bead size on efficiency of the column, two experiments were carried out with two columns filled with different size of beads. The operating parameters of the columns are tabulated in Table 3.34.

Table 3.34 The column operating conditions for different bead sizes in adsorption process

Run #	Feed Li conc. (ppm)	Feed buffer content*	Bead size (mm)	Feed pH	Average flow rate (ml/min)	Total processed solution (ml)	Outlet initial and final pH
3	20	0.48/1.65	3	9	15	16350	2.25 – 3.45
8	20	0.48/1.65	8	9	15	10560	2.25 – 4.10

*($mlNH_3(25\%)/gNH_4Cl$)

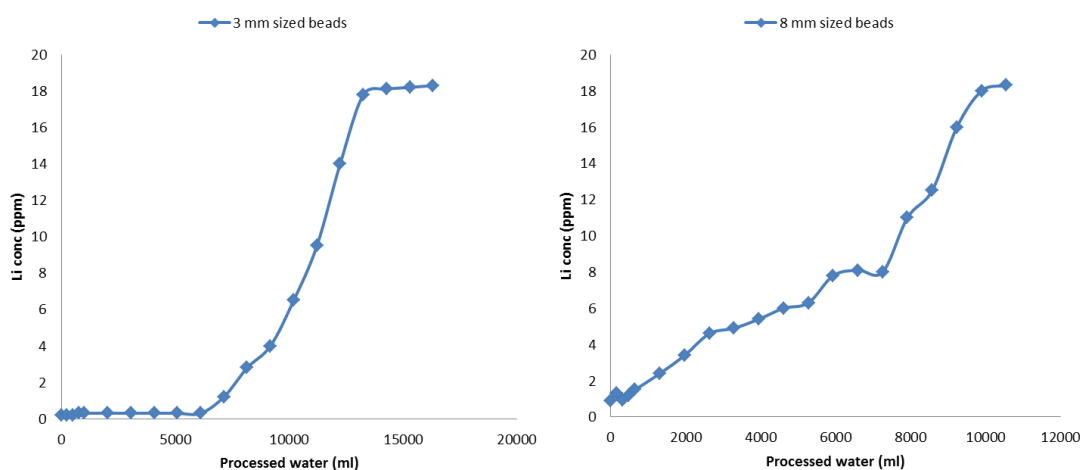


Figure 3.35 The breakthrough curves for different bead sizes

Figure 3.35 shows the effect of bead size and mass transfer clearly. When bead size is increased from 3 mm to 8 mm, the breakthrough curve becomes broader. It is important to note that as the bead size increases, the PSMA content in the beads increases and LiMnO content decreases. 8 mm sized beads can only hold 43 % LiMnO content, while 3 mm sized beads can hold 51 % LiMnO. This brings additional barrier to the diffusion of lithium ions through the beads which have higher PSMA content. Also decrease in the total mass transfer area in the system

leads the broadening of the breakthrough curve. In case of 3 mm sized beads, larger amount of beads can be used in filling the same volume. In this case, 38.5 g of 3 mm sized beads can be filled with 35.4 g of 8 mm sized beads. The capacity usage in each case also validates the findings. In 3 mm sized beads, the capacity of the column is calculated as 221.2 mg Li which is 94 % of the theoretical capacity. Meanwhile the capacity of column filled with 8 mm sized beads is found as 128.4 mg Li which is 70 % of the theoretical capacity. Another significant fact is employing 3 mm sized beads in 20 mm diameter column. The ratio of column diameter to bead diameter is around 7 and coincides with the ratio of 8 mentioned as rule of thumb for adsorption column experiments.

3.4.2 The breakthrough plots for solutions containing foreign ions

Lithium chloride sources are generally poor in lithium content but reach in NaCl, KCl and MgCl. The behavior of adsorbents with solutions containing foreign ions (Na, K, Mg) is questioned in this section. Sodium chloride, potassium chloride and magnesium chloride are very rich in sea water with respect to lithium chloride. For instance, sea water contains 0.17 ppm Li besides 10800 ppm Na, 1290 ppm Mg and 390 ppm K at 3.5 % salinity. Before feeding the column with the mixture of ions, the adsorption capacity of the beads for each foreign ion was analyzed individually. The conditions of the experiments were arranged similar to experiments done with lithium chloride solutions.

3.4.2.1 The breakthrough curve for sodium chloride feed solution

The conditions of the experiments were given in Table 3.35.

Table 3.35 The column operating conditions for feed solutions containing NaCl

Run #	Feed Na conc. (ppm)	Feed buffer content*	Feed pH	Average flow rate (ml/min)	Total processed solution (ml)	Outlet initial and final pH
9	10.1	0.48/1.65	9	15	14440	1.84-3.75

*($m\text{NH}_3(25\%)/g\text{NH}_4\text{Cl}$)

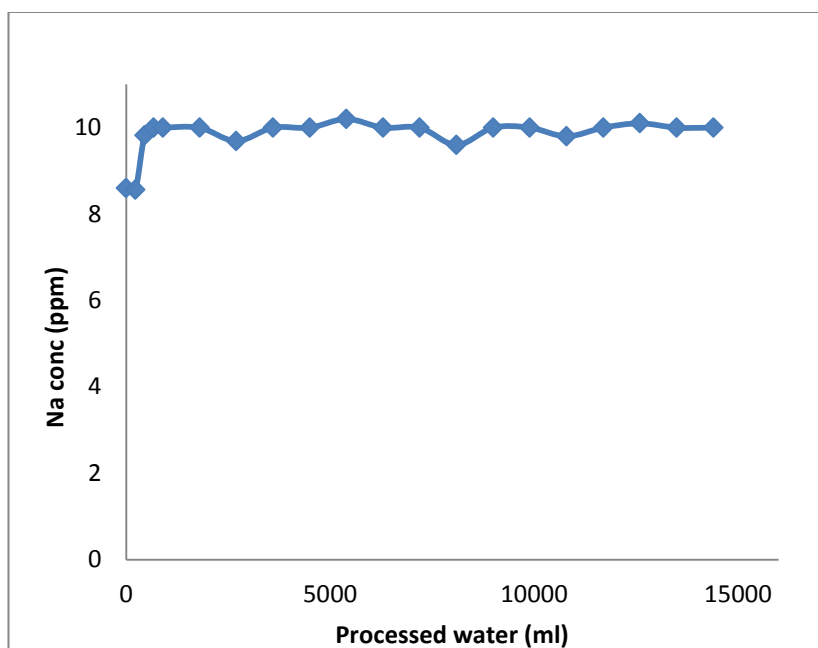


Figure 3.36 The breakthrough curve for sodium chloride feed solution

Figure 3.36 shows that the outlet concentration of the column suddenly reaches to the concentration of the inlet which depicts that the affinity of the adsorbent towards sodium is very low. Generally, a mass transfer zone can be observed in the very first part of the curve which results in a gradual increase in the effluent ion composition. The sudden increase in the composition was attributed to the very low affinity of the beads towards sodium. The capacity of the column was calculated as 2.51 mg Na which was 88 times less than the capacity value for lithium (221.2 mg Li). The adsorption capacity of single LiMnO towards Na was 27 times less than for Li. The selectivity of the beads in column operation towards lithium ions is three times larger with respect to batch operation with single LiMnO.

3.4.2.2 The breakthrough curve for potassium chloride feed solution

The conditions of the experiment were given in Table 3.36.

Table 3.36 The column operating conditions for feed solutions containing KCl

Run #	Feed K conc. (ppm)	Feed buffer content*	Feed pH	Average flow rate (ml/min)	Total processed solution (ml)	Outlet initial and final pH
10	10.3	0.48/1.65	9	15	14440	1.94-3.37

*(mlNH₃(25%)/gNH₄Cl)

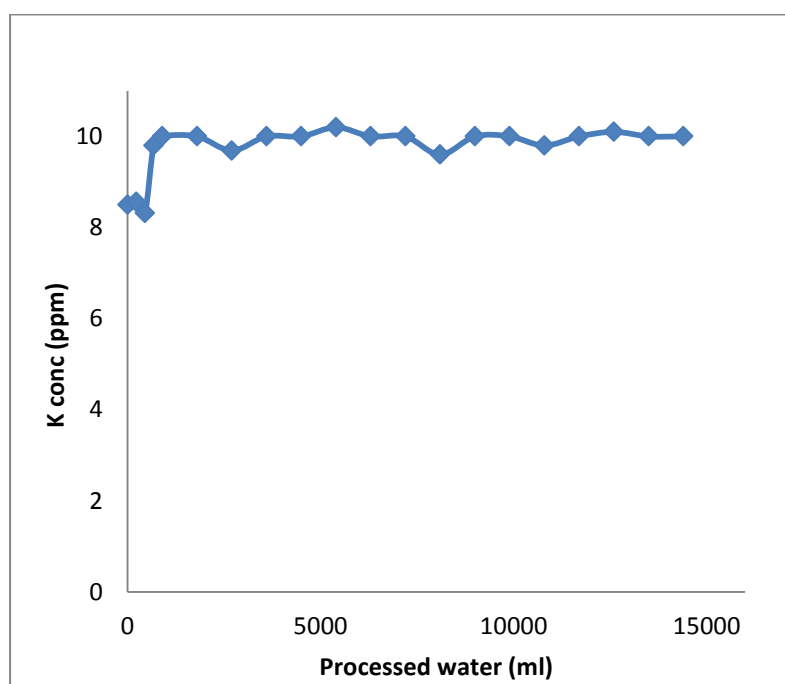


Figure 3.37 The breakthrough curve for potassium chloride feed solution

It is seen from Figure 3.37 that the affinity of the adsorbent towards potassium ions is very low similar to sodium ion. The capacity of the column was found as 5.78 mg K which was 38 times less than the capacity value for lithium. The adsorption capacity of single LiMnO towards K was 12.5 times less than for Li. The selectivity of the beads in column operation towards lithium ions was three times larger with respect to batch operation with single LiMnO similar to the case with sodium.

3.4.2.3 The breakthrough curve for magnesium chloride feed solution

The conditions of the experiment were given in Table 3.37.

Table 3.37 The column operating conditions for feed solutions containing MgCl

Run #	Feed Mg conc. (ppm)	Feed buffer content*	Feed pH	Average flow rate (ml/min)	Total processed solution (ml)	Outlet initial and final pH
11	11	0.48/1.65	9	15	14880	1.05-3.43

*(mlNH₃(25%)/gNH₄Cl)

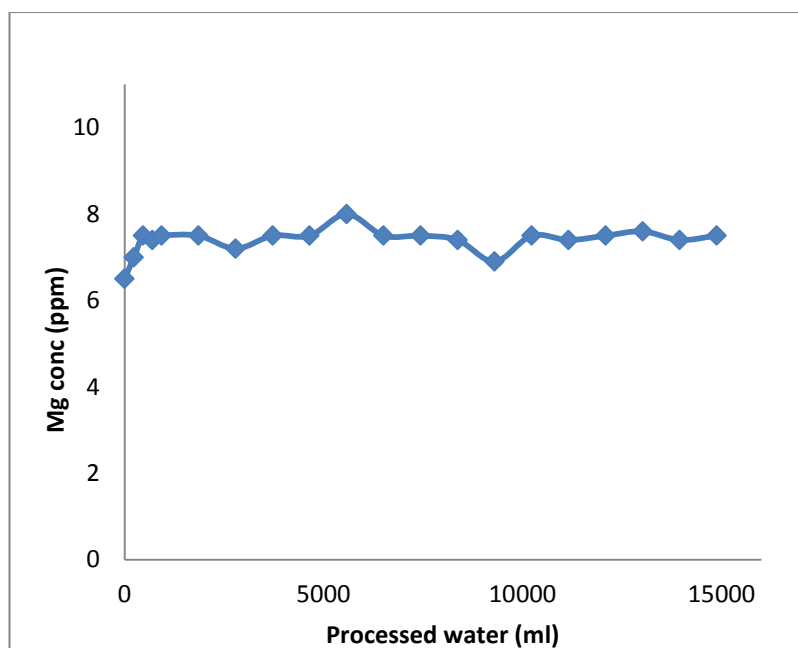


Figure 3.38 The breakthrough curve for magnesium chloride feed solution

In Figure 3.38, it is seen that the outlet of the column does not reach the inlet magnesium concentration. Magnesium ions were adsorbed by the beads partially. The capacity of the column was calculated as 52.9 mg Mg which was 4.2 times less than the capacity value for lithium. The adsorption capacity of single LiMnO towards Mg was 13 times less than for Li, but the selectivity of the beads in column operation towards lithium ions get decreased. The reason of this decrease was attributed to the PSMA content in the beads. The polar OH groups in PSMA may attract the Mg ions and lead to this unexpected result.

3.4.3 The breakthrough plots for the artificial and real brine solutions

The concentrated sea water in Çamaltı Salina (İzmir) and the extract from boron clay in Bigadiç (Balıkesir) are two potential lithium sources that were studied in this thesis work. The concentration of lithium ion in concentrated sea water and boron clay extract is much lower than foreign ion concentration in those solutions.

In order to describe the behavior of LiMnO-PSMA beads when opposed to high salt concentrations, an artificial brine solution of concentrated sea water was prepared first and the following experiments were conducted.

3.4.3.1 The breakthrough plots for the artificial brine solutions

Artificially prepared brine concentration and the experimental conditions were given in Table 3.38.

Table 3.38 The column operating conditions for artificial brine solutions

Run #	Feed solution conc. (ppm)	Feed buffer content*	Feed pH	Average flow rate (ml/min)	Total processed solution (ml)	Outlet initial and final pH
12	0.43 ppm Li 53430 ppm Na 4464 ppm K 9210 ppm Mg	0.2/1.65	8.1	15	37164	0.5-2.52

*(mlNH₃(25%)/gNH₄Cl)

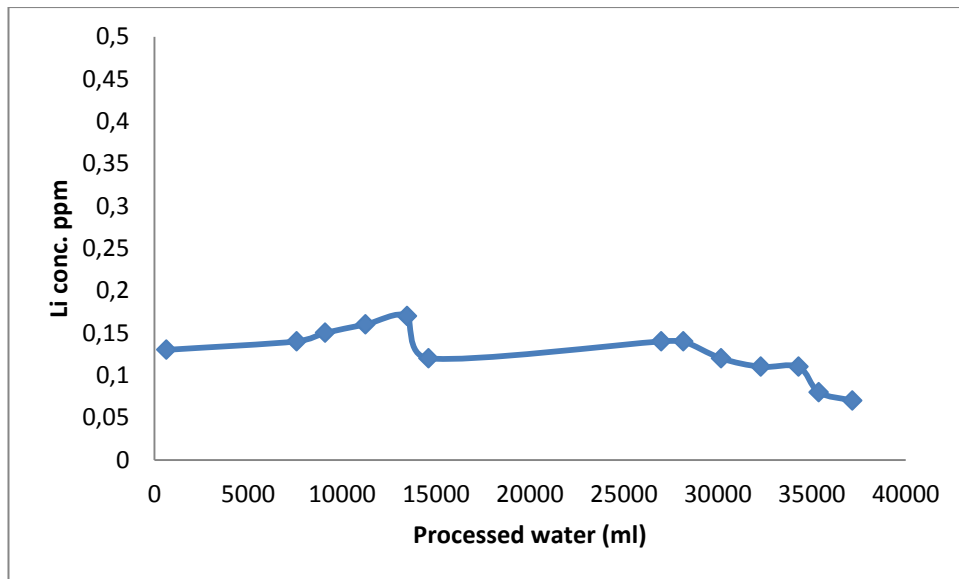


Figure 3.39 The effluent lithium concentration in a column fed with artificially prepared brine solution

Figure 3.39 shows that the outlet concentration of the column oscillates around 0.1 ppm through the experiment. The high ionic strength of the feed solution due to high concentrations of the foreign ions probably plays the major role in this behaviour. The capacity of the column was found as 11.2 mg Li. Breakthrough curves for Na, K and Mg cannot be observed. Due to high concentration of those ions, the feed concentration was suddenly observed in the outlet of the column.

3.4.3.2 The breakthrough plots for the real brine solutions

3.4.3.2.1 The breakthrough plot for concentrated sea water taken from Çamaltı Salina

The sea water in Çamaltı Salina is concentrated around 9 to 10 fold during NaCl production in playa and salt concentration becomes 35 Bome. The concentration of the sea water and the operational conditions of the column were given in Table 3.39.

Table 3.39 The column operating conditions for concentrated brine solution taken from Çamaltı Salina

Run #	Feed conc. (ppm)	Feed pH	Average flow rate (ml/min)	Total processed solution (ml)	Outlet initial and final pH
13	1.25 ppm Li	8.1	15	11473	0.5-2.84
	76750 ppm Na				
	11023 ppm K				
	21000 ppm Mg				

*(mlNH₃(25%)/gNH₄Cl)

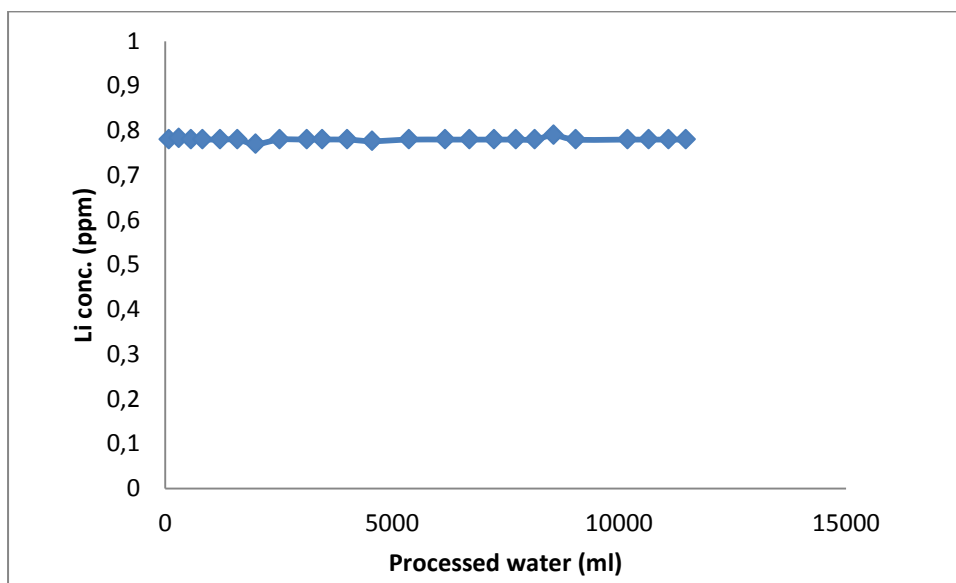


Figure 3.40 The effluent lithium concentration in a column fed with concentrated brine solution from Çamaltı Salina

Figure 3.40 shows that the lithium concentration at the outlet remains constant at 0.78 ppm through the experiment. The capacity of the column was calculated as 5.39 mg Li. The behavior of the column is very similar to the case in artificial brine. The high ionic strength of the concentrated sea water probably suppressed the capacity of the adsorbent by forming an ionic layer around the beads. The breakthrough behavior for the foreign ions was observed similarly to the case in artificial brine solution and the concentration in the outlet of the column suddenly increased to the concentration of the inlet stream.

3.4.3.2.2 The breakthrough plot for boron clay extract taken from Bigadiç

The concentration of the clay extract and the operating conditions are given in Table 3.40.

Table 3.40 The column operating conditions for boron clay extract taken form Bigadiç

Run #	Feed conc. (ppm)	Feed pH	Average flow rate (ml/min)	Total processed solution (ml)
14	388 ppm Li	8.73	15	780
	4880 ppm Na			
	530 ppm K			
	15110 ppm Mg			

The total volume of the boron extract was low to feed to the column continuously; therefore the feed solution was fed to the column in batchwise, where the outlet of the column was circulated back to the feed tank. After 8 h of operation, the following concentrations listed in Table 3.41 were measured for the initial and final concentration in the feed tank.

Table 3.41 The initial and final concentrations in the feed tank before and after the operation

Run #	Li	Na	K	Mg
Run 14 initial conc. (ppm)	388	4880	530	15110
Run 14 final conc. (ppm)	105	4250	460	12400

Table 3.41 shows that nearly 75 percent of the lithium content in the clay extract is adsorbed by the beads. However, besides lithium, sodium and magnesium ions were also adsorbed by the beads, which affect the selectivity of the total process negatively. The selectivity analysis of the process will be covered in following sections.

3.4.4 Recovery of lithium and regeneration of the beads

The recovery of lithium and regeneration of the beads were done with 0.5 M HCl. This process is generally called “elution process” and functions to interchange hydrogen ions with lithium ions and regenerate the beads while recovering lithium. Elution of the columns fed with different feed solutions was analyzed separately.

3.4.4.1 Elution of the column fed with solution having lithium chloride only

The elution was first done with the column fed with solution containing lithium chloride in Run 3.

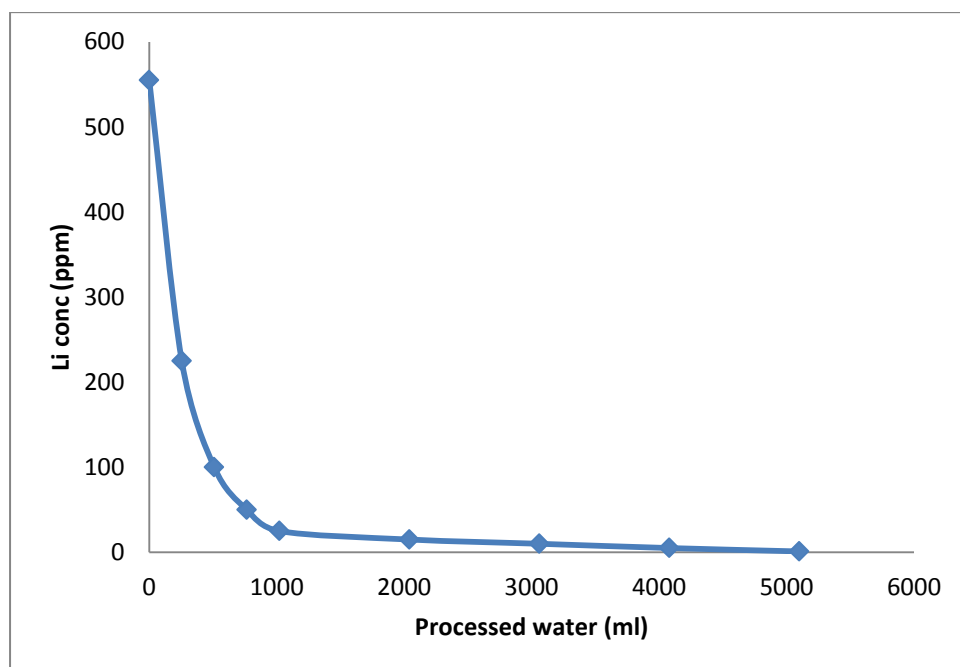


Figure 3.41 The elution curve after Run 3

Figure 3.41 shows the elution curve of the column after Run 3. The total amount of lithium eluted from the column was calculated as 220 mg Li which was nearly equal to capacity value (221.2 mg Li) acquired after Run 3.

In order to have an elution solution with high lithium concentration, Run 3 was repeated and in this case the column was fed with 350 ml 0.5 M HCl solution two times consecutively. The operation was batchwise i.e., the outlet of the column was

returned back to the feed tank. The concentration of the solutions of two consecutive leaching processes is shown in Table 3.42.

Table 3.42 Elution process data of the column after Run 3.

Run #	Total volume (ml)	Li conc. (ppm)
15	350	445
16	350	115

In Run 3, the column capacity was calculated as 221.2 mg Li. After first leaching in Run 15 157.5 mg of Li was leached from the column which was 70 % of the total lithium amount adsorbed in the column. In Run 16, additional 40.3 mg of Li was leached from the column which adds up to total 197.8 mg of Li recovered from the column. At the end, 90 % of total lithium adsorbed in the column was eluted. The leaching process seems to be very effective and nearly all lithium in the column is taken to acid solution. After elution processes, beads were washed with plenty of acid solution and regenerated to be used in following separation process.

3.4.4.2 Elution of the column fed with artificial brine solution

The high concentration of the foreign ions in artificial brine solution leads to adherence of those ions on bead surfaces and partially on LiMnO particles. Therefore a sweeping operation was applied before elution process. In sweeping process the column was fed with tap water or slightly acidic water (pH:6.1) and foreign ions were washed through the column. In that manner, the column fed with artificial brine solution in Run 12 was washed with tap water in Run 17 and washed with acidic water in Run 25 before elution. The results after each sweeping process were analyzed in the following sections.

3.4.4.2.1 Sweeping of the column with tap water

After Run 12, the column was washed with plenty of tap water to get rid of foreign ions. The change of ion concentrations at the outlet of the column is shown in Figure 3.42.

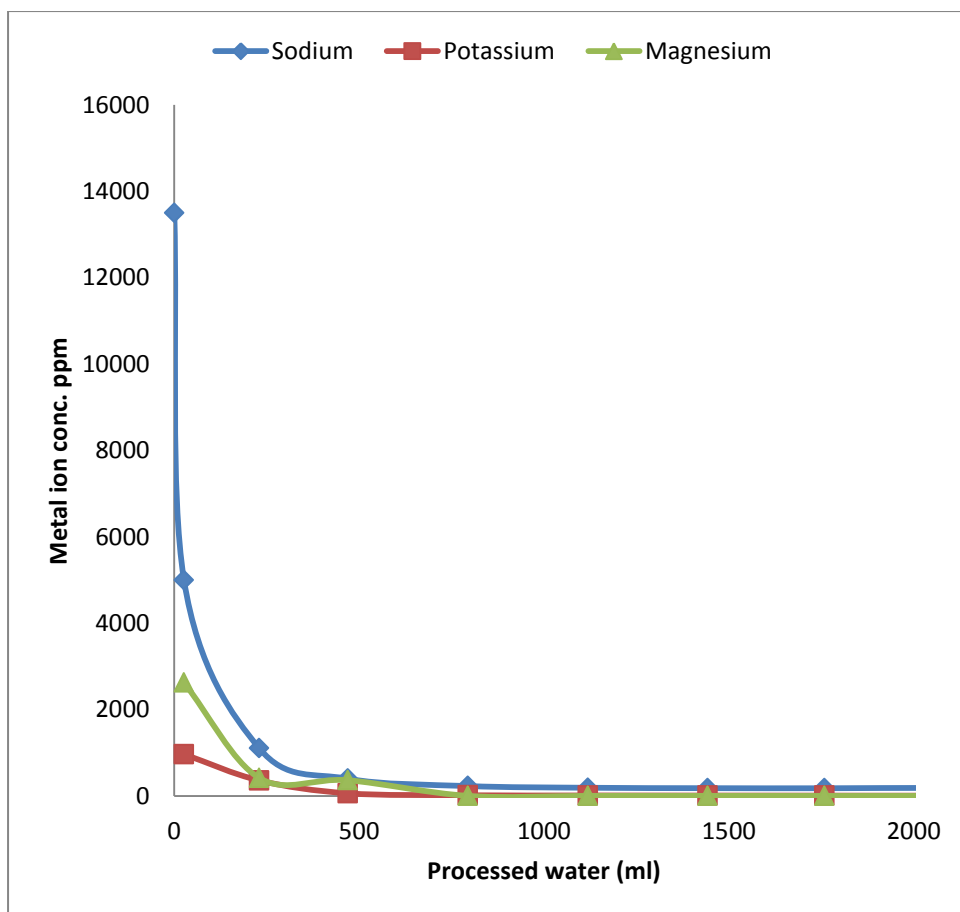


Figure 3.42 The change of ion concentrations in sweeping process applied after Run 12

It is seen from Figure 3.42 that the sweeping rate of sodium ions is very high and 3.33 g Na was swept by 2 L of tap water. The swept amount of potassium ions and magnesium ions were calculated as 234 mg K and 509 mg Mg respectively. During the sweeping process, only 0.326 mg of lithium ions were lost which was 10214 times lower than swept Na, 718 times lower than swept K, 1560 times lower than swept Mg. The sweeping process efficiency decreases after 500 ml of tap water was fed to the system. The concentration of K and Mg becomes 13 ppm and 6 ppm respectively which are nearly equivalent values in ASKİ tap water analysis report [101]. Another graphic representation of the high sweeping rate of foreign ions is given in Figure 3.43, which shows the molar ratio of K and Mg with respect to Li in the column effluent.

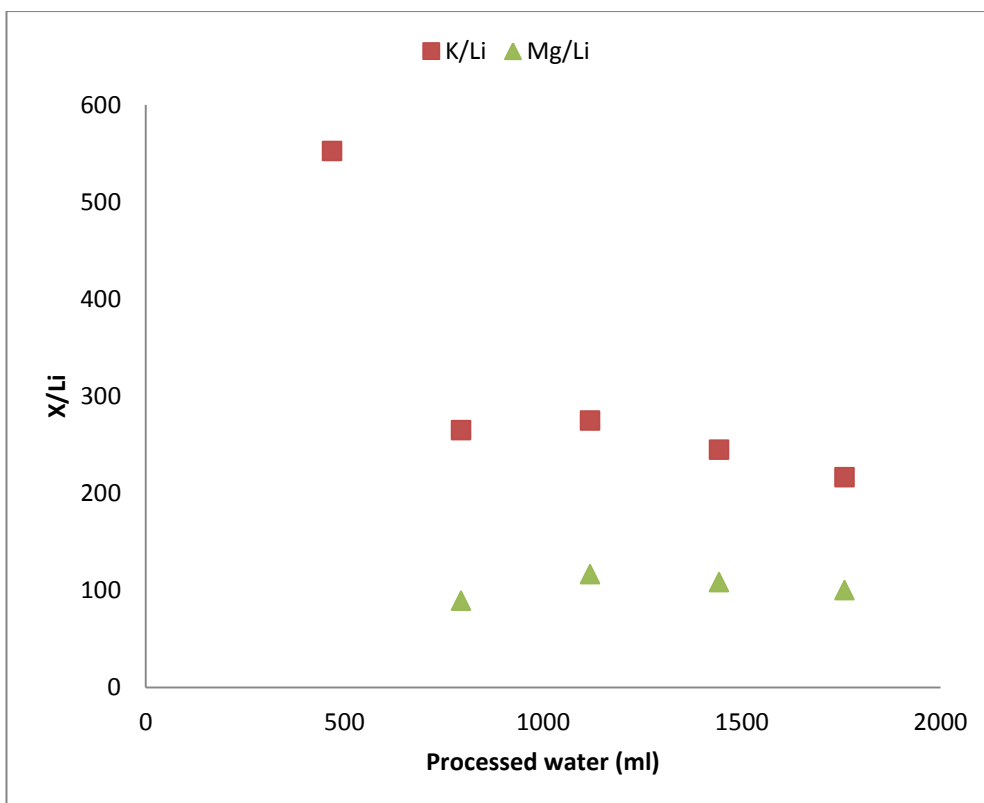


Figure 3.43 The molar ratio of potassium and magnesium with respect to lithium during sweeping process

After the sweeping process was completed, the column was fed with 350 ml 0.5 M HCl batchwise for elution step. The concentration of the elution solution and the summary of the steps up to elution are summarized in Table 3.43

Table 3.43 The elution of the column saturated with artificial brine solution and swept by tap water

Run #	Operation	Total vol. processed (ml)	Li (mg)	Na (mg)	K (mg)	Mg (mg)
12	Adsorbed amount of ions from artificial brine	37164	11.2	Saturated	Saturated	Saturated
17	Amount of ions swept by tap water	2000	0.326	3330	234	509
18	Eluted amount of ions by 0.5 M HCl	350	10.2	53.2	27.7	171.5

Table 3.43 shows the amount of ions adsorbed from artificial brine in Run 12, the amount of ions swept through the column in Run 17 and eluted amount of ions in Run 18 by 0.5 M HCl. The total mass balance holds for lithium and shows small amount of lithium remaining in the column. In order to evaluate the effectiveness of the overall process (feeding-sweeping-eluting), the concentration of the artificial brine and the elution solution are compared in Table 3.44.

Table 3.44 The comparison of the artificial brine and elution solution composition after sweeping by tap water

The composition	Li (ppm)	Na (ppm)	K (ppm)	Mg (ppm)
Artificial brine conc.	0.43	53430	4464	9210
Elution solution conc.	29	152	79	490
Change of concentration	Increased by 67 folds	Decreased by 352 folds	Decreased by 57 folds	Decreased by 19 folds

Table 3.44 shows that the overall process is very highly selective towards lithium compared to sodium and potassium ions and highly selective compared to magnesium ions. The results coincide with the findings in Section 3.4.2 where the column capacity for magnesium was found greater than sodium and potassium.

In order to enrich the lithium content in the eluted solution and decrease the foreign ion content, the overall process was repeated once more with a feed solution of 5 L prepared at a composition of elution solution given in Table 3.44. The new feed solution was prepared in 0.5 M HCl, and the pH of the solution was adjusted to 9 by ammonia addition. After 5 L was fed to the column in batchwise, the column was swept by 4 L of tap water continuously and lastly eluted by 350 ml 0.5 M HCl solution. The compositions of the solutions in each step are shown in Table 3.45.

Table 3.45 The second adsorption-sweeping-elution process composition with the feed solution having concentration of elution process in Run 18

The composition	Li (ppm)	Na (ppm)	K (ppm)	Mg (ppm)
The new feed solution	29	152	79	490
Elution solution conc.	310	151	38	1076
Change of concentration	Increased by 10.7 folds	No change	Decreased by 2 folds	Increased by 2.2 folds

Table 3.45 shows that an additional adsorption-sweeping-elution cycle increases the composition of lithium by 10.7 folds, while decreasing the potassium content by 2 folds and increase the magnesium content by 2.2 folds. The composition of sodium does not change. Increase in magnesium concentration and no change in sodium concentration was attributed to the tap water used in sweeping process. The sodium and magnesium content in tap water probably hinder the desorption of those ions. The low potassium content in tap water (3.1 ppm) explains the decrease in the potassium composition with respect to feed solution.

3.4.4.2.2 Sweeping of the column with acidic water at pH 6.1

As described in Section 3.4.4.2.1, the column was washed with acidic water at pH 6.1 after Run 12 instead of tap water. The logic behind washing the column with a slightly acidic solution was to increase the swept amount of foreign ions, especially Mg ions, while maintaining the lithium content in the column. After sweeping process, the column was eluted with 0.5 M HCl solution, to have the lithium rich solution finally. The concentration of the elution solution and the summary of the steps up to elution are summarized in Table 3.46.

Table 3.46 The elution of the column saturated with artificial brine solution and swept by acidic water at pH 6.1.

Run #	Operation	Total volume processed (ml)	Li (mg)	Na (mg)	K (mg)	Mg (mg)
12	Adsorbed amount of ions from artificial brine	37164	11.2	Saturated	Saturated	Saturated
26	Amount of ions swept by acidic water	2000	0.984	3350	241	612
27	Eluted amount of ions by 0.5 M HCl	350	9.6	28.4	21.4	82.1

Table 3.46 shows that sweeping the column with an acidic water increases the swept amount of all ions through the column including lithium. However, the swept amount of magnesium ions increases to 612 mg from 509, while swept of lithium ions only increases to 0.984 mg from 0.326 mg. By losing 0.658 mg of lithium, 103 mg of magnesium could be swept through the column.

In order to evaluate the effectiveness of the overall process (feeding-sweeping (at pH:6.1)-eluting), the concentration of the artificial brine and the elution solution are compared in Table 3.47.

Table 3.47 The comparison of the artificial brine and elution solution composition after sweeping by acidic solution (pH 6.1)

The composition	Li (ppm)	Na (ppm)	K (ppm)	Mg (ppm)
Artificial brine conc.	0.43	53430	4464	9210
Elution solution conc.	27.4	81.1	61.1	234.6
Change of concentration	Increased by 64 folds	Decreased by 659 folds	Decreased by 73 folds	Decreased by 39 folds

Table 3.47 obviously shows that sweeping of the column by an acidic water increases the lithium content with respect to foreign ion content after elution.

In order to enrich the lithium content in the solution, the adsorption-sweeping-elution cycle was repeated once more with an acidic sweeping solution. The results were tabulated in Table 3.48.

Table 3.48 The second adsorption-sweeping(at pH:6.1)-elution process composition with the feed solution having concentration of elution process in Run 26

The composition	Li (ppm)	Na (ppm)	K (ppm)	Mg (ppm)
The new feed solution	27.4	81.1	61.1	234.6
Elution solution conc.	261	32	20.6	102.5
Change of concentration	Increased by 9.5 folds	Decreased by 2.5 folds	Decreased by 3 folds	Decreased by 2.3 folds

Table 3.48 represents that, an additional adsorption-sweeping-elution cycle increases the lithium content to 261 ppm while reducing the foreign ion concentrations, unlike sweeping with tap water in the previous section. The decreasing ratio of foreign ion concentration is reduced to a number between 2 and 3 which actually implies that the system approaches near its equilibrium point. The repetition of the adsorption-sweeping-elution cycle once more did not change the concentration of the ions significantly and gave nearly equal values.

3.4.4.3 Elution of the column fed with concentrated sea water taken from Çamaltı Salina

Similar to the case in artificial brine solution, sweeping process was applied before elution due to high concentration of foreign ions in concentrated sea water, but the sweeping process was applied batchwise by deionized water or acidic water at pH 6.1 in this case.

3.4.4.3.1 Sweeping of the column with deionized water

After feeding the fresh column with concentrated sea water in Run 13, 1 L of fresh deionized water was fed to the column, 3 times for 2 hours. After that a leaching solution of 0.5 M HCl was fed to the column and the contents of the column were eluted. The overall process starting from feeding the column with concentrated sea water followed by three consecutive sweeping processes and leaching process were given in Table 3.49.

Table 3.49 The elution of the column saturated with concentrated brine solution and swept by demineralized water

Run #	Operation	Total volume processed (ml)	Li (mg)	Na (mg)	K (mg)	Mg (mg)
13	Adsorbed amount of ions from real concentrated brine	11473 (continuous)	5.39	Saturated	Saturated	Saturated
19	Amount of ions swept by water	1000 (batch)	0.72	4443	289.5	617
20	Amount of ions swept by water	1000 (batch)	0.19	479	19.3	8.2
21	Amount of ions swept by water	1000 (batch)	0.1	49	8.4	5.1
22	Eluted amount of ions by 0.5 M HCl	350	4.20	24.4	28.0	72.7

Table 3.49 shows the amount of ions adsorbed from real concentrated brine in Run 13, the amount of ions swept from the column in Run 19 through Run 21 by demineralized water and eluted amount of ions in Run 21 by 0.5 M HCl. The trend of the overall process is very similar to the case with artificial brine solution. The mass balance holds for lithium and shows that only 3.3 % of lithium ions were left in the column and 78 % of lithium ions adsorbed by the column was eluted by 0.5 M hydrochloric acid. In order to evaluate the effectiveness of the overall process (feeding-sweeping-eluting), the concentration of the real concentrated brine and the elution solution are compared in Table 3.50, which shows high selectivity towards lithium similar to the process with artificial brine feed.

Table 3.50 The comparison of the real concentrated brine and elution solution composition after sweeping by deionized water

The composition	Li (ppm)	Na (ppm)	K (ppm)	Mg (ppm)
Real concentrated brine conc.	1.25	76750	11023	21000
Elution solution conc.	12	69.7	80	208
Change of concentration	Increased by 10 folds	Decreased by 1101 folds	Decreased by 138 folds	Decreased by 101 folds

3.4.4.3.2 Sweeping of the column with acidic water at pH 6.1

After Run 13, the column was washed with acidic water at pH 6.1 in this case. The sweeping process was applied in three consecutive runs with 1 L acidic solution in each. The amount of ions adsorbed, swept and eluted is given in Table 3.51.

Table 3.51 The elution of the column saturated with concentrated brine solution and swept by acidic water at pH 6.1.

Run #	Operation	Total vol. processed (ml)	Li (mg)	Na (mg)	K (mg)	Mg (mg)
13	Adsorbed amount of ions from real concentrated brine	11473 (continuous)	5.39	Saturated	Saturated	Saturated
28	Amount of ions swept by acidic water	1000 (batch)	0.84	4474	292	819
29	Amount of ions swept by acidic water	1000 (batch)	0.27	512	28.2	53
30	Amount of ions swept by acidic water	1000 (batch)	0.13	48	9.3	18.4
31	Eluted amount of ions by 0.5 M HCl	350	4.06	16.3	28.0	61.3

Table 3.51 shows that the swept amount of lithium and foreign ions do not change much with respect to the case with deionized water. The reason of this behavior may be attributed to the strong buffer content in concentrated sea water which consumes the hydrogen ions in acidic water. The concentrations for the overall process are shown in Table 3.52.

Table 3.52 The comparison of the real concentrated brine and elution solution composition after sweeping by acidic water at pH 6.1

The composition	Li (ppm)	Na (ppm)	K (ppm)	Mg (ppm)
Real concentrated brine conc.	1.25	76750	11023	21000
Elution solution conc.	11.6	46.6	62	175.1
Change of concentration	Increased by 9.3 folds	Decreased by 1647 folds	Decreased by 178 folds	Decreased by 120 folds

It is seen that, even though the amount of foreign ion swept through the column did not change much, the foreign ion concentration of the elution solution is reduced around 15-20 % with respect to the case where sweeping process was done with deionized water.

3.4.4.4 Elution of the column fed with boron clay extract taken from Bigadiç

The sweeping of the column was done with tap water and acidic water separately after Run 14.

3.4.4.4.1 Sweeping of the column with tap water

After Run 14 was completed, the column was swept by 4000 ml tap water in order to get rid of foreign ions. The outlet concentration through sweeping process is shown in Figure 3.44.

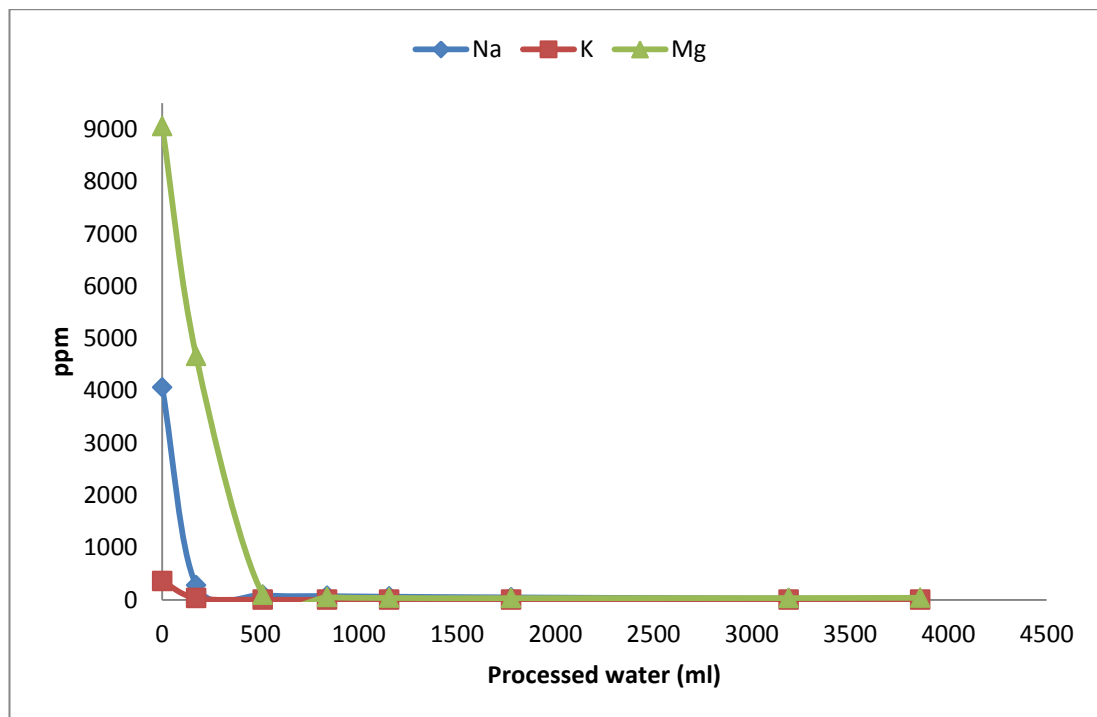


Figure 3.44 The change of ion concentrations in sweeping process applied after Run 14

Figure 3.44 shows that, after 500 ml of tap water was processed in the column, the effect of sweeping process reduces and the ion concentrations in the outlet of the column get equal to tap water ion concentrations. Up to that point, 0.44 g Na, 0.042 g K and 2.0 g Mg were swept through the column while 5.6 mg Li was lost in the operation. After the sweeping process was completed, the column was fed with 350 ml 0.5 M HCl batchwise, in two consecutive steps for elution. The concentration of the elution solution and the summary of the steps before elution were summarized in Table 3.53.

Table 3.53 The elution of the column saturated with clay extract and swept by tap water

Run #	Operation	Total volume processed (ml)	Li (mg)	Na (mg)	K (mg)	Mg (mg)
14	Adsorbed amount of ions from clay extract	780 (batch)	220.7	491.4	54.6	2113.8
23	Amount of ions swept by tap water	500	5.60	440	42.2	1195.6
24	Eluted amount of ions by 0.5 M HCl (First elution)	350	144.0	21.7	6.6	673.4
25	Eluted amount of ions by 0.5 M HCl (Second elution)	350	41.3	9.8	1.6	188.0

Table 3.53 shows the overall process sequence starting with feeding the column by clay extract and followed by two consequent sweeping processes and finally elution step. The overall process selectivity towards lithium compared to potassium and magnesium were seen obviously but similar to the previous processes, magnesium ion seems to behave like lithium ion and decrease the selectivity.

The comparison of the clay extract feed composition with elution solution composition is given in Table 3.54.

Table 3.54 The comparison of the boron clay extract and elution solution composition after sweeping with tap water

The composition	Li (ppm)	Na (ppm)	K (ppm)	Mg (ppm)
Clay extract conc.	388.0	4880.0	530.0	15110.0
Elution solution conc.	411.5	62.1	18.9	1924
Change of concentration	Increased by 1.06 folds	Decreased by 78.6 folds	Decreased by 28 folds	Decreased by 7.9 folds

It is deduced from Table 3.54 that, sodium and potassium ion concentrations were reduced by 28 and 78.6 folds respectively which shows the high selectivity of beads towards lithium ions. However magnesium ion concentration decreases by 7.9 folds while the lithium concentration stays nearly constant.

3.4.4.4.2 Sweeping of the column with acidic water at pH 6.1

Following Run 14, a sweeping process was applied with acidic water at pH 6.1. The amount of processed ions in each step are given in Table 3.55.

Table 3.55 The elution of the column saturated with clay extract and swept by acidic water at pH 6.1

Run #	Operation	Total volume processed (ml)	Li (mg)	Na (mg)	K (mg)	Mg (mg)
14	Adsorbed amount of ions from clay extract	780 (batch)	224.7	512.7	61.1	2184.6
32	Amount of ions swept by acidic water at pH 6.1	500	17.4	491	52.3	1491.4
33	Eluted amount of ions by 0.5 M HCl	350	182.5	17.4	4.3	229.8

In sweeping process with acidic solution, the magnesium could be swept more than the case with deionized water similar to the previous results. The final concentrations of the overall process are given in Table 3.56.

Table 3.56 The comparison of the boron clay extract and elution solution composition after sweeping with acidic water

The composition	Li (ppm)	Na (ppm)	K (ppm)	Mg (ppm)
Clay extract conc.	412.0	4964.0	584.0	15972.0
Elution solution conc.	521.4	49.7	12.3	656.6
Change of concentration	Increased by 1.06 folds	Decreased by 100 folds	Decreased by 48 folds	Decreased by 24 folds

When Table 3.54 and Table 3.56 are compared, it is obviously seen that using an acidic sweeping solution helps to remove more foreign ions from the column and increase the lithium/foreign ion ratio, thus increase the overall separation efficiency. However, higher magnesium ion concentration than lithium ion concentration in clay extract seems to be a problem for recovery of pure lithium carbonate in a real process. A repetition of the overall process would probably decrease the magnesium concentration and increase the lithium concentration however an additional separation unit must be utilized in order to get rid of magnesium content in the resulting lithium chloride rich solution.

After the analysis of column experiments done in Section 3.4, the following conclusions can be written:

- Lithium was obviously separated by adsorbents selectively compared to foreign ions Na, K and Mg.
- Foreign ions were also adsorbed by PSMA content in the beads partially.
- High foreign ion content in feed solution suppressed the capacity of LiMnO beads.
- In sweeping operation, huge amount of Na, K and Mg ions could be swept through the column.

- Employing a slightly acidic solution (pH:6.1) in sweeping process obviously increased the swept amount of foreign ions especially magnesium.
- Most of the lithium adsorbed by the beads stayed within LiMnO content in the column during sweeping by tap water, deionized water and acidic water at pH 6.1.
- It is possible to further concentrate lithium content in a solution by consecutive adsorption-sweeping-elution cycles up to a point where thermodynamic limitation of the process emerges.

3.4.5 Separation of lithium by a post-treatment with LiMnO particles following column adsorption

In this section, the concentrated brine taken from adsorption column was further treated with LiMnO particles in order to increase the lithium and reduce the foreign ion content. The experiments were done batchwise by direct contact of adsorption column effluent with LiMnO particles at pH:9.8 in a large volume beaker. The initial and final concentrations of adsorption process are shown in Table 3.57.

Table 3.57 The initial and final concentrations of the adsorption process done with column effluent

Brine effluent of adsorption column	Volume (ml)	Adsorbent (g)	Initial conc. (ppm)	Final conc. (ppm)	Capacity (mg ion/g ads.)
Artificial brine	1000	15	261 ppm Li	0.3 ppm Li	17.38 mg Li
			32 ppm Na	21.1 ppm Na	0.73 mg Na
			20.6 ppm K	0.35 ppm K	1.35 mg K
			102.5 ppm Mg	83.5 ppm Mg	1.27 mg Mg
Clay extract	1000	30	521.4 ppm Li	0.36 ppm Li	17.37 mg Li
			49.7 ppm Na	28.4 ppm Na	0.71 mg Na
			12.3 ppm K	0.3 ppm K	0.4 mg K
			656.6 Mg	617.9 ppm Mg	1.29 mg Mg

After the adsorption process, LiMnO particles were let to settle down and liquid part was decanted. Then, LiMnO particles were mixed with 100 ml demineralized water

to sweep the foreign ions which was followed by elution of the remaining ion content in the particles. The elution of the particles was done in three consecutive steps by using 100 ml of 0.5 M HCl in each step. The eluted amount of ions and concentrations in each step were tabulated and given in Table 3.58.

Table 3.58 The amount of eluted ions and concentrations in elution process of post-treatment

Brine	Elut. #	Vol. of elut soln (ml)	Recovery (%)	Eluted amount of ions (mg)				Elution solution concentration (ppm)			
				Li	Na	K	Mg	Li	Na	K	Mg
Artificial brine	1. elut.	100	64.2	167.6	6.4	12.9	12.4	1675.6	64.4	128.9	124.1
	2. elut.	100	21.3	55.6	2.2	4.2	4.1	555.9	22.2	42.1	41.2
	3. elut.	100	8	21.1	0.8	1.5	1.5	211.4	8.3	15.4	15.3
	<i>TOTAL</i>	<i>300</i>	<i>93.6</i>	<i>244.3</i>	<i>9.4</i>	<i>18.8</i>	<i>18.1</i>				
Clay extract	1. elut.	100	61.7	321.7	12.6	8.4	23.3	3217.0	126.2	83.8	233.1
	2. elut.	100	19.8	103.2	4.1	2.5	7.5	1032.4	40.6	25.1	75.4
	3. elut.	100	7.4	38.6	1.5	0.9	2.7	385.8	14.9	8.8	27.5
	<i>TOTAL</i>	<i>300</i>	<i>88.9</i>	<i>463.5</i>	<i>18.2</i>	<i>11.8</i>	<i>33.6</i>				

Table 3.58 shows that the effluent lithium concentration from adsorption column can be further concentrated significantly by direct act of LiMnO particles while reducing the foreign ion content of the brine. The efficiency of the overall process starting from feeding the artificial brine/clay extract to the adsorption column in consecutive steps which is followed by the post-treatment with LiMnO particles were analyzed in terms of lithium concentrations, foreign ion concentrations and the amount of lithium lost in each step.

3.4.5.1 Efficiency of the overall process starting from artificial brine

In order to have 1675 ppm Li, 64.4 ppm Na, 128.9 ppm K and 124.1 ppm Mg in 100 ml of water, 1517 L of concentrated sea water was processed with a concentration of 0.43 ppm Li, 53430 ppm Na, 4464 ppm K and 9210 ppm Mg. In the first adsorption-sweeping-elution cycle, 458 mg Li was adsorbed by the LiMnO-PSMA beads, while 65 mg of Li was lost during sweeping process. In the second adsorption-sweeping-

elution cycle, 59 mg of Li was lost during sweeping processes. And lastly, in the post-treatment with LiMnO particles, 17 mg of Li was lost during sweeping processes. In the overall process, 141 mg of Li was lost, which means that 69.2 % of the initially adsorbed lithium could be recovered in the final solution. The lithium concentrations, lithium to foreign ion ratio and lithium loss in each step were summarized in Table 3.59.

Table 3.59 Li concentration, Li/foreign ion ratio, Li loss in each separation step starting from artificial brine

Brine	Na/Li	K/Li	Mg/Li	Li conc. (ppm)	Li	Li Loss (mg)	Li Loss (%)
					percentage among total cations (%)		
Initial brine	124,256	10,381	21,419	0.43	6.408x10 ⁻⁴	-	-
After first ads.-sweep.-elut. cycle	3.0	2.2	8.6	27.4	6.8	65	14.2
After second ads.-sweep.-elut. cycle	0.12	0.08	0.39	261.0	62.7	59	12.9
After post treatment	0.04	0.08	0.07	1675.6	84.0	17	3.7
					TOTAL	141	30.8

A feasibility study of recovering lithium from the concentrated brine in Çamaltı Salina is given in APPENDIX D.

3.4.5.2 Efficiency of the overall process starting from clay extract

In order to have 3217 ppm Li, 126.2 ppm Na, 83.8 ppm K and 233.1 ppm Mg in 100 ml of water, 2.23 L of clay extract was processed with a concentration of 412 ppm Li, 4964 ppm Na, 584 ppm K and 15972 ppm Mg. In the adsorption-sweeping-elution cycle, 642 mg Li was adsorbed, while 42 mg of Li was lost during sweeping process. In the post-treatment with LiMnO particles, 58.4 mg of Li was lost during sweeping processes. In the overall process, 100.4 mg of Li was lost, which means

that 84.4 % of the initially adsorbed lithium could be recovered. The lithium concentrations, lithium to foreign ion ratio and lithium loss in each step were summarized in Table 3.60.

Table 3.60 Li concentration, Li/foreign ion ratio, Li loss in each separation step starting from clay extract

Brine	Na/Li	K/Li	Mg/Li	Li			
				Li conc. (ppm)	percentage among total cations (%)	Li Loss (mg)	Li Loss (%)
Initial clay extract	12.1	1.4	38.8	412.0	1.9	-	-
After ads.-sweep.-elut. cycle	0.09	0.02	1.26	521.4	42.1	42.0	6.5
After post treatment	0.04	0.02	0.07	3217	88.5	58.4	9.1
TOTAL						100.4	15.6

An overall process was proposed for the mass production of lithium carbonate from boron clay and a feasibility study was done which was shown in APPENDIX D.

After the series of operations, lithium concentration in the artificial brine and clay extract was increased to 1675.6 and 3217 ppm respectively while reducing the Li/Na, Li/K, Li/Mg ratio significantly. The concentrated brine would then be sent to pools to let water content evaporate and bischofite salt ($MgCl_2 \cdot 6H_2O$) and lithium carnalite salt ($LiClMgCl_2 \cdot 7H_2O$) precipitate in conventional processes. The remaining magnesium content in the brines may be removed by utilizing lime in the processes.

CHAPTER 4

CONCLUSIONS

The aim of this study is to increase the efficiency of lithium separation from brines by liquid-liquid extraction and adsorption methods with various materials synthesized throughout the study. The conclusions driven from the study can be divided into three parts in terms of the techniques employed.

Liquid-liquid extraction

- Hexyl, octyl, dibutyl and dihexyl formamides were synthesized by direct reaction of formic acid and related alkyl amines in high yields.
- Among those formamides, hexyformamide showed the highest distribution coefficient 0.14 (at 25 °C and pH=4) for LiCl extraction. This is the highest value cited in the literature for a single solvent so far.
- The LiCl extraction process was shown to be highly selective for Li, compared to Na, K ions.
- Li selectivity is somewhat low with respect to calcium ions. However calcium ions are generally absent in concentrated sea water due to its precipitation as sulfates and carbonates during evaporation in ponds.
- It was found that extracted lithium could be eluted with 1.0 M HCl solution, so that 93 % lithium was stripped in the first contact. Full recovery of lithium

could be achieved by repeating the acid treatments. In these conditions no hydrolysis of formamide was detected.

- These results implied that hexyl formamide seemed to be a promising candidate for practical use in extraction of lithium chloride from concentrated brines.

Batch adsorption

- Lithium manganese oxides (LiMnO) were synthesized by solid-solid and hydrothermal reaction procedures. The highest capacity was found as 22.8 mg Li/g adsorbent at pH:10.1 by the method used in the study of Ooi et al.
- As pH increases from 6.3 to 10.2, the capacity values increases from 5.2 to 22.8 mg Li/g adsorbent.
- The initial lithium concentration did not affect the capacity value of the adsorbents.
- The kinetics study showed that the adsorption process was totally completed in 20 hours.
- The equilibrium isotherm calculations showed that, the adsorption process was mostly fitted into Langmuir isotherm with an R^2 value of 0.997.
- The stability experiments of the adsorbents indicated that the capacity of the adsorbents decreased by around 1 % in each consecutive cycle.
- LiMnO adsorbents showed strong selectivity towards lithium; 27 times higher than sodium, 12.5 times higher than potassium and 13.3 times higher than magnesium ions.

Column adsorption

- The LiMnO particles were integrated into poly(styrene-maleic anhydride-glycidyl methacrylate) (PSMA) polymer and employed in column adsorption.
- PSMA has been utilized as organic metal oxide support for the first time and gave superior results compared to similar polymers cited in the literature.
- The properties which make PSMA superior than the other polymers are its self-crosslinking and swelling ability.

- Self-crosslinking makes PSMA-LiMnO beads easy to process, tough and stable.
- PSMA-LiMnO beads were stable up to pH:9. At basic pH 9 it swells 4 %, which increased the diffusion rate of lithium and hydrogen ions in and out of the beads.
- The capacity of the column filled with LiMnO beads was calculated as 221.2 mg Li at pH 9 with a 20 ppm Li feed solution which was the 94 % of the theoretical capacity.
- The capacity of the column was found as 2.51 mg Na, 5.78 mg K and 52.9 mg Mg when each foreign ion was fed to the column in equal operating conditions.
- It was found out that, the capacity value of the column for lithium was suppressed in the presence of high foreign ion concentrations.
- Sweeping process before eluting the column decreased the foreign ion concentration in elution solution. Sweeping with acidic water at pH:6.1 gave the most satisfactory results.
- For artificial brine, after two adsorption-sweeping-elution cycles and post-treatment by LiMnO, the lithium concentration was increased to 1675.6 ppm from 0.43 ppm. The lithium concentration among the cations in the brine was increased to 84 % from 6.408×10^{-4} % while 30.8 % of the lithium in the brine was lost during the process.
- For clay extract, after one adsorption-sweeping-elution cycle and post-treatment by LiMnO, the lithium concentration was increased to 3217 ppm from 412 ppm. The lithium concentration among the cations in the brine was increased to 88.5 % from 1.9 % while 15.6 % of the lithium in the brine was lost during the process.
- It is finally concluded that, adsorption via LiMnO-PSMA beads can be used to concentrate lithium content in brines selectively which makes adsorption process a promising method to be employed in conventional lithium separation processes.

CHAPTER 5

RECOMMENDATIONS

Adsorption via LiMnO particles is a promising method to be conjugated with conventional lithium carbonate production process from brines especially where the foreign ion content is remarkably high. Boron clay disposed in Bigadiç is a valuable source of lithium with its 3000 ppm Li content. The experiment held on this study shows a way to recover lithium from the clay in a feasible way. As a future prospect, a pilot plant project can be proposed to produce an industrial grade lithium carbonate which will also incorporate the knowledge and infrastructure in ETİ Mining Company.

For further investigation,

- The optimum pH of the sweeping process can be determined where the minimum amount of lithium is lost and maximum amount of foreign ions are swept
- The recycle pathways must be determined in the overall process to loose minimum amount of lithium in consecutive elution operations
- The precipitation regimes of the magnesium salts like bischoffite and carnalite in pools must be determined to get rid of the magnesium content in the processed brine

- A more realistic feasibility analysis can be done which takes into account the total cost and time needs of the process while considering to produce whole possible goods (i.e KCl, MgCl₂, boron derivatives) from the clay as by-products of lithium carbonate.

REFERENCES

- [1] D. Linden and T. B. Reddy, *Handbook of Batteries*. 2002, p. 328.
- [2] J. H. Fishwick, *Applications of lithium in ceramics*. Boston Cahners, 1974, p. 156.
- [3] USGS Report, “Mineral Commodity Summaries 2010”
- [4] Kirk-Othmer, “Lithium and lithium compounds,” *Kirk-Othmer Encyclopedia of Chemical Technology, Volume 15*. 2005.
- [5] “Is Lithium-ion the Ideal Battery?,” 2010. [Online]. Available: http://batteryuniversity.com/learn/article/is_lithium_ion_the_ideal_battery/3. [Accessed: 17-Aug-2014].
- [6] E. Cairns, “Batteries and Fuel Cells,” *Newsletter, Coll. Chem., U. Calif., Berkeley*, vol. 10, no. 3, p. 4, 2002.
- [7] Anon, “New Lithium Battery Design,” *Sci. News 158*, p. 399, 2000.
- [8] M. A. Delucchi and T. E. Lipman, “An analysis of the retail and lifecycle cost of battery-powered electric vehicles,” *Transp. Res. Part D*, vol. 6, pp. 371–404, 2001.
- [9] E. E. Richard L. Nailen, “Grease: What it is; How it Works,” *Electr. Appar.*, vol. April, 2002.
- [10] K. Murakami, H. Sato, and K. Watanabe, “A new bubble-point-pressure correlation for the binary LiBr/H₂O solution,” *Int. J. Thermophys.*, vol. 16, no. 3, pp. 811–820, May 1995.
- [11] E. A. Starke, T. H. Sanders, and I. G. Palmer, “New Approaches to Alloy Development in the Al-Li System,” *JOM*, vol. 33, no. 8, pp. 24–33, Dec. 2013.
- [12] G. W. Edward W. Abel, Francis Gordon Albert Stone, *Comprehensive Organometallic Chemistry 2*. Elsevier, p. 667, 1995.

- [13] I. Natori, "Synthesis of Polymers with an Alicyclic Structure in the Main Chain. Living Anionic Polymerization of 1,3-Cyclohexadiene with the n - Butyllithium/N,N,N',N'-Tetramethyl-ethylenediamine System" *Macromolecules*, vol. 30, no. 12, pp. 3696–3697, Jun. 1997.
- [14] "FMC Lithium-More than lithium-World Pharmaceutical Frontiers." [Online]. Available: <http://www.worldpharmaceuticals.net/contractors/chemicals-and-catalysts/fmc-lithium/>. [Accessed: 17-Aug-2014].
- [15] H. Zerriffi, *Tritium: The environmental, health, budgetary, and strategic effects of the Department of Energy's decision to produce tritium*. Institute for Energy and Environmental Research, 1996.
- [16] N. Tsoulfanidis, *Measurement and Detection of Radiation*. Washington, D.C.: Taylor & Francis, pp. 467 – 501, 1995.
- [17] National Research Council (U.S.). Committee on Separations Technology and Transmutation Systems and N.R.C. (U.S.) C. on S.T. and T. Systems, *Nuclear wastes: technologies for separations and transmutation*. National Academies Press, 1996.
- [18] M. Makara-studzińska, A. Koćelak, J. Moryłowska-topolska, and A. Urbańska, "Lithium Therapy – The effectiveness of the medicine, side symptoms, complications and their influence on the quality of the life in affective diseases," *J. Elem.*, vol. 15, no. 2, pp. 393–403, 2010.
- [19] T. Ichikawa, S. Isobe, N. Hanada, and H. Fujii, "Lithium nitride for reversible hydrogen storage," *J. Alloys Compd.*, vol. 365, no. 1–2, pp. 271–276, Feb. 2004.
- [20] Z. Xiong, C. K. Yong, G. Wu, P. Chen, W. Shaw, A. Karkamkar, T. Autrey, M. O. Jones, S. R. Johnson, P. P. Edwards, and W. I. F. David, "High-capacity hydrogen storage in lithium and sodium amidoboranes.," *Nat. Mater.*, vol. 7, no. 2, pp. 138–41, Feb. 2008.
- [21] Donald E. Garrett, *Handbook of Lithium and Natural Calcium Chloride*. Elsevier, 2004.
- [22] USGS Report, "Mineral Commodity Summaries 2012."
- [23] USGS Report, "Mineral Commodity Summaries 2013."
- [24] USGS Report, "Mineral Commodity Summaries 2014."
- [25] M. . D. M. Saller, "Lithium takes charge, supply and demand reviewed," *Ind. Miner.*, vol. 37, no. March, 2000.

- [26] Schaller W.T., “Lithium Minerals Industrial Minerals and Rocks,” *Am. Inst. Min. Met. Eng.*, p. 427, 1937.
- [27] E. Siame and R. D. Pascoe, “Extraction of lithium from micaceous waste from china clay production,” *Miner. Eng.*, vol. 24, no. 14, pp. 1595–1602, Nov. 2011.
- [28] S. D. M. Norton J. J., “Lithium Resources of North America,” *Geol. Surv. Bull.*, vol. 1027, no. G, 1955.
- [29] M. Tamlin, A. Sheth, and D. J. McCracken, “Lithium,” *Min. Eng.*, 2002.
- [30] M. J. J., “Lithium and lithium compounds,” *Encyclopedia of Chemical Processing and Design*. p. Vol 28, 1988.
- [31] W. A. Averill and D. L. Olson, “A review of extractive processes for lithium from ores and brines,” *Energy*, vol. 3, no. 3, pp. 305–313, Jun. 1978.
- [32] G. O. G. Löf and W. K. Lewis, “Lithium Chloride from Lepidolite,” *Ind. Eng. Chem.*, vol. 34, no. 2, pp. 209–216, Feb. 1942.
- [33] “Salar Brines.” [Online]. Available: <http://www.sqm.com/en-us/acercadesqm/recursosnaturales/salmuera.aspx>. [Accessed: 19-Aug-2014].
- [34] “Resources & Recycling | Rockwood Lithium.” [Online]. Available: <http://www.rockwoodlithium.com/resources-recycling/>. [Accessed: 19-Aug-2014].
- [35] “Company Overview.”
[Online]. Available: http://www.orocobre.com/About_Us.htm. [Accessed: 19-Aug-2014].
- [36] “Who We Are: the sustainable materials technology company| Simbol, Inc.” [Online]. Available: http://www.simbolmaterials.com/who_we_are.htm. [Accessed: 20-Aug-2014].
- [37] R. and S. J. Hollender, “Bolivia and its Lithium,” 2010.
- [38] W. Huang, X. Wang, .Z. Sun, Z. Nie, Z. Sha, “Zabuye Salt Lake solar pond in Tibet , China: Construction and operational experience,” *Nat. Resour. Environ. Issues*, vol. 15, 2009.
- [39] “South Korea aims to produce lithium from seawater | Business Spectator.” [Online]. Available: <http://www.businessspectator.com.au/news/2011/1/21/cleantech/south-korea-aims-produce-lithium-seawater>. [Accessed: 20-Aug-2014].

- [40] “Posco cuts lithium recovery time from 12 months to 8 hours - BNamericas.” [Online]. Available: <http://www.bnamericas.com/news/mining/posco-cuts-lithium-recovery-time-from-12-months-to-8-hours>. [Accessed: 20-Aug-2014].
- [41] Anon, “Nevada Brine Supports a Big New Lithium Plant,” *Chem. Eng.*, pp. 86–88, 1966.
- [42] D. E. Garrett, *Potash; Geology, Processing, Uses and Phase Data*. London: Chapman & Hall, 1996.
- [43] D. E. Garrett, *Borates : Handbook of Deposits , Processing , Properties , and Use , 1998 , 483 pages ,.* San Diego, CA: Academic Press, 2001.
- [44] Coad M., “Lithium production in Salar de Atacama,” *Industrial Miner.*, vol. Nov., p. 27, 1984.
- [45] I. F. Wilkomirsky, “Extractive Metallurgy of Lithium,” *Miner. Rev.*, vol. 53(221), pp. 31–36, 1998.
- [46] J. Susan, “Production of lithium metal grade lithium chloride from lithium-containing brine,” 1990.
- [47] W. C. Baumann, “Composition for the recovery of lithium values from brine and process of making/using said composition,” 2001.
- [48] A. N. Mordoğan H., Helvacı C., Malayoğlu U., “Lityumun Tersiyer bor yatakları ve güncel göllerdeki varlığı, dağılımı ve kazanılma olanakları,” 1994.
- [49] B. Holdorf, H., Ziegenbalg, G., and Schmidt, “Recovery of Lithium Compounds from Natural Salt Brines.,” in *Seventh Symposium on Salt*, pp. 571–595, 1993
- [50] G. G. Gabra and A. E. Torma, “Lithium chloride extraction by n-butanol,” *Hydrometallurgy*, vol. 3, no. 1, pp. 23–33, Jan. 1978.
- [51] J. A. Hermann, “Preparation and purification of lithium chloride,” 1966.
- [52] S. Kaneko and W. Takahashi, “Adsorption of lithium in sea water on alumina—magnesia mixed-oxide gels,” *Colloids and Surfaces*, vol. 47, pp. 69–79, Jan. 1990.
- [53] K. Schwochau, “Extraction of Metals from Sea Water,” *Top. Curr. Chem.*, vol. 124, pp. 91–133, 1984.
- [54] R. D. Goodenough, “Recovery of Lithium,” 1960.
- [55] M. P. Neipert and C. K. Bon, “Method of lithium recovery,” 1967.

- [56] K. Rothbaum, H. P., and Middendorf, "Lithium extraction from Wairakei geothermal waters," *NZ J. Technol.*, vol. 2, no. 4, pp. 231–235, 1986.
- [57] H. Pauwels and C. Fouillac, "Lithium recovery from geothermal waters of Cesano (Italy) and Cronembourg (Alsace , France)," in *12th New Zealand Geothermal Workshop*, pp. 117–123, 1990.
- [58] I. Pelly, "Pelly," *Biotechnol., J. Appl. Chem.*, vol. 28, pp. 469–475, 1978.
- [59] Y. Epstein, J. A., Feist, E. M., Zmora, J., and Marcus, "The Recovery of Lithium from the Dead Sea," *Hydrometallurgy*, vol. 6, pp. 269–275, 1981.
- [60] A. D. Ryabtsev, L. T. Menzheres, and A. V. Ten, "Sorption of Lithium from Brine onto Granular $\text{LiCl}\cdot 2\text{Al}(\text{OH})_3\cdot m\text{H}_2\text{O}$ Sorbent under Dynamic Conditions," *Russ. J. Appl. Chem.*, vol. 75, no. 7, pp. 1069–1074, Jul. 2002.
- [61] A. H. Hamzaoui, B. Jamoussi, and A. M'nif, "Lithium recovery from highly concentrated solutions: Response surface methodology (RSM) process parameters optimization," *Hydrometallurgy*, vol. 90, no. 1, pp. 1–7, Jan. 2008.
- [62] M. Abe, Y. Kanzaki, and R. Chitrakar, "Synthetic inorganic ion-exchange materials. 44. NMR study of the ion-exchange reaction of lithium on titanium antimonate and tin antimonate," *J. Phys. Chem.*, vol. 91, no. 11, pp. 2997–3001, May 1987.
- [63] L. Ma, B. Chen, X. Shi, and K. Zhang, " Li^+ extraction/adsorption properties of Li-Sb-Mn composite oxides in aqueous medium," *Trans. Nonferrous Met. Soc. China*, vol. 21, no. 7, pp. 1660–1664, Jul. 2011.
- [64] Y. S. Kim, K. S. No, K. S. Chung, J. C. Lee, and K. Ooi, "Li⁺ extraction reactions with spinel-type $\text{LiM}_{0.5}\text{Mn}_{1.5}\text{O}_4$ (M=Ti, Fe) and their electronic structures," *Mater. Lett.*, vol. 57, no. 26–27, pp. 4140–4146, Sep. 2003.
- [65] C.-M. Park, Y.-U. Kim, and H.-J. Sohn, "Topotactic Li Insertion/Extraction in Hexagonal Vanadium Monophosphide," *Chem. Mater.*, vol. 21, no. 23, pp. 5566–5568, Dec. 2009.
- [66] L. Fransson and K. Edstro, "Structural investigation of the Li⁺ ion insertion / extraction mechanism in Sn-based composite oxide glasses," vol. 62, pp. 1213–1218, 2001.
- [67] C. V. Ramana, a. Mauger, F. Gendron, C. M. Julien, and K. Zaghbi, "Study of the Li-insertion/extraction process in $\text{LiFePO}_4/\text{FePO}_4$," *J. Power Sources*, vol. 187, no. 2, pp. 555–564, Feb. 2009.
- [68] E. I. Kachibaya, R. a. Imnadze, T. V. Paikidze, and R. a. Akhvlediani, "Cathodic materials for lithium-ion batteries based on spinels $\text{Li}_x\text{Mn}_{2-y}\text{Me}_y\text{O}_4$: Synthesis, phase composition, and structure of $\text{Li}_x\text{Mn}_{2-y}\text{Cr}_y\text{O}_4$ at $x = 1.0\text{--}1.2$

- and $y = 0-0.5$,” *Russ. J. Electrochem.*, vol. 42, no. 11, pp. 1224–1234, Nov. 2006.
- [69] Z. Gong and Y. Yang, “Recent advances in the research of polyanion-type cathode materials for Li-ion batteries,” *Energy Environ. Sci.*, vol. 4, no. 9, p. 3223, 2011.
- [70] R. Chitrakar, H. Kanoh, Y. Miyai, and K. Ooi, “Recovery of Lithium from Seawater Using Manganese Oxide Adsorbent ($\text{H}_{1.6}\text{Mn}_{1.6}\text{O}_4$) Derived from $\text{Li}_{1.6}\text{Mn}_{1.6}\text{O}_4$,” *Ind. Eng. Chem. Res.*, vol. 40, pp. 2054–2058, 2001.
- [71] X. M. Shen, “Phase transitions and ion exchange behavior of electrolytically prepared manganese dioxide,” *J. Solid State Chem.*, vol. 64, p. 270, 1986.
- [72] K. Ooi and M. Abe, “Topotactic Li^+ Insertion to X-MnO_2 in the Aqueous Phase,” *Langmuir*, no. 5, pp. 150–157, 1989.
- [73] K. Ooi, Y. Miyai, and J. Sakakihara, “Mechanism of lithium(1+) insertion in spinel-type manganese oxide. Redox and ion-exchange reactions,” *Langmuir*, vol. 7, no. 6, pp. 1167–1171, Jun. 1991.
- [74] Q. Feng, Y. Miyai, H. Kanoh, and K. Ooi, “ Li^+ Extraction/Insertion with Spinel-Type Lithium Manganese Oxides. Characterization of Redox-Type and Ion-Exchange-Type Sites,” *Langmuir*, vol. 8, pp. 1861–1867, 1992.
- [75] H. Welfare, “Manganese oxide minerals: Crystal structures and economic and,” vol. 96, no. March, pp. 3447–3454, 1999.
- [76] Q. Feng, “Hydrothermal Synthesis of Lithium and Sodium Manganese Oxides and Their Metal Ion Extraction-Insertion Reactions,” no. 23, pp. 1226–1232, 1995.
- [77] R. J. Amundsen Brett, Jones Deborah J., “Mechanism of Proton Insertion and Characterization of the Proton Sites in Lithium Manganate Spinel,” *Chem. Mater.*, vol. 7, no. 11, pp. 2151–2160, 1995.
- [78] M. H. Kazuharu YOSHIKAZU, Ayuko KITAJOU, “Lithium recovery from geothermal waters of Cesano (Italy) and Cronembourg (Alsace, France),” *Ars Separatoria Acta*, vol. 4, pp. 78–85, 2006.
- [79] S. N. and K. Y. A Kitajou, T Suzuki, “Selective recovery of lithium from seawater using a novel MnO_2 type adsorbent II – Enhancement of lithium ion selectivity of the adsorbent,” *Ars Separatoria Acta*, vol. 2, pp. 97–106, 2003.
- [80] K. Yoshizuka, A. Kitajou, and M. Holba, “Selective recovery of lithium from seawater using a novel MnO_2 type adsorbent III - benchmark evaluation,” *Ars Separatoria Acta*, vol. No. 4, pp. 78–85, 2006.

- [81] S. Nishihama, K. Onishi, and K. Yoshizuka, "Selective Recovery Process of Lithium from Seawater Using Integrated Ion Exchange Methods," *Solvent Extr. Ion Exch.*, vol. 29, no. 3, pp. 421–431, May 2011.
- [82] L. Wang, W. Ma, R. Liu, H. Y. Li, and C. G. Meng, "Correlation between Li^+ adsorption capacity and the preparation conditions of spinel lithium manganese precursor," *Solid State Ionics*, vol. 177, no. 17–18, pp. 1421–1428, Jul. 2006.
- [83] L. Wang, C. G. Meng, M. Han, and W. Ma, "Lithium uptake in fixed-pH solution by ion sieves," *J. Colloid Interface Sci.*, vol. 325, no. 1, pp. 31–40, Sep. 2008.
- [84] L. Wang, C. G. Meng, and W. Ma, "Study on Li^+ uptake by lithium ion-sieve via the pH technique," *Colloids Surfaces A Physicochem. Eng. Asp.*, vol. 334, no. 1–3, pp. 34–39, Feb. 2009.
- [85] L. Tian, W. Ma, and M. Han, "Adsorption behavior of Li^+ onto nano-lithium ion sieve from hybrid magnesium/lithium manganese oxide," *Chem. Eng. J.*, vol. 156, no. 1, pp. 134–140, Jan. 2010.
- [86] C. Özgür, "Preparation and characterization of LiMn_2O_4 ion-sieve with high Li^+ adsorption rate by ultrasonic spray pyrolysis," *Solid State Ionics*, vol. 181, no. 31–32, pp. 1425–1428, Oct. 2010.
- [87] K. Ooi and J. Sakakihara, "Mechanism of Li^+ Insertion in Spinel-Type Manganese Oxide. Redox and Ion-Exchange Reactions," *Langmuir*, vol. 7, pp. 1167–1171, 1991.
- [88] Q.-H. Zhang, S.-P. Li, S.-Y. Sun, X.-S. Yin, and J.-G. Yu, " LiMn_2O_4 spinel direct synthesis and lithium ion selective adsorption," *Chem. Eng. Sci.*, vol. 65, no. 1, pp. 169–173, Jan. 2010.
- [89] R. R. Rashmi, "Preparation and characterization of manganous manganic oxide (Mn_3O_4)," *J. Mater. Sci. Mater. Electron.*, vol. 3, pp. 257–262, 2002.
- [90] Z. M. O. Rzaev, "Complex-Radical Terpolymerization of Glycidyl (Methyl) Methacrylates , Styrene , and Maleic Anhydride," no. May 1998, pp. 1095–1102, 1999.
- [91] L. Alders, *Liquid-liquid extraction : theory and laboratory practice / Alders L.* Elsevier, 1959.
- [92] Y. Uludag, H. Ö. Özbelge, and L. Yilmaz, "Removal of mercury from aqueous solutions via polymer-enhanced ultrafiltration," *J. Memb. Sci.*, vol. 129, no. 1, pp. 93–99, Jun. 1997.

- [93] W. G. H. George E. P. Box , J. Stuart Hunter, *Statistics for Experimenters*, 2nd ed., vol. 21, no. 3. J. Wiley, 2005.
- [94] J. M. Paulsen and J. R. Dahn, “Phase Diagram of Li-Mn-O Spinel in Air,” *Chem. Mater.*, vol. 4, pp. 3065–3079, 1999.
- [95] et al Gerhard Ertl, Helmut Knözinger, Ferdi Schüth, *Handbook of Heterogeneous Catalysis*. WILEY, 2008, p. 4270.
- [96] C. Valley, “Product Bulletin,” 2014.
- [97] G. Xiao, K. Tong, L. Zhou, J. Xiao, S. Sun, P. Li, and J. Yu, “Adsorption and Desorption Behavior of Lithium Ion in Spherical PVC – MnO₂ Ion Sieve,” *Ind. Eng. Chem. Res.*, vol. 51, pp. 10921–10929, 2012.
- [98] L.-W. Ma, B.-Z. Chen, Y. Chen, and X.-C. Shi, “Preparation, characterization and adsorptive properties of foam-type lithium adsorbent,” *Microporous Mesoporous Mater.*, vol. 142, no. 1, pp. 147–153, Jun. 2011.
- [99] T. Ryu, J. Shin, J. Ryu, I. Park, H. Hong, B.-G. Kim, and K.-S. Chung, “Preparation and Characterization of a Cylinder-Type Adsorbent for the Recovery of Lithium from Seawater,” *Mater. Trans.*, vol. 54, no. 6, pp. 1029–1033, 2013.
- [100] Q. H. Zhang, S. Sun, S. Li, H. Jiang, and J. G. Yu, “Adsorption of lithium ions on novel nanocrystal MnO₂,” *Chem. Eng. Sci.*, vol. 62, no. 18–20, pp. 4869–4874, Sep. 2007.
- [101] “Kaliteli ve Güvenli Şebeke Suyu, ASKİ Genel Müdürlüğü.” [Online]. Available: <http://www.aski.gov.tr/tr/kaliteli-sebeke-suyu/index.html>. [Accessed: 24-Aug-2014].
- [102] A. Seidell and W. F. Linke, *Solubilities of Inorganic and Organic Compounds*. Van Nostrand, 1952.
- [103] Rockwood Lithium, *Quotation # 20019109*, no. 047. 2014, pp. 1–3, 2014

APPENDIX A

ALTERNATIVE MATERIALS EMPLOYED IN LITHIUM SEPARATION

In this thesis work, various alternative materials were synthesized and employed in lithium separation besides the materials used in liquid-liquid extraction and adsorption methods. Successfully synthesized alternative materials are comb like polyethylene glycol (C-PEG), poly glycidyl methacrylate, poly vinyl formamide and epoxy-lithium complex. In addition to that, synthesis trials for water soluble crown ether polymer and water insoluble crown ether polymer were done, unfortunately the synthesis of those polymers cannot be achieved throughout the study.

The synthesis, characterization and the lithium separation performance of the successfully synthesized materials were described below.

Comb like poly ethylene glycol (C-PEG)

C-PEG has tines in the form of long poly ethylene glycol chains which are supposed to form coordination complexes with lithium ions. The aim was to dissolve C-PEG in lithium brine and form coordination bonds between lithium ions and oxygen atoms in tines. The coordination bond would selectively separate lithium from brines with multi-ion content. After the coordination bonds formed the mixture was ultrafiltrated in a ultrafiltration set-up, so that the lithium would be separated from the rest of the solution in an efficient and selective way.

The synthesis of comb like poly ethylene glycols (C-PEG) was first started from the monomer synthesis. Polyethylene glycol with a certain molecular weight was reacted with methacryloyl chloride in toluene. After that the resulting monomer was radically polymerized and comb-like poly ethylene glycol was synthesized. The reaction sequence is shown in Figure A.1.

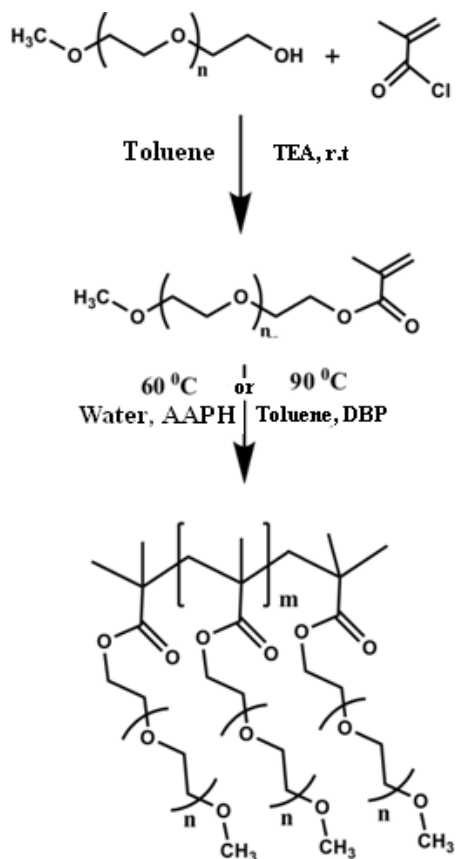


Figure A.1 Reaction sequence of comb like poly ethylene glycol

The characterization of the monomer was done by $^1\text{H-NMR}$ spectrum as given in Figure A.2.

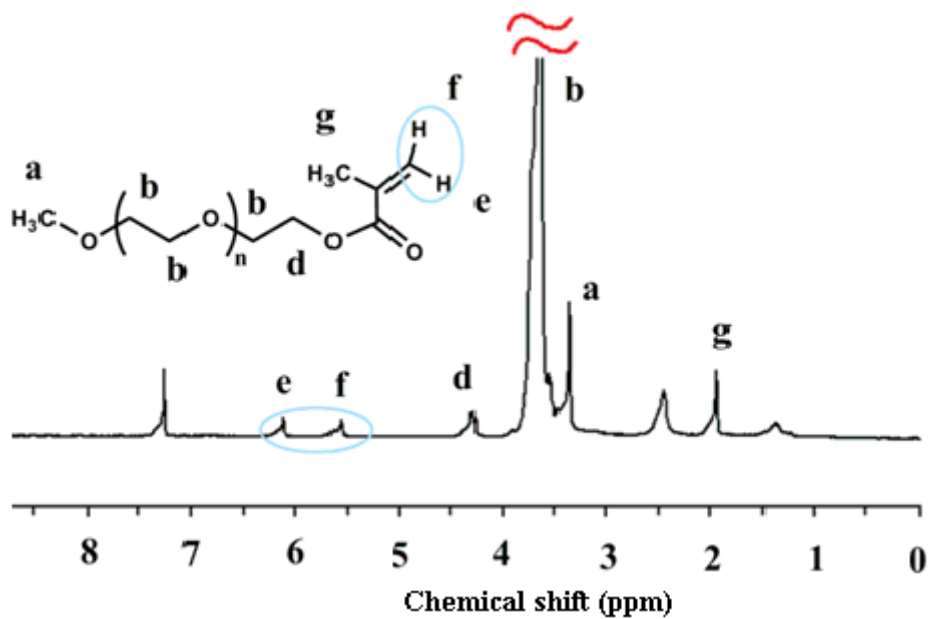


Figure A.2 ¹H-NMR spectrum of C-PEG monomer

The signals observed at different ppm values were paired with relevant chemical groups. The signal at 3.3 ppm belongs to methyl end group attached to oxygen. The strong signal at 3.7 ppm shows the methylene bridge protons in polymer backbone. Two signals at 5.6 and 6.2 belong to olefinic hydrogens and signal at 2 ppm shows the methyl group protons attached to double bond.

The characterization of the polymer (C-PEG) was done by ¹H-NMR spectrum as given in Figure A.3.

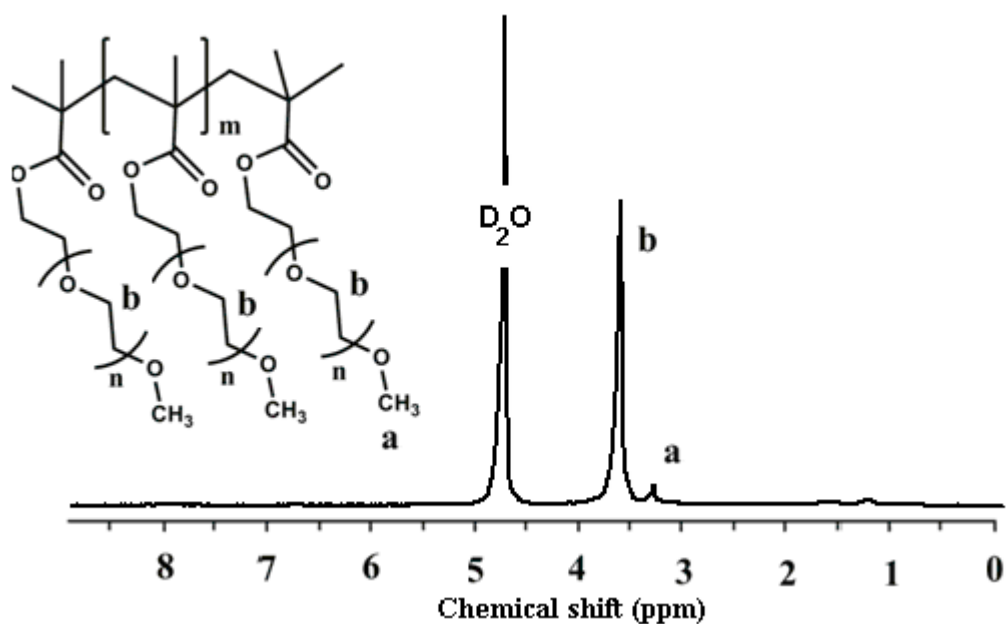


Figure A.3 ^1H -NMR spectrum of C-PEG

In the structure of polymer, two types of protons were observed in 3.3 ppm and 3.6 ppm which belong to methyl end group and methylene bridge protons respectively. The detailed synthesis procedure was given in two steps.

- Synthesis of PEG functionalized with methacrylate;

75 g (100 mmol) of polyethylene glycol (PEG, Mn:750 Da) was weighed, dissolved in toluene and put into a 250 ml volume flask. Then 11.2 g (110 mmol) of distilled triethyl amine was added to the mixture. When this mixture was stirred at 0 °C, 13.25 g (110 mmol) methacryloyl chloride was added dropwise. When the first drops fed into the mixture, a precipitate of triethyl ammonium was appeared in the solution. After the precipitate was filtered from the solution, the excess of toluene was evaporated and PEG with functionalized with methacrylate was precipitated in hexane. The resulting product (MPEG) was dried in vacuum dryer at 40 °C for 12 hours.

- Synthesis of comb like PEG (C-PEG)

8.35 g (100 mmol) of MPEG was weighed and dissolved in 100 ml water in a 100 ml volume erlenmeyer. After nitrogen gas passed through the mixture, the erlenmeyer

was placed into an oil bath at 60 °C and 54 mg (2mmol) 2,2'-Azobis(isobutyramidine) dihydrochloride (AABH), ([AABH]/[MPEG]: 1/50) was added to the mixture. The reaction continued until the magnet in the Erlenmeyer cannot mix the solution due to the increase in the viscosity. Then, the resulting solution was filtrated with a proper size membrane in order to use in polymer enhanced ultrafiltration (PEUF) experiments. The final concentration was measured by taking a sample from it and dried in a drying oven.

The separation efficiency of C-PEG was analyzed by utilizing a polymer enhanced ultrafiltration set-up. To observe the time where the permeate flux and concentration reaches steady state, results of a representative experimental run was given in Table A.1. It was seen that steady state was attained after two hours.

Table A.1 A representative experimental run for a PEUF experiment

Polymer	: C-PEG				
Polymer MW	: ~50 kDa				
Loading	: 0.01				
pH	: 7.3				
ΔP	: 200kPa				
MWCO	: 20 kDa				
Time (hour)	0	1	2	3	4
F_p (L/m ² h)		4.8	4.6	4.6	4.6
pH(Feed)	7.3	7.4	7.3	7.3	7.3
T (°C)	25.0	25.2	25.4	25.3	25.3
Li C_f (ppm)	8.0	7.9	7.9	7.9	7.9
Li C_p (ppm)		6.8	6.7	6.7	6.7
R		0.14	0.15	0.15	0.15
	$F_{p,avg}=0.15$	$C_{f,avg}=7.9$	$C_{p,avg}=6.7$		$R_{avg}=0.15$

In order to understand whether C-PEG works in PEUF or not, some preliminary experiments at different pH values with constant loading (0.01) and temperature (25 °C) were performed and retention values were calculated. The results are shown in Figure A.4.

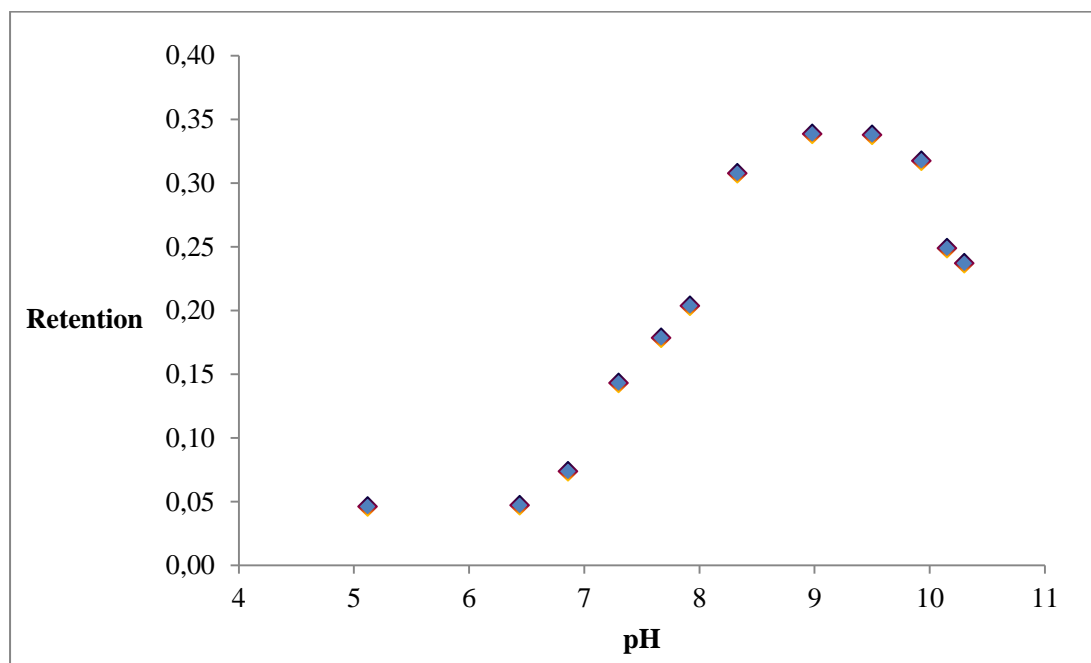


Figure A.4 Retentions for different pH values at 25 °C and constant loading (0.01) for C-PEG

As it can be deduced from Figure A.4, a maximum retention value of 0.35 could be acquired with C-PEG (Mn:950) around pH 9.

Effect of loading value on retention was also investigated at pH=9 and the results listed in Table A.2 were acquired.

Table A.2 Retention values for different loadings at 25 °C and pH:9

Retention	Loading
0.21	0.1
0.35	0.01
0.28	0.002

It was deduced that, when loading value increased above 0.01, retention value started to decrease. This unusual behavior was attributed to the decrease in polymer solubility resulting in coiling up of polymer chains.

Next, the selectivity of C-PEG polymers on PEUF was investigated with concentrated sea water taken from Çamaltı Salina under varying loading values and the results listed in Table A.3 were obtained.

Table A.3 Retention values for concentrated brine taken from Çamaltı Salina in PEUF utilizing C-PEG under pH:7.4 and 25 °C

Metal ion	Retention values (R)		
	Loading:0.1	Loading:0.01	Loading:0.001
Na	0.060	0.090	0.041
K	0.014	0.049	0.001
Mg	0.093	0.134	0.136
Li	0.086	0.178	0.136

It was seen that C-PEG is selective to lithium near sodium and potassium in 2 to 4 folds. For magnesium, the retention values came out to be similar for different loading values. Only when loading value is 0.01, the retention value of lithium seems to be higher than magnesium. At this point, the selectivity values of C-PEG were found as $S_{Li/Na}=2$, $S_{Li/K}=3.6$, $S_{Li/Mg}=1.3$.

Even though the selectivity values are below the expectations, when the high concentration of potassium (around 10000 ppm), magnesium (around 20000 ppm) and sodium (around 75000 ppm) near lithium (around 1.25 ppm) is considered, the results were found meaningful for utilizing PEUF method in separation of lithium.

After these results were examined, the synthesis of C-PEG was done by different molecular weight PEG methacrylate to highlight the definite separation efficiency of PEUF with C-PEGs. Additional C-PEGs were synthesized having different Mn values (300, 500, 950 and 2000). The most satisfactory results were obtained by C-PEG with a monomer MW around 950 g/mol. The higher MW polymer which was

synthesized by PEG methacrylate with Mn: 2000 had a solubility problem and PEUF set-up could not be utilized.

The synthesis experiments with monomers having Mn values of 300 and 500 did not give expected retention values. The retention values for C-PEG (Mn: 300) and C-PEG (Mn: 500) were given in Table A.4 for different pH values at loading: 0.01.

Table A.4 Retention values for different Mn C-PEG under various pH at loading: 0.01

pH	C-PEG	C-PEG
	(Mn: 300)	(Mn: 500)
	Retention	Retention
7	0.04	0.11
8	0.05	0.21
9	0.12	0.21
10	0.33	0.21
11	0.20	0.15

After that, PEUF experiments were conducted without any polymer in order to understand the effect of membrane on retention values, and the results were tabulated in Table A.5Table .

Table A.5 Retention values for membrane (PES MWCO: 5kDa) on separation of lithium via PEUF under varying pH.

pH	Retention
6.7	0.15
7.5	0.16
9	0.24
10	0.32
11	0.19

Table A.4 and Table A.5 show that C-PEG does not actually interact with lithium ions and cause their separation, the main reason of separation is the membrane barrier. The membrane employed in PEUF experiments was polyether sulfone with a

molecular weight cut-off 5 kDa. The molecular structure of PES membrane is seen in Figure A.5.

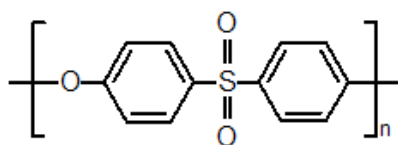


Figure A.5 The molecular structure of PES membranes

The interaction of lithium ions with PES membrane can be occurred via unshared electrons of sulfone and ether group. Since oxygen atoms tend to be more electrophilic than sulfur atoms, the electron cloud between sulfur and oxygen atoms is oriented towards oxygen, which means slightly negative charge on oxygen atoms. The remaining positive charge on sulfur atom can also be stabilized by the resonance effect of benzene rings in the structure. If we consider that lithium ions present in solution are in Li^+ form, an interaction of lithium ions with sulfone group oxygens is predictable.

After these findings, the selectivity of membrane towards lithium near foreign ions was questioned and a mixture of lithium, sodium, potassium, magnesium each having a concentration around 10 ppm in solution was fed to the PEUF set-up with the same membrane (PES MWCO: 5 kDa). The results are tabulated in Table A.6.

Table A.6 Retention values for Na⁺, K⁺, Mg²⁺ and Li⁺ with PES membrane at varying pH values.

pH	Retention (Li⁺)	Retention (Na⁺)	Retention (K⁺)	Retention (Mg²⁺)	Retention (Total)
7.1	0	0.03	0.04	0.05	0.12
7.5	0.02	0.03	0.04	0.01	0.10
8.25	0.01	0.04	0.04	0.03	0.12
9.5	0.03	0.05	0.05	0.10	0.23
10.1	0.03	0.05	0.07	0.07	0.22

As it is obviously deduced from Table A.6, retention values for lithium near foreign ions are smaller which means that the membrane does not have selectivity towards lithium. Mg²⁺ ions have the highest retention value around pH=9.5. It can be explained by the +2 charge, which attracts magnesium towards slightly negative sulfur more than other cations. When we look to the total retention values and compare them with the values in Table A.6, it is seen that the capacity of membrane to hold cations is somewhat filled by separate individual cations. The small difference in total retention values can be attributed to the steric effects especially caused by the magnesium ion which is the largest cation among them with the highest charge.

Poly glycidyl methacrylate

The synthesis of poly glycidyl methacrylate was started with the reaction of glycidyl methacrylate with dilute sulfuric acid for overnight in order to enhance its water solubility with introduced hydroxyl groups. The reaction sequence is as shown in Figure A.6;

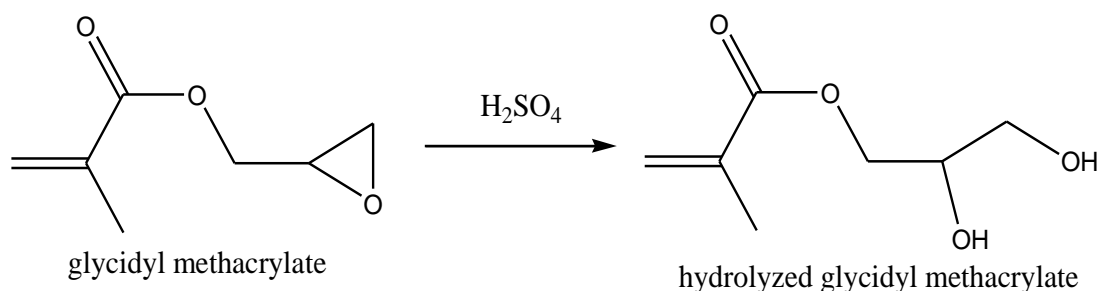


Figure A.6 The reaction sequence for hydrolyzed glycidyl methacrylate synthesis

Afterwards, the polymerization of the hydrolyzed monomer was done with 2,2'-Azobis (isobutyramidine) dihydrochloride in 1/100 molar ratio with 15 % monomer concentration in water at 65 °C for 4 hours. The resulting polymer has the molecular structure shown in Figure A.7.

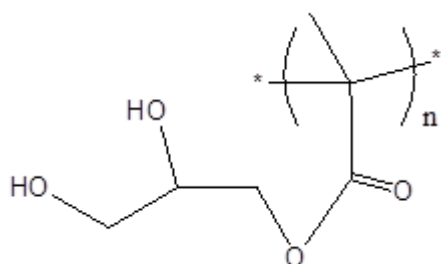


Figure A.7 Molecular structure of hydrolyzed poly glycidyl methacrylate

The resulting poly glycidyl methacrylate polymer becomes insoluble in water due to slight crosslinking occurs during the polymerization reaction. The gel like polymer

was than chopped for 2-3 minutes at 300 rpm in a blender and washed with water several times. The hydroxyl groups in gel-like polymer are supposed to make coordination bonds with lithium ions and then separate the lithium ions from aqueous phase. The logic behind this technique is very similar to the technique used with comb like poly ethylene glycols. Expect that, this material does not dissolve in water and does not require a polymer enhanced ultrafiltration technique.

In the separation experiments simply the lithium solution was mixed with gel like polymer and pH of the solution was adjusted to 10 by ammonium chloride and ammonia buffer. The solution was mixed for 24 hours and then wait for another 24 hours to gel-like polymers settle down. The supernatant solution was analyzed in atomic absorbance spectrophotometer. 47.2 ppm feed solution was mixed with 0.33 g gel-like polymer and the capacity was found as 1.2 mg Li/g polymer. This value appears to be so small compared to the values acquired with manganese oxide adsorbents. Therefore further experiments with hydrolyzed poly glycidyl methacrylate gel-like polymers were not held on.

Poly vinyl formamide

Formamides are very polar molecules and have strong solvation powers. In Chapter 3.2, alkyl formamides were employed as extraction solvents for lithium chlorides and fairly high distribution coefficient values were acquired in the experiments. Therefore, it was thought that, to synthesize a polymer of vinyl formamide can lead us to high retention values in polymer enhanced ultrafiltration method. The synthesis of poly vinyl formamide was accomplished by addition polymerization technique starting from vinyl formamide monomer. 2,2'-Azobis (isobutyramidine) dihydrochloride was used as an initiator. The final product was dissolved in water and the polymer solution was first filtrated with a membrane having molecular weight cut-off: 3-20 kDa. Adjustment of the pH was done by ammonia-ammonium chloride buffer. The final mixture was fed to the polymer enhanced ultrafiltration (PEUF) set-up and the experiment was repeated for two different pH values at loading:0.01 and 25 °C. The resulting retention values are tabulated in Table A.7 and shown below.

Table A.7 PEUF experiment results by poly vinyl formamide

	pH: 8	pH:9
Feed conc. (ppm)	45.68	45.165
Permeate conc. (ppm)	44.64	43.21
Retention	0.023	0.043

As it can be seen from Table A.7, poly vinyl formamide has no functionality in separation of lithium. Therefore further experiments were not held on.

Epoxy-lithium complex

Epoxy lithium complex was synthesized by mixing 1,2 epoxy octane by lithium chloride solution in NMP and react the epoxide groups by triethyl amine addition at high temperature. The final product was supposed to have a structure shown in Figure A.8.

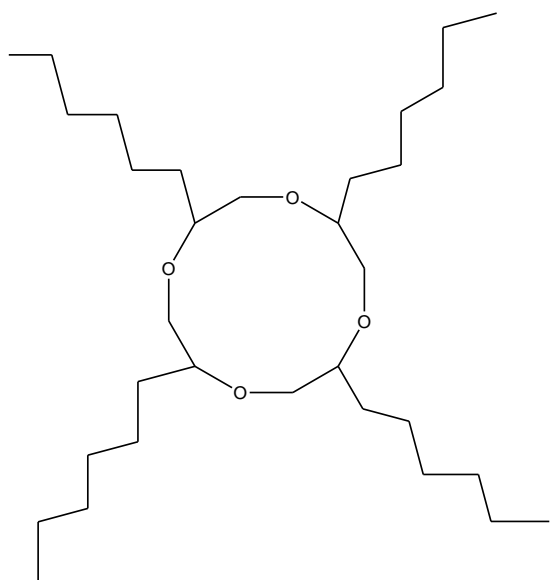


Figure A.8 4 octyl 12-crown-4 ether

This hypothetical molecule does not mix with water due to alkyl groups and can make complexes with lithium ions by oxygen atoms. Therefore it could be used as selective liquid-liquid extraction agent to separate lithium from brines.

The H-NMR spectrum of the resulting product is given in Figure A.9.

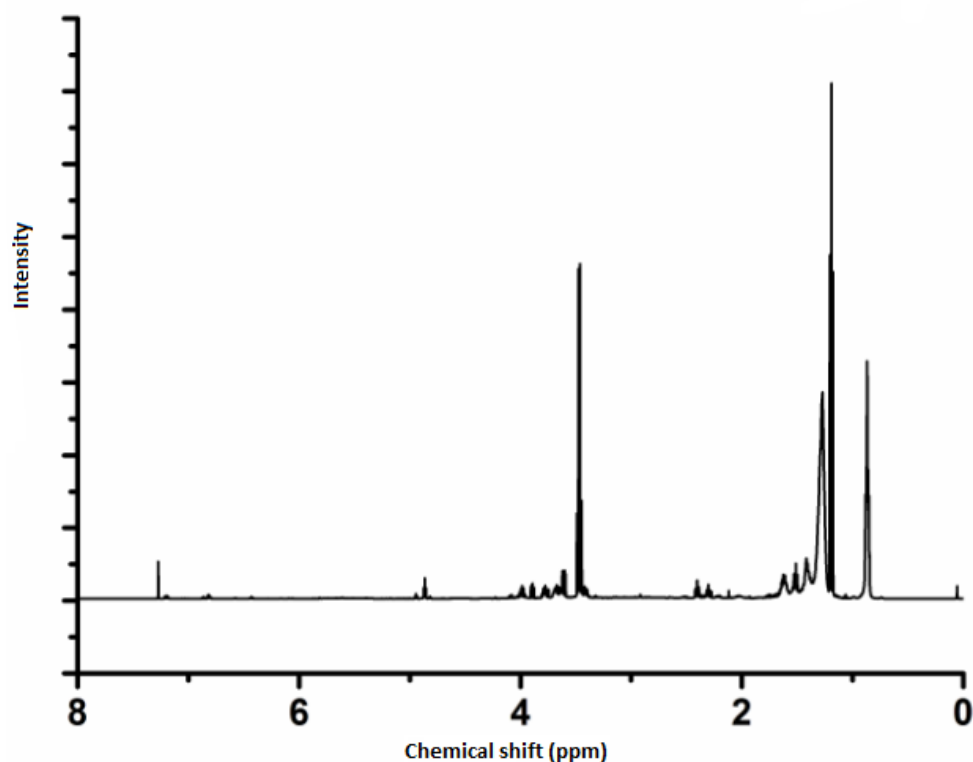


Figure A.9 H-NMR spectrum of 4 octyl 12-crown-4 ether

Figure A.9 shows that the peak which is divided into three at 0.9 ppm represents methyl groups at the end of four octyl groups. The signals around 1.3 and 1.5 show the methylene bridge protons near to oxygen. In signal at 3.5 ppm, $-\text{CH}_2-$ groups on the ring are detected. They are shifted to right which may be caused by the lithium ions coordinated in the middle of the ether ring. The synthesis of 4 octyl 12-crown-4 ether started with dissolving lithium chloride in minimum amount of N-methyl pyrrolidone. Then, 1,2 epoxy octane was added into the mixture. The molar ratio of lithium chloride to 1,2 epoxy octane was 1:4. The mixture was then heated to 140 °C and 2 ml of triethyl amine was added to the mixture. Under a reflux, the reaction continued for 12 hours. The resulting black mixture was mixed with water and boiled to recover the desired product with water. After 10 hours of distillation, the water and slightly yellow colored organic material were condensed and mixed with diethyl ether to extract the organic material from water. The ether phase was separated by a separation funnel and remaining solvent was evaporated in rotary evaporator which left the desired product. The resulting product was very low in quantity, so the

extraction experiments with that solvent could not be held on. The synthesis route was presented for further research about topic.

Water soluble 12-crown-4 etheric polymer

12-Crown-4 ethers are known to bind with lithium ions by coordination bonds. In order to employ ethers in PEUF system, water soluble polymers with 12-crown-4 ether side groups must be synthesized. The hydrophobic nature of crown ethers makes it very difficult to integrate them into a water soluble polymer structure. The problem was handled by a new synthesis pathway which was proposed to integrate crown ethers in a water soluble polymer as shown in Figure A.10.

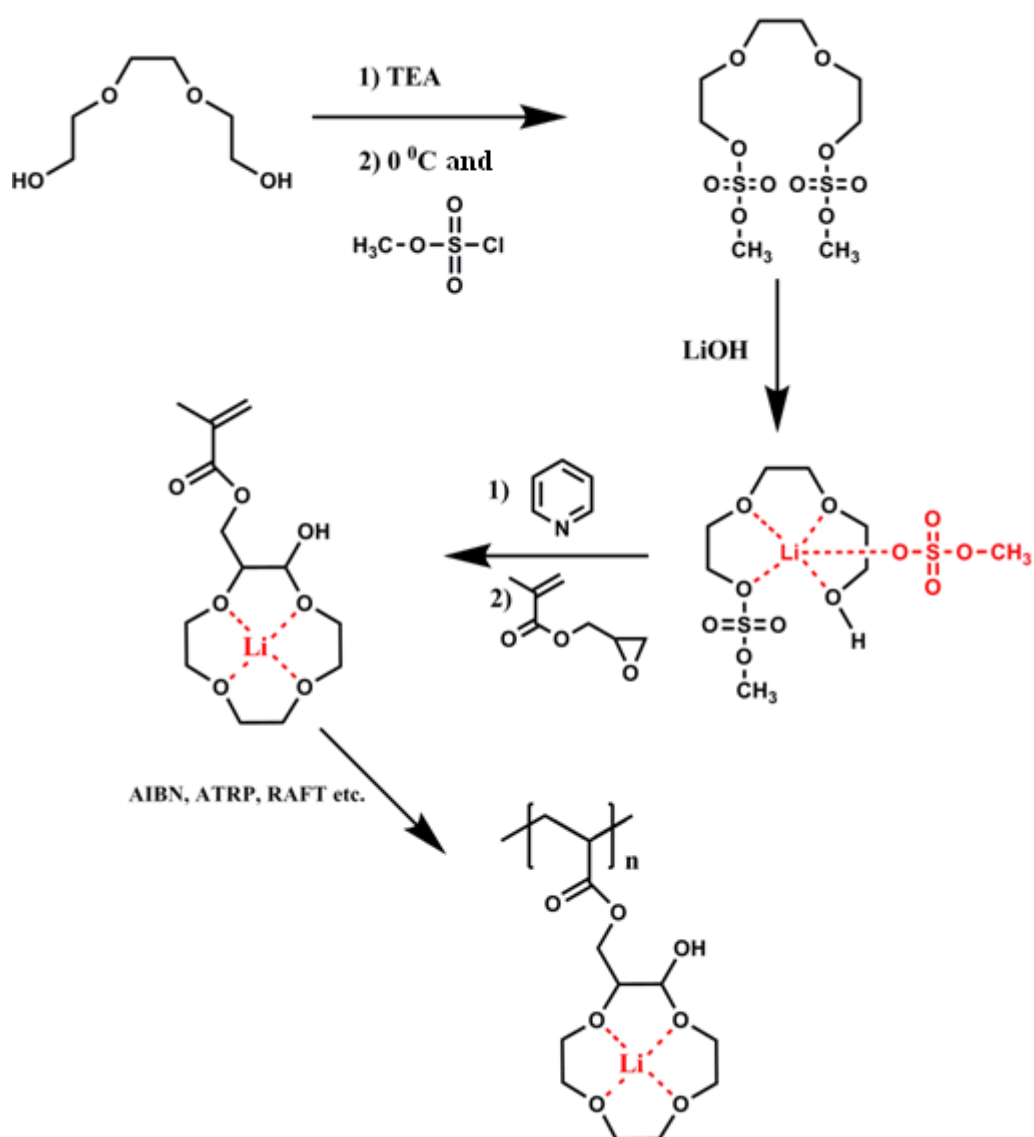


Figure A.10 The pathway of synthesis of water soluble crown ether polymers

The synthesis was started with dripping 0.2 mol sulfonyl chloride by a funnel into an erlenmeyer flask which had 0.1 mol triethylene glycol. The reaction took place in

the presence of triethyl amine at 0 °C by the aid of an ice bath. In the second step, 0.1 mol LiOH was dissolved in N-methyl pyrrolidone and mixed with the product. After the addition of LiOH, no reaction was observed and the sequence was terminated.

The synthesis experiments couldn't be successful throughout the study, because during the synthesis, candidate crown ether monomer structure with SO₄ leaving groups must dissolve the lithium hydroxide in step 2. However the candidates could not dissolve the lithium. Therefore a successful synthesis route could not be established, but the proposed reaction sequence was given for further investigation.

Water insoluble 14-crown-4 etheric polymer

Lastly, another synthesis route was studied to synthesize a 14-crown-4 ether monomer in order to polymerize it and get a water insoluble adsorbent. The proposed synthesis has eight steps.

In the first step, equimolar 1,3 propanediol and metallic sodium was mixed (See Figure A.11). Although sodium metal is very reactive against OH groups the synthesis could only be done by adding additional methanol (petrol ether is also tried but does not give reaction). The reaction proceeded under vacuum (100 mbar) at 90 °C for 24 hours. In order to get rid of methanol, the mixture was heated up to 130 °C under vacuum in final step.

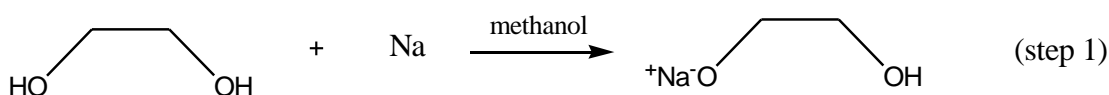


Figure A.11 14-crown-4 monomer synthesis step 1

In the second step, sodium propanediol salt was mixed with dibromoethane (See Figure A.12). In order to sustain a well-mixed system, propanediol salt was first heated to 60 °C, then dibromoethane was dripped onto it. The reaction took place very fast, and due to the heat release during reaction, the temperature of the mixture increased rapidly. The reaction continued for 24 hours at 70 °C. The resulting product was tried to be separated by dissolving it in diethyl ether, but it didn't work out. Then methanol was used to dissolve the mixture and the precipitated salt was filtered. During the next step which was the evaporation of methanol from the mixture, additional salt was precipitated, so it was thought that, methanol also dissolved the salt. In order to get rid of salt, the liquid part was decanted and used in the next step.

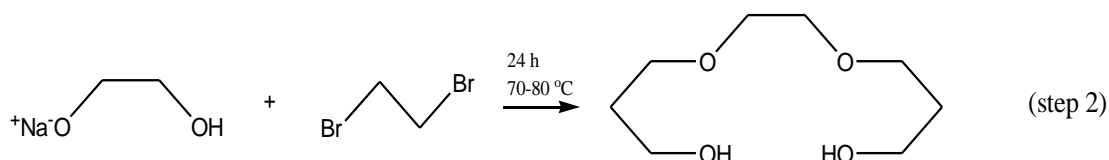


Figure A.12 14-crown-4 monomer synthesis step 2

In third step, the product was mixed with butyl lithium in a molar ratio of 1:2 (See Figure A.13). Butyl lithium could be stored in hexane solution, therefore the reaction continued in hexane medium at room temperature for 8 hours.

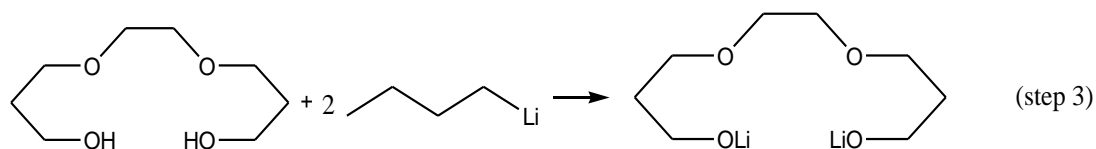


Figure A.13 14-crown-4 monomer synthesis step 3

In the fourth step, glycidol was dissolved with equivolume dichloromethane (See Figure A.14). Then, benzoyl chloride was dissolved with equivolume dichloromethane and pyridine was dissolved with equivolume dichloromethane. Equimolar benzoyl chloride and pyridine solutions were dripped onto equimolar glycidol solution simultaneously. The reaction was held on in an ice bath under vigorous stirring for 15 hours. After the reaction was completed, the product mixture was taken into separation funnel. Ice-water and sodium chloride was added to funnel and the funnel was shaken vigorously. Then the phase separation was observed in the funnel. The dichloromethane phase was taken and mixed with sodium sulfate in order to separate remaining water residues. In the rotary evaporator, the dichloromethane was evaporated and an orange colored viscous liquid was taken as a product.



Figure A.14 14-crown-4 monomer synthesis step 4

In the fifth step, the product was mixed with mesyl chloride (See Figure A.15). Mesyl chloride was put into a reaction balloon which was placed in an ice bath and the product of step 4 was dripped onto it. After dripping, the mixture was taken into room temperature and mixed for 60 hours.

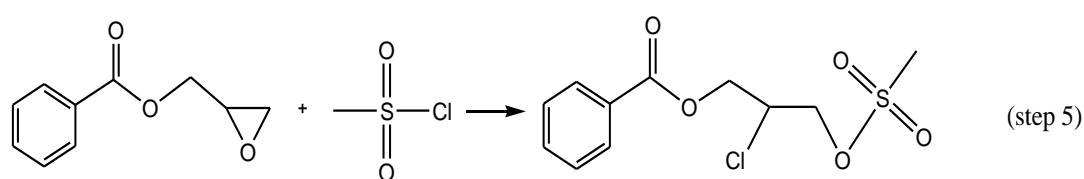


Figure A.15 14-crown-4 monomer synthesis step 5

In the sixth step, the product after step 5 was mixed with the product which was acquired after step 3 and a condensation reaction was expected to synthesize a crown-4-ether structure (See Figure A.16). While dripping, a phase separation occurred in the mixture. The reaction was continued for 15 hours at 80 °C. The hexane phase was separated into another erlenmeyer and put aside. The remaining black residue was held in the balloon.

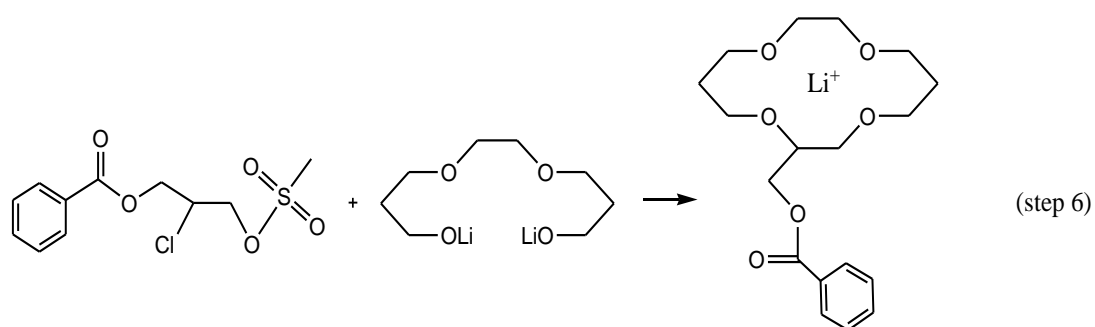


Figure A.16 14-crown-4 monomer synthesis step 6

Afterwards a TLC experiment was done in order to understand how many products were in the hexane phase. TLC paper showed, 7 separate dots, which designates 7

different products. At that point, different products could not be separated and the next two steps could not be done.

The final two steps were designed as shown in Figure A.17 and Figure A.18.

In step 7, the product at step 6 was supposed to mix with acryloyl chloride and a monomer of 14-crown-4 ether form would form.

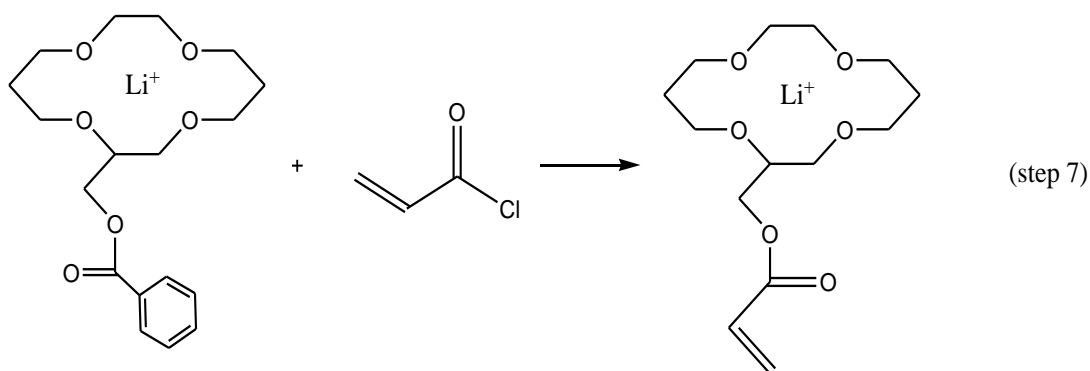


Figure A.17 14-crown-4 monomer synthesis step 7

In the final step, 14-crown-4 ether monomer would be polymerized by AIBN at 65 °C and finally a candidate water insoluble polymer to be used as an adsorbent in lithium separation from brines would be synthesized.

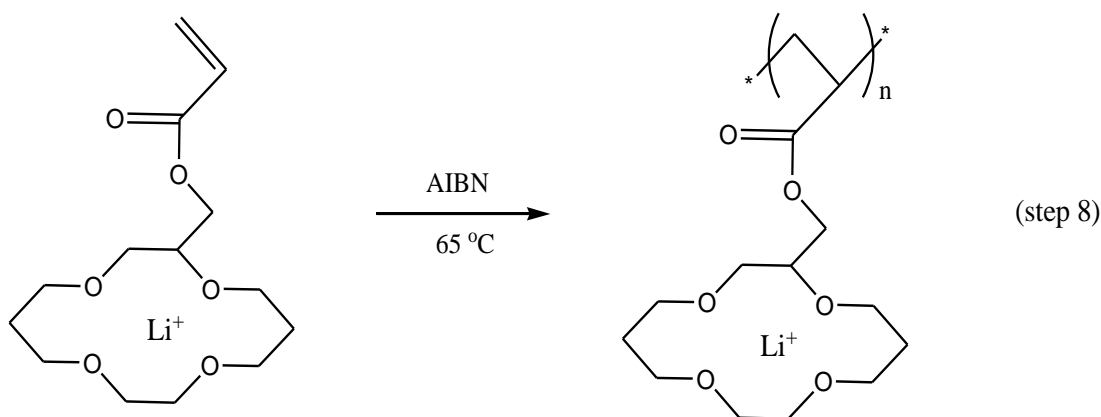


Figure A.18 14-crown-4 monomer synthesis step 8

APPENDIX B

XRD MEASUREMENTS OF SYNTHESIZED LITHIUM MANGANESE OXIDES

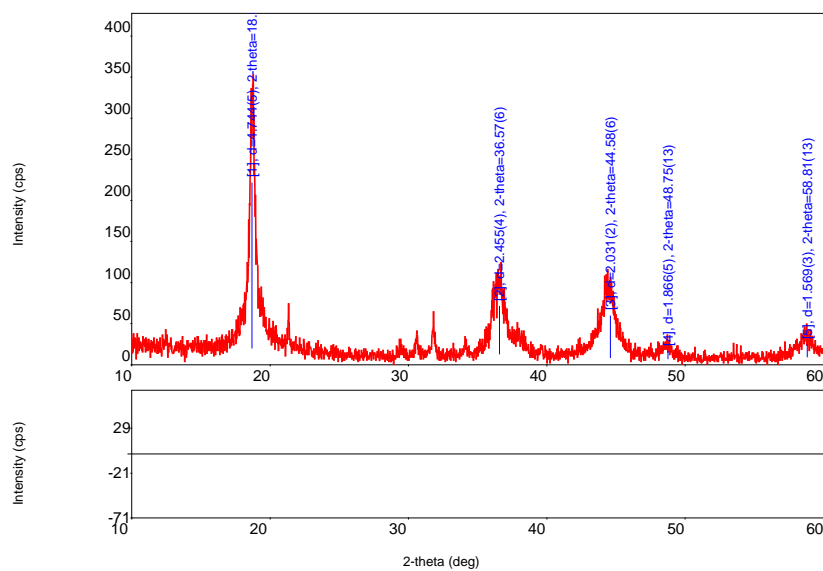


Figure B.1 XRD pattern of spinel lithium manganese oxide LMO (350 °C, Li/Mn=1)

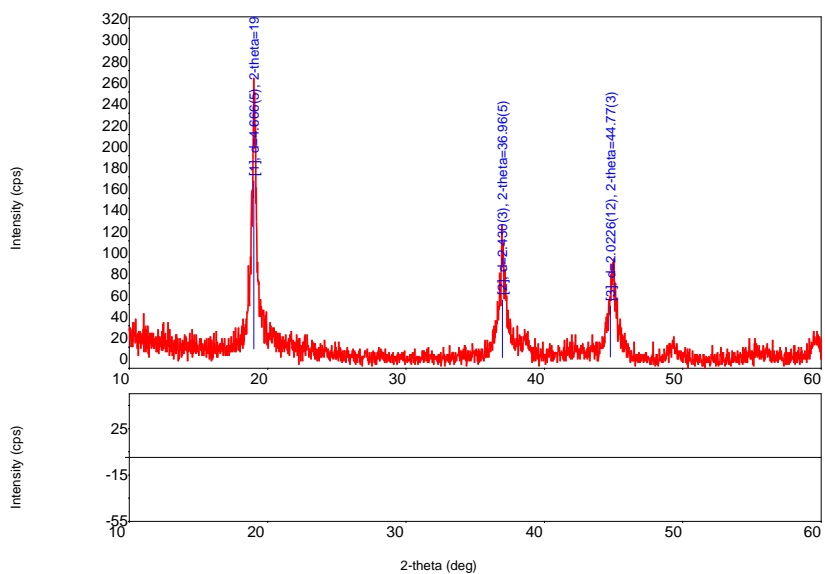


Figure B.2 XRD pattern of the spinel lithium manganese oxide HMO (350 °C, Li/Mn=1)

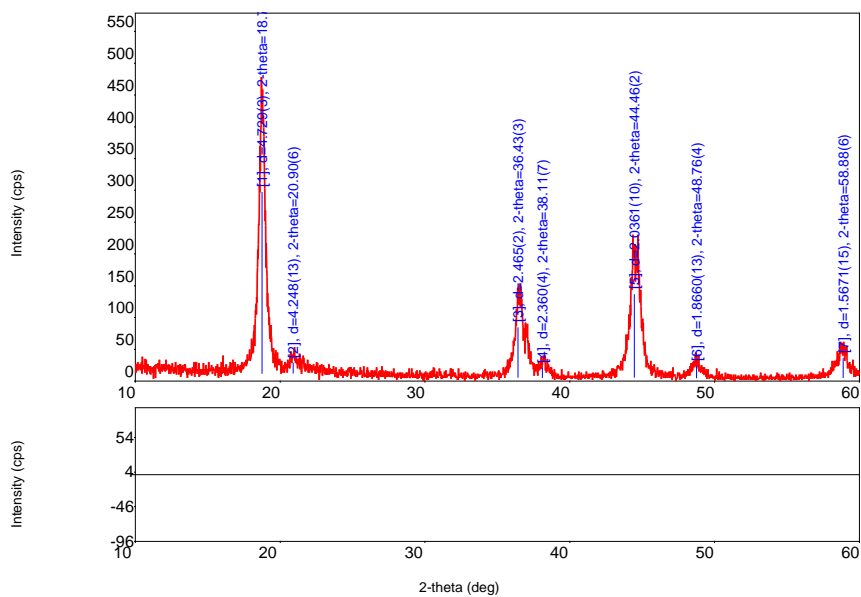


Figure B.3 XRD pattern of the spinel lithium manganese oxide LMO (550 °C, Li/Mn=1)

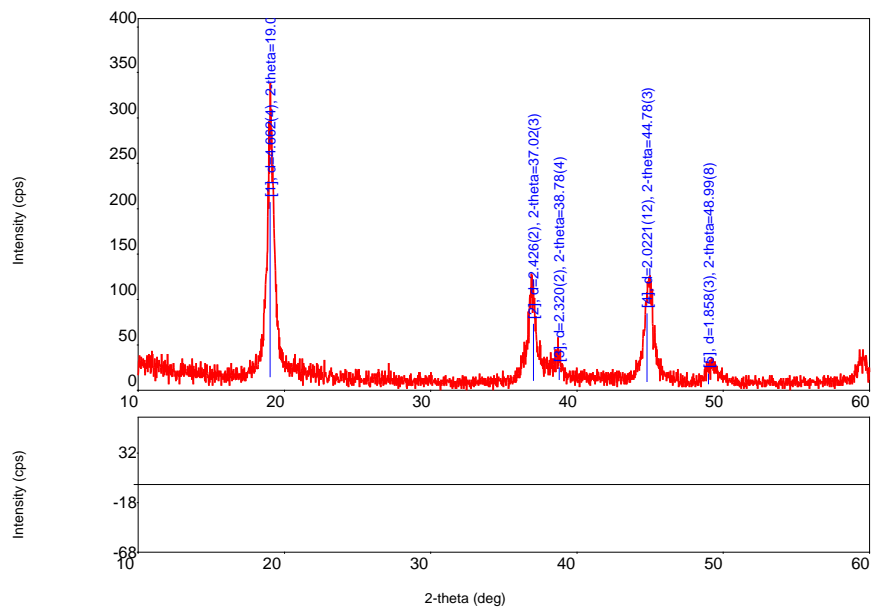


Figure B.4 XRD pattern of the spinel lithium manganese oxide HMO (550 °C, Li/Mn=1)

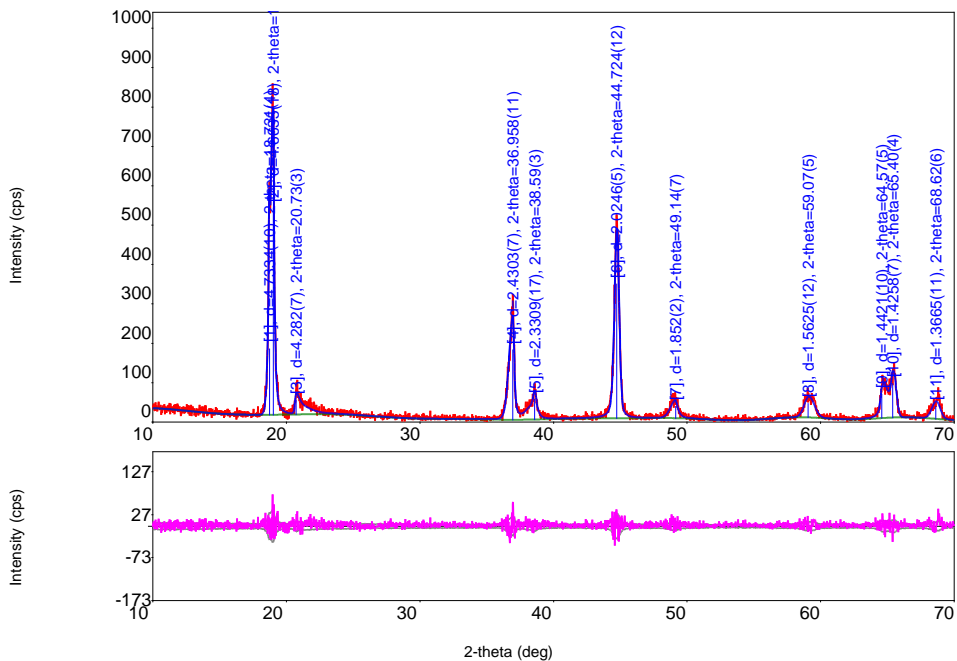


Figure B.5 XRD pattern of HMO for the synthesis at 750 °C

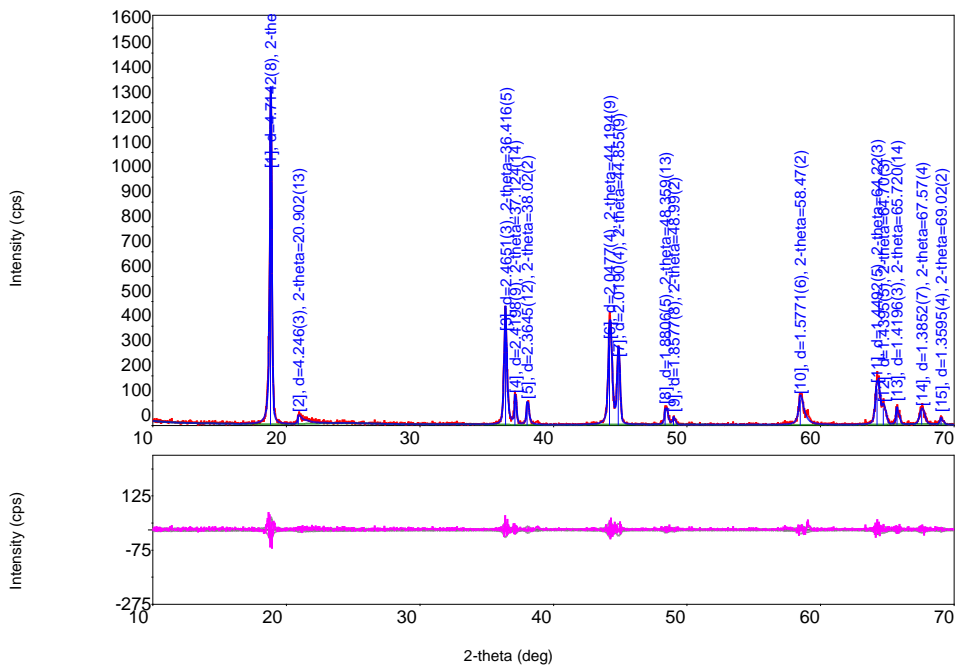


Figure B.6 XRD pattern of LMO for the synthesis at 750 °C

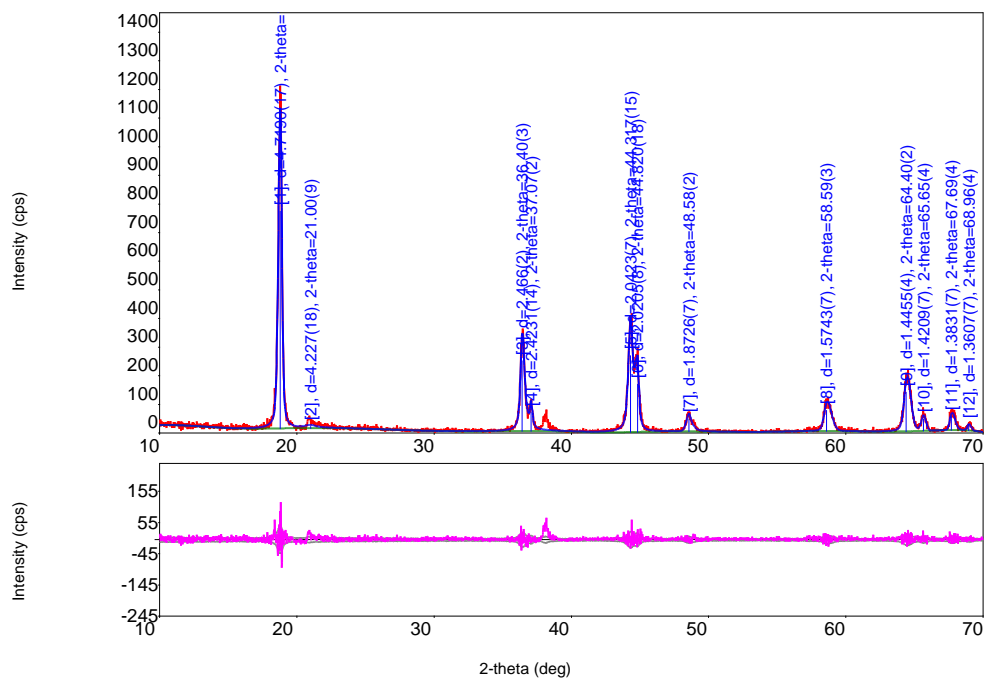


Figure B.7 XRD pattern of LMO for the synthesis at 650 °C

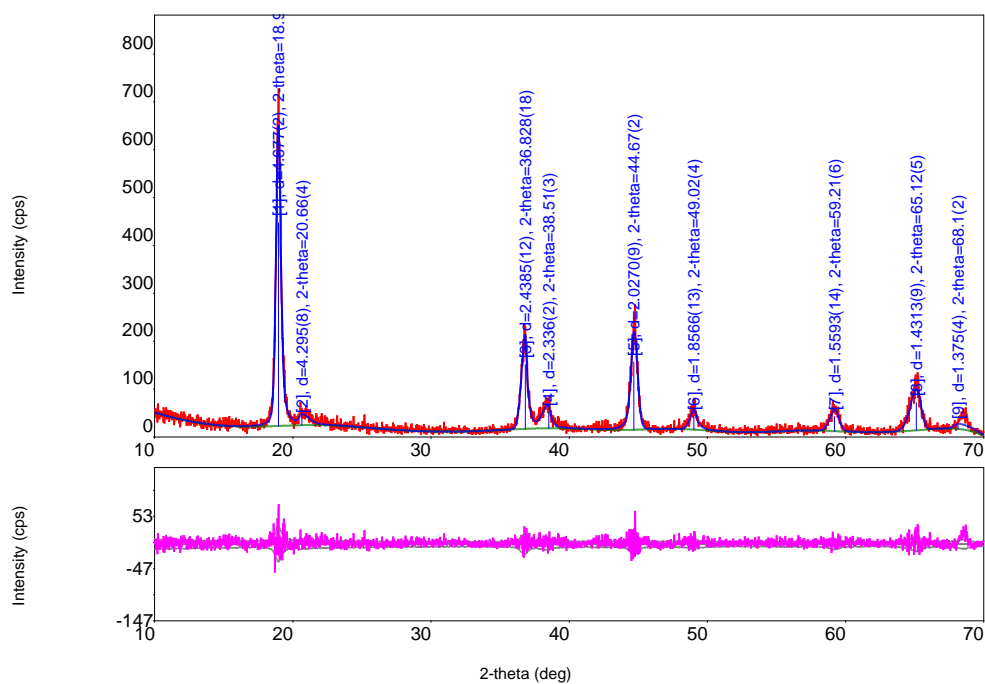


Figure B.8 XRD pattern of HMO for the synthesis at 650 °C

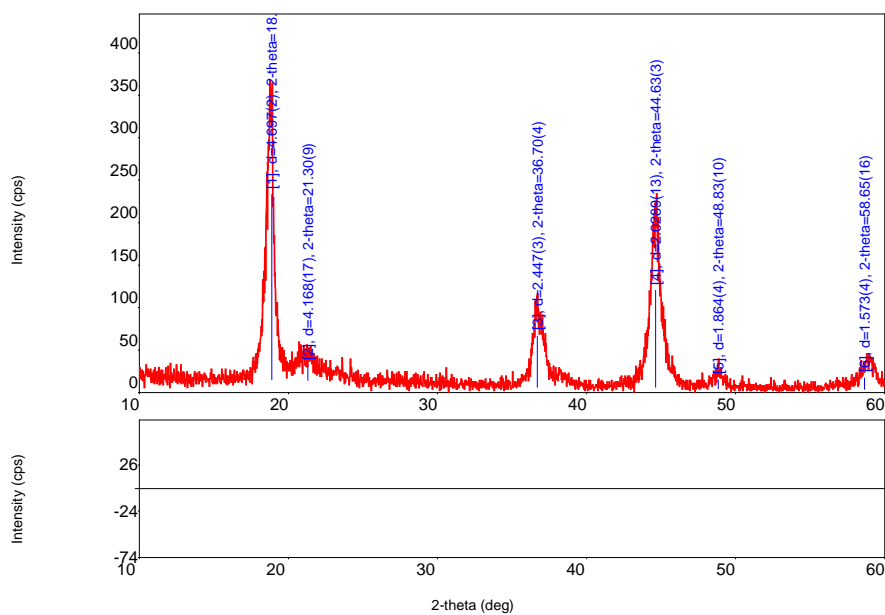


Figure B.9 XRD pattern of the spinel lithium manganese oxide LMO (450 °C, Li/Mn=1.25)

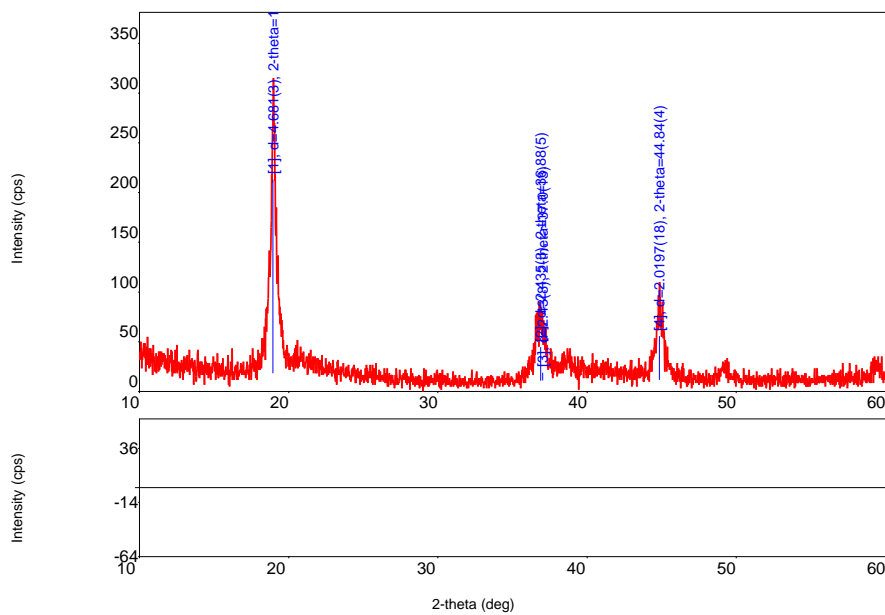


Figure B.10 XRD pattern of the spinel lithium manganese oxide HMO (450 °C, Li/Mn=1.25)

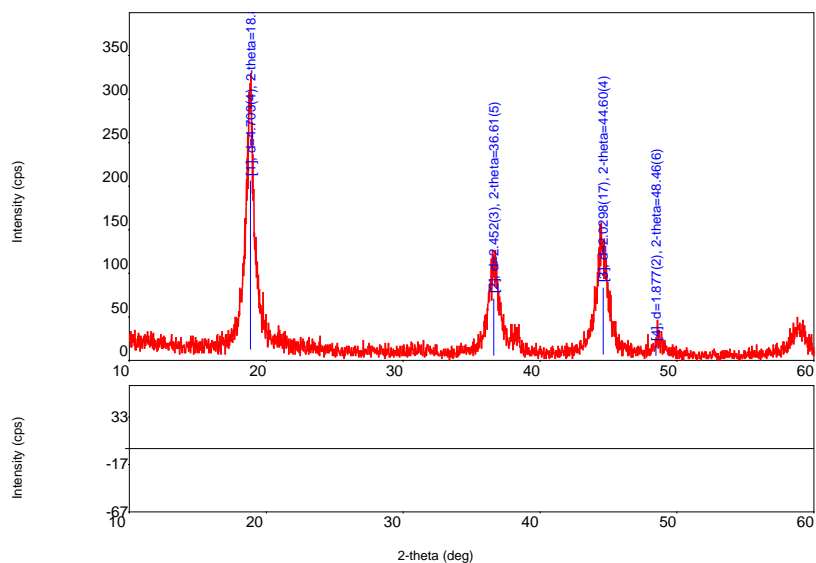


Figure B.11 XRD pattern of the spinel lithium manganese oxide LMO (450 °C, Li/Mn=0.8)

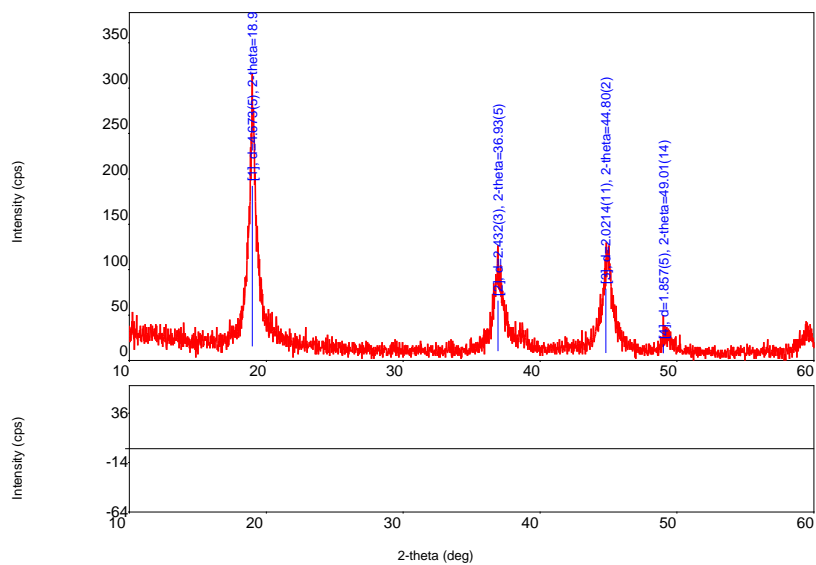


Figure B.12 XRD pattern of the spinel lithium manganese oxide HMO (450 °C, Li/Mn=0.8)

APPENDIX C

SEM PHOTOGRAPHS OF SYNTHESIZED PSMA-LiMnO BEADS

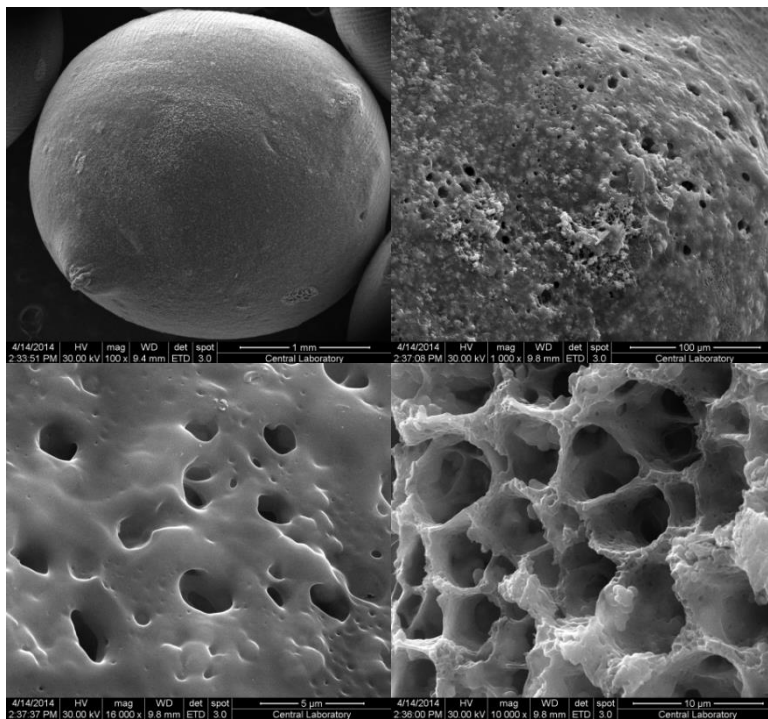


Figure C.1 SEM photographs for Bead T14

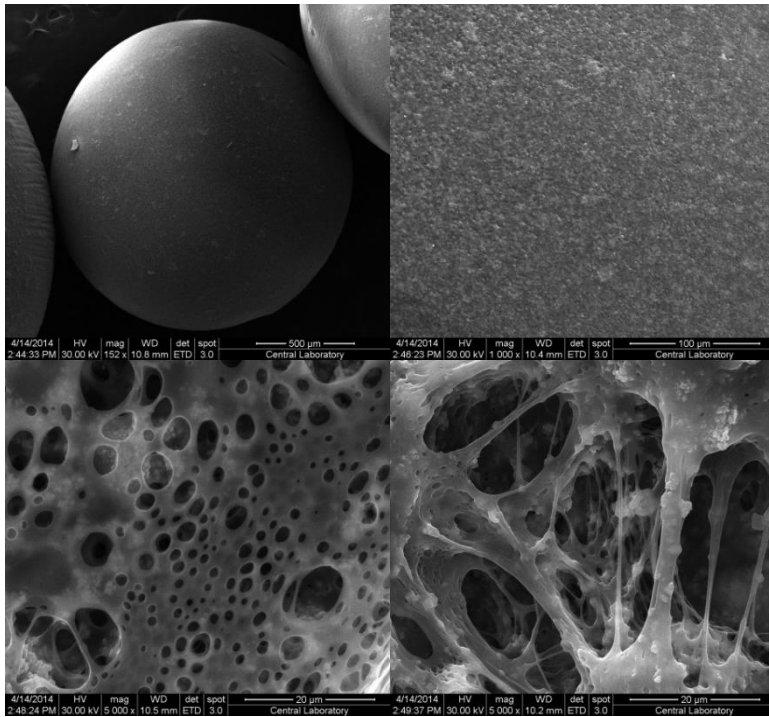


Figure C.2 SEM photographs for Bead T15

APPENDIX D

THE FEASIBILITY STUDY TO RECOVER LITHIUM CARBONATE FROM ÇAMALTI SALINA AND BORON CLAY EXTRACT

The potential sources to produce lithium conventionally in Turkey are Çamaltı Salina, Salt Lake and boron clay extract as mentioned in this study. The low concentration of lithium especially in seawater is the major problem with the high magnesium ion content. However a selective separation process including lithium manganese oxides can resolve the problems and lead a way to an industrial production of lithium carbonate.

In this section, the feasibility studies to recover lithium from the potential resources; Çamaltı Salina and boron clay extract in Bigadiç.

Li₂CO₃ production from Çamaltı Salina

Lithium carbonate production may be achieved by a system which is drawn in Figure D. 1.

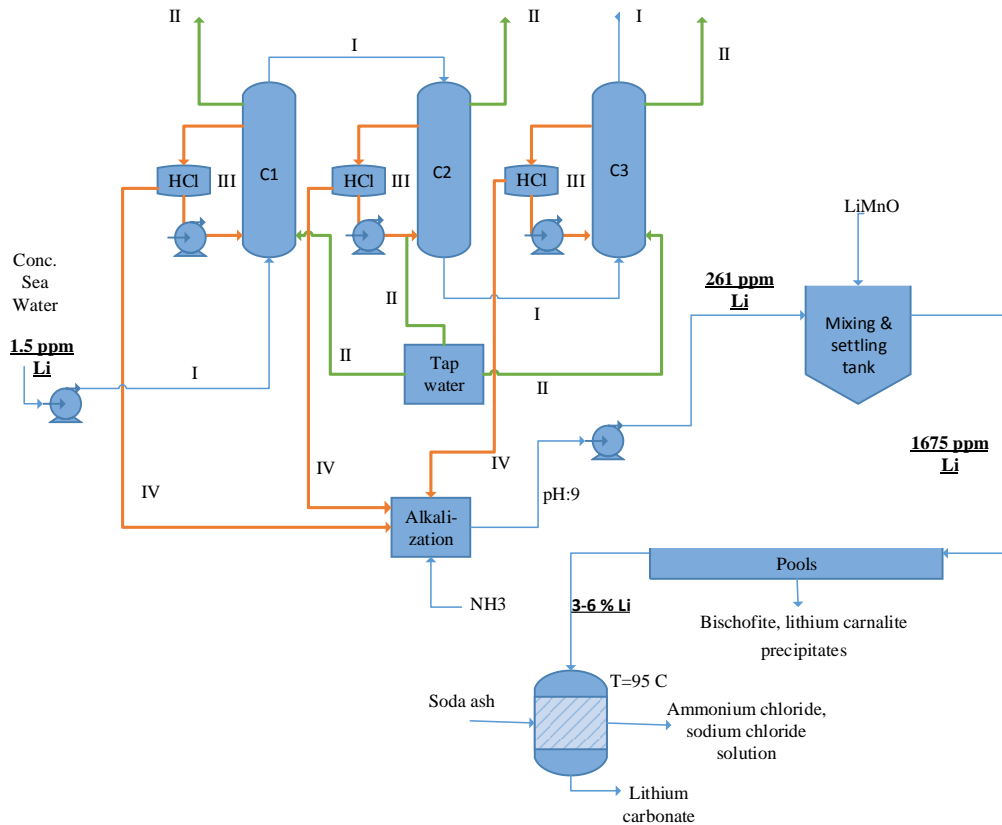


Figure D. 1 Li_2CO_3 production process from concentrated brine in Çamaltı Salina

The aim of the proposed process is to enrich the lithium content in concentrated brine solution from 1.2-1.5 ppm to 3000 ppm. The adsorption of lithium chloride is done by feeding the concentrated brine through (Line I) series of columns filled with PSMA-LiMnO beads (C1, C2 and C3). The effluent of C3 which has trace amount of lithium is sent back to sea. After that, tap water is fed to the columns for a while until the outlet concentration of foreign ions remains constant Line 2. The outlet of tap water may be recycled back to C1, when it has a lithium content higher than 1.5 ppm. After sweeping process is completed, dilute hydrochloric acid solution is fed to each column batchwise and the lithium content in the column is eluted (Line 3). After elution process is completed, 261 ppm Li solution is acquired. After that, a post-treatment process with LiMnO particles is done and the concentration of lithium is increased to 1675 ppm. The neutralization of hydrochloric acid content in solution can be done by ammonia. The concentrated brine would then be sent to pools to let water content evaporate and bischofite salt ($\text{MgCl}_2 \cdot 6\text{H}_2\text{O}$) and lithium carnalite salt ($\text{LiCl} \cdot \text{MgCl}_2 \cdot 7\text{H}_2\text{O}$) precipitate in conventional processes. The remaining magnesium

content in the brines may be removed by utilizing lime in the processes. The solutions enriched in lithium content are finally precipitated by adding soda ash (Na_2CO_3) in the form of Li_2CO_3 . Before this operation, the lithium content must be at least saturated to 3000 ppm and the solution should be heated to 95 °C. The high temperature lowers the carbonate solubility, therefore increases precipitated lithium carbonate amount. The dependency of lithium carbonate solubility in water towards temperature is given in Table D. 1.

Table D. 1 Temperature dependency of lithium carbonate solubility [102]

Temperature (°C)	Solubility (g/100 ml)
25	1.29
100	0.69

In this study, an experiment was performed in order to produce lithium carbonate from 3000 ppm LiCl solution. The simple experiment set-up is as shown below.

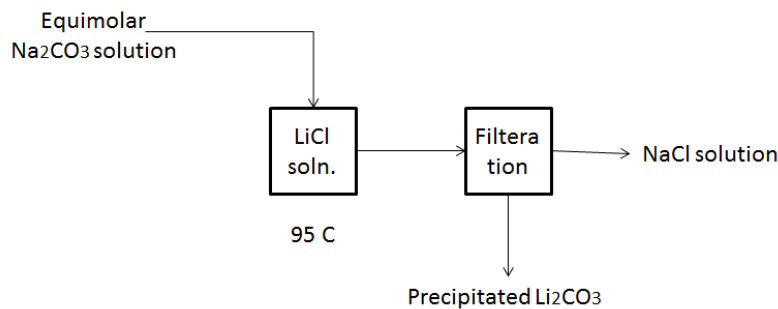


Figure D. 2 Li_2CO_3 production from LiCl

By this experiment, some amount of lithium carbonate was produced while using artificially prepared 3000 ppm LiCl solution. Sodium and potassium carbonates dissolves in water rapidly but magnesium carbonate solubility in water is 0.0063 g/100 ml [102] which means that, all the magnesium remaining in the solution precipitates with lithium in the last step. Therefore enriching the brine in lithium content is as important as decreasing the magnesium content in the brine.

In Çamaltı Salina, 500,000 tons of NaCl is produced in a year. That means 14,285,714 tons of sea water is processed in NaCl production. The sea water is concentrated up to 10 folds which means the total amount of sea water reduces approximately to 1.5 M tons. After NaCl is produced, the residue is fed back to sea directly. In order to process that much of water in a year one has to use pumps with a capacity of 260 kg/min. Totally 13 tons of Li₂CO₃ can be produced from that amount of sea water. The price of lithium carbonate is 8540 USD/ton commercially [103] which means 111,020 USD annual income.

The cost of the system is roughly estimated by utilizing a standard 22” diameter column with a 4 m height. The volume of each column is calculated as 1 m³. The density of the beads is known as 1 g/cm³. 1 ton of beads can adsorb 7 kg Li, which means 30 kg Li₂CO₃. In order to have 13 tons of Li₂CO₃ as a product, columns must be saturated 430 times in a year. In the basis of lab-scale experiments done in this thesis work, approximately 0.5 L of water is enough to sweep 38.5 g of beads which scales up to 12.5 m³ of water to sweep 1 ton of beads. 14.35 ml HCl is enough to elute 38.5 g of beads, which scales up to 372 kg HCl to elute 1 ton of beads. Half of the acid is required as ammonia to neutralize it.

According to these rough estimations, the expenses were listed in Table D. 2.

Table D. 2 Rough estimation of the cost of 13 tons lithium carbonate production in a year from Çamaltı Salina

Expenditure	Amount	Price (\$)
Fixed costs		
Pumps	3	12,000
Columns, tanks and flow elements	3	100,000
Total		112,000
Operational costs		
Tap water	5,000 tons	25,000
	160 ton HCl	
HCl, NH ₃ , Na ₂ CO ₃	50 ton NH ₃ 18 ton Na ₂ CO ₃	30,000

Table D.2 continued.

PSMA-LiMnO beads (d: 1000 kg/m ³)	3 tons	100,000
Electrical cost of pumps in one year	0.7 kWh(10 TL/hour)	4,500
	Total	159,500
	GRAND TOTAL	271,500

It is obviously seen that, under these circumstances there is no chance to extract lithium carbonate from Çamaltı Salina in a feasible way due to the very low concentration of lithium in sea water. However, in terms of energy considerations and the strategic role that the lithium element will play in the future, the economical drawback of the process might be reconsidered.

To reduce the magnesium content in the concentrated brine, a pretreatment process can be integrated to the design which utilizes soda ash before feeding the concentrated brine into the adsorption column. In this study, preliminary experiments were done about using soda ash to reduce the magnesium content in the concentrated brine. The brine and equimolar amount of sodium carbonate with respect to magnesium was heated to 95 °C and mixed in a beaker. Suddenly a white precipitate was observed and after 15 min of mixing time, the precipitate was filtered. When the magnesium content of the initial and final solutions was analyzed in AAS, it was seen that the magnesium content was reduced to 8614 ppm from 21000 ppm while maintaining the lithium concentration constant at 1.25 ppm. This additional process would distress the sweeping duty of the system but would not be sufficient to overcome the high magnesium concentration problem.

Li₂CO₃ production from boron clay in Bigadiç-Balıkesir

Besides acquiring lithium from sea water, boron clay in Bigadiç seems to be a very promising candidate to gather lithium with its 3000 ppm Li content. The system will not require that much of tap water used for sea water and also it won't need high performance pumps and operational costs. On the other hand it will need additional sulfuric acid and ammonia expenses.

The proposed flow diagram to extract lithium carbonate from boron clay is shown in Figure D. 3.

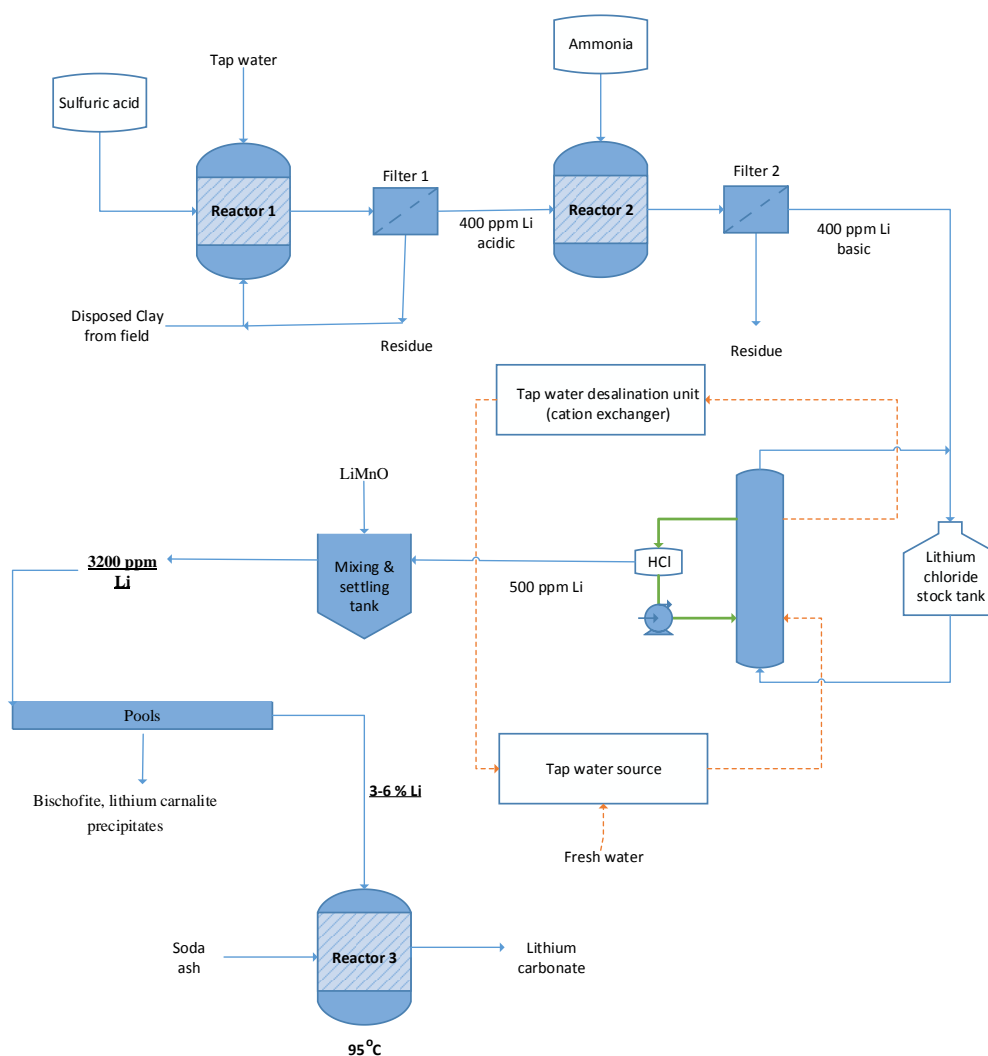


Figure D. 3 Flow diagram of extraction lithium carbonate from boron clay.

The aim of the proposed process is to recover lithium from boron clay and make a production of lithium carbonate. The process starts by the treatment of clay with sulfuric acid so that, leaching the lithium content and taking into brine. The mixture is then sent to filter where clay residues are separated. In the second reactor, ammonia is added to the lithium solution to increase the pH near 9 which is the operational pH of the beads. Filter 2 after Reactor 2 helps to get rid of white precipitate formed after ammonia addition. The basic lithium chloride rich solution is then sent to the adsorption column where adsorption, sweeping and elution processes are done. Following the post-treatment of brine with LiMnO in settling tanks, the brine is sent to pools to further concentrate. After that by addition of ammonia and soda ash the final lithium carbonate product is acquired. When the expenses in the system are roughly estimated, the following table is acquired.

Table D. 3 Expenses of the lithium carbonate plant from Bigadic boron clay.

Expenditure	Amount	Properties	Price (TL)
Fixed costs			
Reactors	4	316 Stainless steel 4 m ³	100,000
Columns	2	316 Stainless steel	50,000
Filters	2	316 Stainless steel 250 kg/h filtering capacity	25,000
Flow elements	1	316 Stainless steel	10,000
Storage tanks	4	316 Stainless steel 4 m ³	20,000
Desalination unit	1	Cation exchanger	20,000
Pumps	5		10,000
Total			235,000 TL
Operational costs			
PSMA-LiMnO beads	1000 kg/ton clay/year	Needs a production unit	30,000
Sulfuric acid	600L/ton clay	Commercial	120
Ammonia	300L/ton clay	Commercial	120
Soda ash	25 kg/ton clay	Commercial	20
HCl	300 L/ton clay	Commercial	120
Tap water	5000 L/ton clay	Industrial water (or well water)	10
Heating and electricity	7 kWh/ton clay		10
Total			400 TL/ton clay + 30,000 TL/year

Table D.3 continued.

GRAND TOTAL	235,000 TL Fixed 10,000TL/year Oper. + 400 TL/ton clay
--------------------	--

28.7 kg lithium carbonate can be produced from 1 ton of clay (3000 ppm lithium content). Lithium carbonate price is 8540 USD/ton commercially. If 1000 tons of clay is processed in a year, 430,000 TL is spent to the operational cost and 525,000 TL will be income. Gross profit in a year is around 100,000 TL. 2.5 years will be enough to pay the expenses for the fixed costs.

Two and a half year time to return investment money will make the process feasible. Also, the strategic importance of lithium in energy market and expected raises in lithium carbonate price make the process promising.

CURRICULUM VITAE

PERSONAL INFORMATION

Surname, Name: Erdoğan, Barış
Nationality: Turkish (TC)
Date and Place of Birth: 25 February 1983, Zonguldak
Marital Status: Single
Phone: +90 312 297 61 57 (128)
Fax: +90 312 297 61 57 (128)
email: barise@logoskimya.com

EDUCATION

Degree	Institution	Year of Graduation
MS	METU Chemical Engineering	2008
BS	METU Chemical Engineering	2006
High School	KDZ Ereğli Anadolu High School, Zonguldak	2001

WORK EXPERIENCE

Year	Place	Enrollment
2012- Present	LOGOS Chemical Technologies	Co-Founder
2008-2012	METU Department of Chemical Engineering	Research Assistant
2005 July	İstanbul Elyaf Intern Engineering	Student
2004 August	ERDEMİR Intern Engineering	Student

FOREIGN LANGUAGES

Advanced English

PUBLICATIONS

Sinan Korpe, Baris Erdogan, Goknur Bayram, Serkan Özgen, Yusuf Uludag, Niyazi Bıçak, Crosslinked DADMAC polymers as cationic superabsorbants, Reactive Functional Polymers, 69, 9, September 2009, sayfa 660-665

PUBLICATIONS IN REVIEW

Baris Erdogan, H. Onder Ozbelge, Niyazi Bicak, Direct synthesis of N-alkyl formamides and their utility in lithium extraction from artificial brines and concentrated seawater, Journal of Environmental Chemical Engineering

ABSTRACTS IN INTERNATIONAL CONFERENCES

Baris Erdogan, H. Onder Ozbelge, Niyazi Bıçak, Extraction of Lithium from Seawater by N-Alkyl Formamides, 12. Mediterranean Congress of Chemical Engineering, November 2011; Barcelona, Spain

Baris Erdogan, H. Onder Ozbelge, Niyazi Bıçak, Separation of Lithium by Polymer Enhanced Ultrafiltration, 12. Mediterranean Congress of Chemical Engineering, November 2011; Barcelona, Spain

HOBBIES

Mountaineering, Microcontrollers